ULTRAFAST ERBIUM DOPED FIBER LASERS USING 2D NANOMATERIAL BASED SATURABLE ABSORBERS

MAHMOUD HAZZAA MOHAMMED AHMED

FACULTY OF ENGINEERING
UNIVERSITY OF MALAYA
KUALA LUMPUR

2018

ULTRAFAST ERBIUM DOPED FIBER LASERS USING 2D NANOMATERIAL BASED SATURABLE ABSORBERS

MAHMOUD HAZZAA MOHAMMED AHMED

THESIS SUBMITTED IN FULFILMENT OF THE REQUIREMENTS FOR THE DEGREE OF DOCTOR OF PHILOSOPHY

FACULTY OF ENGINEERING
UNIVERSITY OF MALAYA
KUALA LUMPUR

2018

UNIVERSITY OF MALAYA

ORIGINAL LITERARY WORK DECLARATION

Name of Candidate: MAHMOUD HAZZAA MOHAMMED AHMED

Registration/Matric No: KHA150005

Name of Degree: DOCTOR OF PHILOSOPHY

Title of Project Paper/Research Report/Dissertation/Thesis ("this Work"):

ULTRAFAST ERBIUM DOPED FIBER LASERS USING 2D NANOMATERIAL BASED SATURABLE ABSORBERS

Field of Study: PHOTONIC

I do solemnly and sincerely declare that:

(1) I am the sole author/writer of this Work;
(2) This Work is original;
(3) Any use of any work in which copyright exists was done by way of fair dealing and for permitted purposes and any excerpt or extract from, or reference to or reproduction of any copyright work has been disclosed expressly and sufficiently and the title of the Work and its authorship have been acknowledged in this Work;
(4) I do not have any actual knowledge nor do I ought reasonably to know that the making of this work constitutes an infringement of any copyright work;
(5) I hereby assign all and every rights in the copyright to this Work to the University of Malaya ("UM"), who henceforth shall be owner of the copyright in this Work and that any reproduction or use in any form or by any means whatsoever is prohibited without the written consent of UM having been first had and obtained;
(6) I am fully aware that if in the course of making this Work I have infringed any copyright whether intentionally or otherwise, I may be subject to legal action or any other action as may be determined by UM.

Candidate's Signature Date:

Subscribed and solemnly declared before,

Witness's Signature Date:

Name:

Designation:

ULTRAFAST ERBIUM DOPED FIBER LASERS USING 2D NANOMATERIAL BASED SATURABLE ABSORBERS

ABSTRACT

The importance of ultrafast fiber lasers technology in science and engineering continues to grow as their performance offers great advantages. Therefore, ultrafast erbium-doped fiber lasers (EDFLs) have been demonstrated in this thesis using various new two-dimensional (2D) nanomaterials as a mode-locker. Here, new 2D nanomaterials like graphene, molybdenum disulfide (MoS_2) and black phosphorus were explored as saturable absorbers (SAs) device. These SAs were fabricated, characterized and integrated into various EDFL cavities for realizing ultrafast laser. At first, a simple and compact mode-locked EDFL was demonstrated using nonconductive graphite pencil-core based SA. Then, stretched pulse and soliton femtosecond pulse generation with graphene SA were obtained by manipulating cavity dispersion. With dispersion management, the net cavity total dispersion can be decreased to -0.028 ps^2, where stable stretched pulse with pulse width of 750 fs can be generated at a repetition rate of 35.1 MHz. Also, by varying the net cavity dispersion to -0.3 ps^2, anomalous dispersion cavity has been achieved to generate soliton mode-locked pulses train with a pulse width of 820 fs and repetition rate of 11.5 MHz. Next, a few-layer molybdenum disulfide (MoS_2) based SA was developed by mechanically exfoliating the material using scotch tape. A self-started mode-locked soliton pulse was successfully generated at a central wavelength of 1598.94 with pulse width and repetition rate of 830 fs, and 17.1 MHz, respectively. After that, a free-standing few-layer MoS_2 polymer composite was fabricated by liquid phase exfoliation of chemically pristine MoS_2 crystals and use this to demonstrate a soliton mode-locked EDFLs. A stable soliton pulse started at a low threshold pump power of 25 mW and has shorter pulse duration of 630 fs. Furthermore, a dissipative soliton with square pulse train was obtained by using MoS_2 in the ultra-long cavity. Finally, through

mechanically exfoliating a black phosphorus (BP) crystal, the BP-SA was obtained. A small piece of the BP flakes was then integrated into an EDFL cavity to achieve a self-started soliton mode-locked pulse operation at 1560.7 nm with shorter pulse duration of 570 fs and high pulse energy of 0.74 nJ. Overall, the emerging 2D nanomaterials as SA in fiber lasers cavity designs could be leveraged to yield tangible benefits for ultrafast lasers technology and we place our results in the full-text publication of ongoing research. The developed lasers will find possible applications in high-speed telecommunications, environmental sensing, metrology and biomedical diagnostics.

Keywords: Ultrafast lasers, Fiber lasers, Mode-locked laser, Nanomaterial

LASER GENTIAN TERDOP ERBIUM ULTRA-PANTAS MENGGUNAKAN PENYERAP TEPU BERASASKAN BAHAN NANO 2D

ABSTRAK

Kepentingan teknologi ultralaju gentian laser dalam bidang sains dan kejuruteraan terus berkembang sejajar dengan kelebihan prestasi yang ditawarkan. Dalam tesis ini, kami memperagakan mod terkunci ultralaju erbium terdop gentian laser (ETGL) menggunakan dua-dimensi (2D) bahannano. 2D bahannano seperti graphene, molibdenun disulfida (MoS_2) dan fosforus hitam yang disentesis, dicirikan dan besepadu kedalam rongga gentian laser untuk bertindak sebagai penyerap bolehtepu (PB). Pada peringkat pertama, generasi denyut femtosaat dan regangan dengan PB graphene diperoleh dengan memanipulasi rongga serakan. Dengan menguruskan penyebaran rongga bersih, jumlah penyebaran boleh dikurangkan kepada -0.028 ps^2, denyut regangan stabil dengan lebar denyut 750 fs dihasilkan pada kadar pengulangan 35.1 MHz. Juga, dengan variasi penyebaran rongga bersih, jumlah penyebaran boleh ditingkatkan kepada -0.3 ps^2, dimana penyebaran ganjil boleh dicapai dengan menghasilkan mod terkunci soliton dengan denyut lebar 820 fs pada kadar pengulangan 11.5 MHz. Pada peringkat kedua, kami menyediakan beberapa lapisan molibdenum disulfida (MoS_2) dengan cara mekanikal pengelupasan menggunakan pita scotch dan menetapkan serpihan MoS_2 yang diperoleh ke permukaan penyambung denyut FC/PC standard. Mod dikunci denyut soliton dihasilkan pada panjang gelombang tengah 1598.94 nm dengan masing-masing lebar denyut dan kadar pengulangan 830 fs, dan 17.1 MHz. Kami juga membikin beberapa lapisan MoS_2 komposit polimer yang berdiri bebas oleh cecair pengelupasan fasa kristal MoS2 kimia yang bersih dan digunakan untuk menghasilkan mod terkunci soliton ETGL. Denyut nadi yang stabil bernula pada kuasa pam di ambang yang rendah iaitu 25 mW dan mempunyai tempoh denyut yang pendek iaitu 630 fs. Tambahan pula, soliton lesap

dengan panjang denyut persegi yang diperoleh dengan menggunakan MoS_2 dalam rongga ultra-panjang. Akhir sekali, melalui mekanikal pengelupasan kristal fosforus hitam (FH), FH-PB diperoleh dengan melekatkan kepingan FH yang diperoleh ke pita scotch. Kepingan kecil pita kemudiannya diintegrasikan dalam rongga ETGL untuk mencapai mod terkunci denyut soliton yang beroperasi pada 1560.7 nm dengan tempoh denyut yanf pendek iaitu 570 fs dan tenaga denyut yang tinggi iaitu 0.74 nJ. Secara keseluruhannya, bahannano 2D muncul sebagai penyerap bolehtepu dalam reka bentuk rongga gentian laser boleh dimanfaatkan untuk teknologi ultralaju laser dan kami meletakkan keputusan kami dalam penerbitan penyelidikan teks penuh yang berterusan. Peranti laser mempunyai aplikasi dalam bidang telekomunikasi berkelajuan tinggi, menderia alam sekitar, metrologi dan diagnostik bioperubatan.

Kata kunci: Ultra-pantas laser, Gentian laser, Laser mod terkunci, Bahan nano

ACKNOWLEDGEMENTS

First and foremost praise is to ALLAH for giving me the opportunity and granting me the capability to proceed my research successfully.

I would like to thank and express my greatest gratitude to my supervisor Prof. Ir. Dr. Sulaiman Wadi Harun for his excellent guidance, supervision, and support, which have made my research highly interesting and enjoyable. He had spent his valuable time with me to discuss any problems and issues arise during the study and make sure that I have produced my best effort. I would also like to express my gratitude to Dr. Norfizah Mohamad Ali for helping me get started in the lab and gave me many illuminating thoughts and suggestions. My sincere appreciation goes to Prof. Dr. Hamzah Arof for helping me in my research. Indeed, his constructive comments were really helpful.

In addition, I would like to take this opportunity and thank all my colleagues and friends at Photonic Engineering Lab and Photonic Research Centre (PRC) for discussions and suggestions, you all have made the PhD process more enjoyable despite the many challenges we have faced. I would also like to express my gratitude to my friends back home for encouraging me throughout my study.

I gratefully acknowledge the scholarship awarded by the Malaysian International Scholarship (MIS) to undertake my PhD.

I owe everything to my family for their endless love and continuous support, especially my parents who always care for my study and tried to be patient for my absence to see this achievement come true, thanks to them for giving me this chance to complete my research.

TABLE OF CONTENTS

LIST OF FIGURES

LIST OF TABLES

LIST OF SYMBOLS AND ABBREVIATIONS

β_2	:	Group velocity dispersion parameter
I	:	Light intensity
I_{sat}	:	Saturation intensity
α_s	:	Modulation depth
α_{ns}	:	Non-saturable absorption
f_{rep}	:	Pulse repetition rate
λ	:	Wavelength
$\Delta\lambda$	:	Spectral bandwidth (at FWHM)
n	:	Refractive index
c	:	Speed of light
υ	:	Frequency of optical wave
$\Delta\nu$	:	Optical spectral bandwidth (in hertz)
dB	:	Decibel
μs	:	Microsecond
ps	:	Picosecond
fs	:	Femtosecond
nm	:	Nanometer
τ_p	:	Pulse duration
$sech^2$	:	Secant hyperbolic
2D	:	Two-dimensional
AC	:	Auto-correlator
BP	:	Black Phosphorus
CNTs	:	Carbon Nanotubes
CW	:	Continues Wave

EDF	:	Erbium-Doped Fiber
EDFL	:	Erbium-Doped Fiber Laser
FESEM	:	Field Emission Scanning Microscopy
FWHM	:	Full-Width at Half Maximum
GVD	:	Group Velocity Dispersion
LASER	:	Light Amplification by Stimulated Emission of Radiation
LPE	:	Liquid Phase Exfoliation
MoS_2	:	Molybdenum disulfide
NA	:	Numerical Aperture
NOLM	:	Nonlinear Optical Loop Mirror
NPR	:	Nonlinear Polarization Rotation
OTDM	:	Optical Time Division Multiplexing
OSA	:	Optical Spectrum Analyzer
OSC	:	Oscilloscope
PC	:	Polarization Controller
PVA	:	Poly Vinyl Alcohol
RF	:	Radio Frequency
SA	:	Saturable Absorber
SESAMs	:	Semiconductor Saturable Absorption Mirrors
SMF	:	Single Mode Fiber
SNR	:	Signal to Noise Ratio
SPM	:	Self-Phase Modulation
SWCNT	:	Single-Walled Carbon Nanotubes
TBP	:	Time Bandwidth Product
TMD	:	Transition Metal Dichalcogenide
WDM	:	Wavelength Division Multiplexing

CHAPTER 1: INTRODUCTION

1.1 Background and Motivation

Ultrafast photonics is a relatively new and rapidly growing field of research. It is not only limited to scientific research but is also found in many industrial applications like optical communications (Salehi et al., 1990), medical diagnostics (Nagy et al., 2009; Plamann et al., 2010), micromachining (Gattass et al., 2008), multiphoton imaging (C Xu et al., 2013), spectroscopy and microscopy (Freudiger et al., 2014). Over the past decade, ultrafast fiber laser technology has been developed quickly and as our understanding develops so will the applications of these lasers. It is also interesting to observe how advances in fiber optics have revolutionized laser technology, especially for ultrahigh-speed optical systems and networks. Optical fiber provides an appropriate platform for the developments and monolithic integration of a laser system, therefore fiber technology has a significant impact on the area of laser engineering and holds a dominant position in the commercial laser market. Ultrafast fiber lasers with pulse width on the order of a few picosecond or femtosecond have been progressed with an emphasis focusing on the nature of the gain medium and the modulation techniques that dynamically promote the formation of the ultrashort pulse generation. The near and mid-infrared (~1.0–2.0 μm) region is now well addressed by silica glass fiber amplifiers, including active medium doped with ytterbium (Yb) (Zhou et al., 2008), erbium (Er) (Tausenev et al., 2008), bismuth (Bi) (Kelleher et al., 2010) and thulium (Tm) (Zhang et al., 2012), allowing almost continuous coverage of this wavelength region.

Erbium-doped fiber laser (EDFL) is one of the most widely developed fiber lasers that operating in 1.5 μm region. Recently, they have achieved huge interest for optical communication, medicine, and fiber sensor applications. For instance, in the optical communication field, ultrashort pulsed EDFLs have been utilized in long-distance communications networks due to their practical advantages, such as compact,

inexpensive, robust, efficient heat dissipation, and so on (Chong, 2008). Recently, with the increasing demands of higher data rate transmission, people have expanded the telecommunications window from the conventional C-band (1530 – 1565 nm) to the long wavelength L-band (1565 – 1625 nm) by reason of the lowest losses of silica fibers in this region, and researchers have also paid more attention to the L-band ultrafast fiber laser (Agrawal, 2005). In addition, to achieve a high capacity transmission, multiplexing with Wavelength Division Multiplexing (WDM) and Optical Time Division Multiplexing (OTDM) are effective solutions in current technology. Mode-locked fiber laser can also be used in the OTDM system. For instance, the ultra-high speed at 5.1 Tb/s in OTDM transmission over 70 km had been demonstrated using ultrashort femtosecond soliton with 10 GHz per channel at the transmitter (Mulvad et al., 2010; Nakazawa, 2000).

To generate ultrashort fiber laser pulses, either active or passive techniques can be utilized. The active technique is typically performed by inserting optical modulators and bulk devices into the cavity to electronically synchronize the cavity repetition rate (El-Sherif et al., 2003). However, this technique is often relatively complicated and bulky due to the existence of the external modulators and other bulk devices in the cavity. On the other hand, the passive technique is not required external synchronization, but rather adopts an all-optical nonlinear process in a laser resonator based on saturable absorbers (SAs). Passive pulse based on SAs represents convenient technique and additional advantages such as simplicity, compact construction, cost efficiency, robustness and ultrafast pulse generation (F Ahmad et al., 2013; Chang et al. (2012)). The efficient generation of ultrashort pulses is the strong key qualifying technology in optical communication. Typically, this is recently done by the passive technique based on various SAs. SA is a nonlinear optical material which changes its absorbance depends on the intensity of light. It absorbs the low intensity of light while the absorbance decreases for

the high intensity of light. Generally, SA is used to generate passively Q-switched and mode-locked fiber lasers.

To date, various types of SAs have been intensively investigated and implemented to realize passive Q-switching and mode-locking pulses trains, such as nonlinear optical loop mirror (NOLM) (Zhong et al., 2010), nonlinear polarization rotation (NPR) (A Luo et al., 2011), semiconductor saturable absorption mirrors (SESAMs) (Gomez, 2004; Z-C Luo et al., 2011), single wall carbon nanotubes (SWCNTs) (Ahmed et al., 2014; Set et al., 2004) and graphene SAs (Sun, Hasan, Torrisi, et al., 2010; Han Zhang et al., 2009). In the NOLM approach, a long fiber must be used to produce sufficient nonlinear phase shifts. The NPR technique utilizes dispersion and nonlinearity management to generate the laser. However, it is often sensitive to ambient factors such as vibration and temperature, which limits its practical applications. SESAM is the dominated passive mode locking. However, SESAMs require complex design to improve their damage threshold and work only in a narrow wavelength range. A simpler and cost-effective alternative relies on SWCNTs. However, SWCNTs have a low damage threshold and their operating wavelength depends on the diameters of the nanotube (Ahmed et al., 2014). Therefore, a strong aspiration to seek new high-performance of SAs with the broadband operation for fiber laser systems. Since the first demonstration of two dimensional (2D) nanomaterial like graphene based SA (Bao et al., 2009), graphene has been studied and developed for passive Q-switching and mode locking applications (Cui et al., 2013; Luo et al., 2010). Compared to the previous SAs, graphene has the advantages of ultrafast recovery time and broadband saturable absorption. But the absence of band gap and the low absorption co-efficiency (2.3%/layer) of graphene have also restraint its applications. These limitations lead to the intensive research on other 2D nanomaterials which can complement the graphene.

Recently, various 2D nanomaterials have been explored as an SA for ultrafast laser applications, due to their thickness dependent band-gap and excellent optical properties (Wang et al., 2013; Robert I. Woodward et al., 2014; H Zhang et al., 2014). Since the nonlinear saturable property of molybdenum disulfide (MoS_2) nanosheet was firstly reported by Wang et al. in 2013 (Wang et al., 2013), few works have been carried out on demonstrating Q-switched fiber lasers using a MoS_2 based SA (Huang et al., 2014; Robert I. Woodward et al., 2014). Another kind of 2D nanomaterial is black phosphorus (BP), which is considered as a new promising nanomaterial for optoelectronic applications (Churchill et al., 2014; F Xia et al., 2014). Black phosphorus is the most thermo-dynamically stable allotrope of phosphorus, which has recently joined the family of 2D nanomaterials (Churchill et al., 2014). BP is a high-mobility layered semiconductor with band-gap sensitively dependent on the number of layers from 0.3 eV (bulk) to 2 eV (monolayer layer) (Rudenko et al., 2014; Tran et al., 2014). Up to date, there are only a few reported works on 2D nanomaterial used as a broadband SAs within the laser cavity to realize passive mode-locked fiber lasers (Y Chen et al., 2015).

This thesis focuses on developing new ultrafast fiber lasers operating at C-band and L-band wavelength regions using 2D nanomaterials like graphene, MoS_2, and black phosphorus as a saturable absorber.

1.2 Thesis Objectives

Ultrafast fiber laser is important and widely used in communication and industrial applications. This work aims to construct and demonstrate practical ultrafast fiber lasers based on 2D nanomaterials SAs. To achieve this, several objectives have been outlined to guide the research direction toward the goal:

1. To fabricate and characterize new passive SAs based on 2D nanomaterials like graphene, MoS_2, and black phosphorus.
2. To design and optimize EDFL cavities to generate mode-locking pulses train in different dispersion regimes.
3. To generate and evaluate mode-locked EDFL using graphene and MoS_2 based SAs.
4. To generate and develop mode-locked EDFL with shorter pulse width and high pulse energy using black phosphorus saturable absorber.

1.3 Contributions

The major contributions of this research work are summarized as below:

1. A simple and compact mode-locked EDFL is successfully demonstrated using nonconductive graphite pencil-core based SA. The SA is prepared by exfoliating a low-cost graphite- pencil-core flakes on adhesive tape surface. Then a small piece of the tape is sandwiched between two ferrules and integrate into EDFL ring cavity to realize a self-started mode-locked pulse train at 1562 nm wavelength with a pulse width of 3.05 ps.
2. Demonstration of stretched and soliton femtosecond mode-locked EDFLs with graphene SA by manipulating the cavity dispersion.

3. Demonstration of various mode-locked EDFLs using MoS_2 SA. Soliton mode-locked EDFL is realized with mechanically exfoliated MoS_2 SA. Femtosecond mode-locked EDFL is achieved using a fabricated few-layer MoS_2 polymer composite film. A dissipative soliton mode-locked EDFL with square pulse train is generated by using MoS_2 in ultra-long cavity based on dispersion shifted fiber (DSF).
4. Demonstration of ultrafast EDFL based on mechanically exfoliated multi-layer black phosphorus SA. The ultrafast pulse operates at 1560.7 nm wavelength with 570 fs pulse width and pulse energy of 0.74 nJ.

1.4 Thesis Overview

This thesis consists of six chapters. In these chapters, a comprehensive study of mode-locked fiber laser based on 2D nanomaterials is presented. This chapter describes the background and motivation of ultrafast fiber laser study. The objectives and contributions of this research are also outlined in this chapter.

Chapter 2 highlights the literature review of this work, where theoretical aspects including theoretical equations for pulse propagation in optical fiber, historical evolution of the saturable absorbers technologies and review of the fundamental optical properties of 2D nanomaterials like graphene, MoS_2, and black phosphorus are described. The mode-locking technique and the important parameters of the mode-locked laser output are also briefly reviewed and described.

Chapter 3 demonstrates three mode-locked EDFLs using new graphene based SAs. At first, the usability of nonconductive graphite pencil-core as SA for mode-locked EDFL was demonstrated. Then, the development of two different femtosecond mode-locked EDFLs using graphene SA was reported. It was shown that the variation of net cavity dispersion in the laser cavity can produce stretched and soliton pulses.

Chapter 4 reports various passively mode-locked EDFLs using MoS_2 based SA. Firstly, the MoS_2 is obtained via mechanical exfoliation method to generate a soliton mode-locked pulse. Next, few-layer MoS_2-PVA is fabricated as a thin film for mode locking pulse generation in both anomalous and ultra-long normal dispersion regimes.

Chapter 5 demonstrates the employment of black phosphorus (BP) based SA as an effective SA for the ultrafast EDFLs. The BP is prepared by a simple mechanical exfoliation technique. Depending on the thickness of the BP-SA used, the EDFL can operate either in Q-switching or mode-locking regime. It is found that thick BP-SA produces Q-switching pulses while thinner BP-SA is capable to be used in generating soliton mode-locked pulses.

Finally, chapter 6 concludes the thesis with the summary and review of the research finding. Also, this chapter provides a recommendation for future works.

CHAPTER 2: LITERATURE REVIEW ON PULSED FIBER LASER

2.1 Overview of Ultrafast Fiber Laser Development

Ultrafast lasers have been developed over the past few decades and are becoming ubiquitous tools in a wide variety of applications every year. Since the invention of optical laser in 1958 (Schawlow et al., 1958), several fields of research have been developed in optics and photonics, especially ultrafast optics that began in 1964, with the generation of short pulses by incorporation an acousto-optic modulator inside a He–Ne laser (DiDomenico Jr, 1964; LE Hargrove et al., 1964). In 1970, Kuizenga and Siegman firmly established the analytic theory of active mode-locking using a Gaussian pulse analyses (Kuizenga et al., 1970). However, the intra-cavity filter was not reported in the analysis, which is used to stabilize the laser. Later in 1975, Haus introduced the MASER equation approach for the mode-locking theory (Haus, 1975). Since the early demonstration of the optical fiber, the application of optical fiber to laser has attracted very much attention after the development of high brightness laser diode pump source in the 1980s and the demonstration of erbium-doped fiber amplifier (Desurvire et al., 1987; Mears et al., 1987). In 1989, Hanna et al. reported the first mode-locking operation in a Ytterbium Erbium co-doped fiber laser (Hanna et al., 1989). The mode-locking operation was realized by using an AM modulator with a repetition rate of 100 MHz and pulse width of 70 ps. However, active mode locking based on modulators faces major problem with the stability and the availability of fast external modulators and other bulk devices.

To distinguish between active and passive mode locking, the passive mode locking can generate much shorter pulses using saturable absorbers (SAs) (Keller, 2003). Six years after the first demonstration of the laser, De Maria et al. had produced the first ultra-short pulsed laser based on Nd:glass using a passive technique (Schmidt et al., 1968). They had an underlying problem, it did not measure a regular pulse train. This lack of a regular pulse train remained a problem for passive mode-locked laser for more than 20

years. Finally, the problem was solved in 1992 by utilizing semiconductor saturable absorber mirrors (SESAMs) (U Keller et al., 1992; Keller et al., 1996). Currently, the ultrafast pulse can range from few picoseconds to femtoseconds, depending on the laser material and the parameters of the SAs. The developments in ultrafast fiber lasers performance keep advancing the outlines of ultra-short pulse duration, repetition rate, pulse energy and peak power, which will be discussed in this thesis.

2.2 Spectroscopy of Erbium-Doped Fiber

In the late 1980s, a tremendous interest in erbium-doped fiber amplifiers (EDFAs) led up to a wide availability of related components and necessary equipment. This spurred initial research in a variety of erbium-doped fiber lasers (EDFLs) in the early 1990s, including multiple-wavelength lasers, Q-switched and mode-locked lasers for potential application in a telecommunication system. Figure 2.1 shows the energy level diagram of trivalent erbium Er^{3+} in silicate glass. The main transition in EDFA is the $^4I_{13/2} \rightarrow {}^4I_{15/2}$ transition, which provides gain for the 1.55-μm spectral region, because the $^4I_{13/2}$ is the only metastable state for common oxide glasses at room temperature and gain is only available for these materials at 1.55-μm $^4I_{13/2} \rightarrow {}^4I_{15/2}$ emission band (Ngo, 2010). The peak absorption and emission wavelengths occur around 1530 nm; therefore, the operating wavelength must be chosen in the band that the emission cross section is much greater than the absorption cross section, which is around 1.55-μm.

With current technology, the EDFAs are pumped with a laser diode at around 810, 980, and 1480 nm. However, the pump wavelength of 810 nm suffers from strong excited state absorption (ESA), which causes an undesirable waste of pump photons. Therefore, the pumping wavelengths of 980 and 1480 nm are more commonly used. Pumping at 980 nm (InGaAs/GaAs-based lasers), which excites Er^{3+} ions to the $^4I_{11/2}$ level is one of the most common pumping schemes, due to the higher gain efficiency and signal-to-noise

ratio (SNR) for small signal amplifiers (Digonnet, 2001). It also gives better noise Figures (NFs) and quantum conversion efficiencies for power amplifiers.

The Erbium-doped fiber (EDF) has a broad spectrum range and the fiber dispersion at 1.5 μm is irregular, thus the EDF has advantageous for ultrashort pulse fiber lasers. Irregular dispersion supports the soliton pulse regime of mode locking fiber lasers. In this thesis, EDF was used extensively, which was often commercial unit from *Moritex PureCore*™. We used single-mode InGaAs laser diode at 980 nm to pump and typically achieved lasing at ~1530-1600 nm.

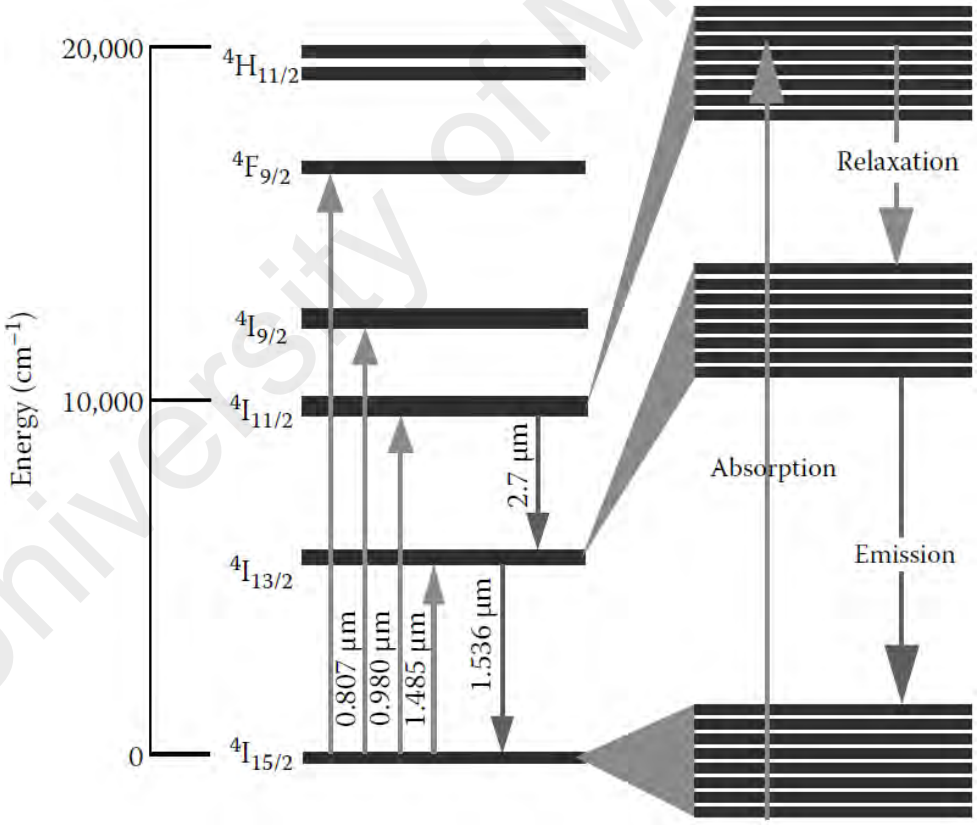

Figure 2.1: Erbium transition diagram (Ngo, 2010)

2.3 Pulse Propagation in Optical Fiber

To understand the nonlinear phenomena in optical fibers, it is necessary to consider the theory of electromagnetic wave propagation in dispersive nonlinear media. In the 1860s, James Clerk Maxwell famously identified the connection between electromagnetism and optics leading to a set of four equations which can be used to describe all electromagnetic phenomena (GP Agrawal, 2007; Maxwell, 1865).

$$\nabla \times \boldsymbol{E} = -\frac{\partial \boldsymbol{B}}{\partial t} \tag{2.1}$$

$$\nabla \times \boldsymbol{H} = \boldsymbol{J} + \frac{\partial \boldsymbol{D}}{\partial t} \tag{2.2}$$

$$\nabla \cdot \boldsymbol{D} = \rho f \tag{2.3}$$

$$\nabla \cdot \boldsymbol{B} = 0 \tag{2.4}$$

where $\boldsymbol{E}$ and $\boldsymbol{H}$ are the electric and magnetic field vectors, $\boldsymbol{D}$ and $\boldsymbol{B}$ are electric and magnetic flux densities, $\boldsymbol{J}$ is the current density vector, ρf is the charge density and t is the time coordinate. In the absence of free charges in a medium such as optical fibers, $\mathbf{J} = 0$ and $\rho f = 0$. The flux densities D and B arise in response to the electric and magnetic fields E and H propagating inside the medium and are related to them through the constitutive relations given by (Diament, 1990).

$$D = \epsilon_0 E + P \tag{2.5}$$

$$B = \mu_0 H + M \tag{2.6}$$

where P and M are the induced electric and magnetic polarizations, ϵ_0 is the vacuum permittivity and μ_0 is the vacuum permeability. For propagation in a nonmagnetic medium such as optical fibers, $M = 0$. Maxwell's equations without charges ($\rho f = 0$) or

currents (J= 0), can be used to obtain the wave equation that describes light propagation in optical fibers. By taking the curl of Eq. (2.1) and using Eq (2.2), (2.5), and (2.6), one can eliminate *B* and *D* in favor of *E* and *P* and obtain a single wave equation:

$$\nabla \times \nabla \times \boldsymbol{E} = -\frac{1}{c^2}\frac{\partial^2 \boldsymbol{E}}{\partial t^2} - \mu_0 \frac{\partial^2 \boldsymbol{P}}{\partial t^2} \tag{2.7}$$

where *c* is the speed of light in a vacuum and the relation $\mu_0\epsilon_0 = 1/c^2$ was used. The electric polarization P is the dipole moment per unit volume of the medium, resulting from electrons oscillating about their equilibrium positions in response to an oscillating electric field. The strength of the electric field and induced polarization are related by the electric susceptibility tensor x of the material, which can be Taylor expanded into $x^{(n)}$ terms, describing the nth order susceptibility (Boyd, 2008):

$$\boldsymbol{P} = \epsilon_0\left(x^{(1)} \cdot \boldsymbol{E} + x^{(2)} : \boldsymbol{EE} + x^{(3)} \vdots \boldsymbol{EEE} + \cdots\right) \tag{2.8}$$

When a material polarization is induced by a field, the oscillating dipoles can radiate new fields with a phase delay. Since the electric field and induced polarization are vector quantities, the susceptibilities are tensors. Consequently, Eq (2.8) can be used to relate the direction of the induced material polarization (and new radiated fields) to the direction of the incident electric field (Woodward, 2015). This enables much information about the nonlinear response of materials to be determined by comparing the polarization of incident light and light generated through nonlinearity.

The study of most nonlinear effects in optical fibers involves the use of short pulses with widths ranging from ~10 ns to 10 fs. When such optical pulses propagate inside a fiber, both dispersive and nonlinear effects influence their shapes and spectra. The following nonlinear Schrödinger (NLS) equation is a nonlinear partial differential equation for describing wave propagation in nonlinear medium;

$$i\frac{\partial A}{\partial z} - \frac{\beta_2}{2}\frac{\partial^2 A}{\partial T^2} + \gamma|A|^2 A = 0 \qquad (2.9)$$

A(z, t) represents the amplitude of the pulse envelope, β_2 is the Group Velocity Dispersion (GVD) parameter, and the nonlinear parameter γ is responsible for Self-Phase Modulation (SPM). GVD and SPM are presented in this equation, whereby both dispersive and nonlinear effects have an impact on the shape and spectrum. The Kerr effect is assumed to be instantaneous nonlinear response which results from optical interaction with electrons of the medium, which lead to an intensity dependent refractive index. This depends on the real part of $x^{(3)}$ in Eq (2.8) and leads to nonlinear effects such as self-phase modulation (SPM), cross-phase modulation (XPM) and four-wave mixing (FWM). Other effects such as Stimulated Raman Scattering (SRS) and Stimulated Brillouin Scattering (SBS) are also considered in fiber, which are non-instantaneous. The SRS arises from interaction between light and optical phonons, whereas SBS is due to acoustic phonon interaction. Each of these effects can be usefully exploited to achieve a particular optical function, or can manifest as an unwanted source of loss or distortion depending on the application.

2.3.1 Chromatic Dispersion

The frequency dependence of the refractive index $n(\omega)$ dictates that the phase velocity in a medium depends on the optical frequency ω. This property, referred to as chromatic dispersion (GP Agrawal, 2007). On a fundamental level, the chromatic dispersion is related to the characteristic resonance frequencies at which the medium absorbs the electromagnetic radiation through oscillations of bound electrons. For wavelengths far from the medium resonances, the material refractive index is well approximated by the *Sellmeier equation* (GP Agrawal, 2007)

$$n^2(\omega) = 1 + \sum_{j=1}^{m} \frac{B_j \omega_j^2}{\omega_j^2 - \omega^2} \tag{2.10}$$

where ω_j is the resonance frequency and B_j is the strength of j[th] resonance. The sum in extends over all material resonances that contribute to the frequency range of interest.

To consider the effect of chromatic dispersion mathematically, the propagation constant β, is Taylor expanded about the center frequency of the propagating light, ω_0 (Govind, 2013):

$$\beta(\omega) = n(\omega)\frac{\omega}{c} = \beta_0 + \beta_1(\omega - \omega_0) + \frac{1}{2}\beta_2(\omega - \omega_0)^2 + \frac{1}{6}\beta_3(\omega - \omega_0)^3 + .., \tag{2.11}$$

where

$$\beta_m = \left(\frac{d^m \beta}{d\omega^m}\right)_{\omega=\omega_0} \quad (m = 0, 1, 2, \dots) \tag{2.12}$$

Dispersion has a particularly important effect on pulsed light, since narrow pulses possess a broad spectrum. The envelope of the pulse propagates at the group velocity v_g, which is related to the first-order propagation constant term by:

$$v_g = \frac{1}{\beta_1} \tag{2.13}$$

The group velocity of different spectral components within the envelope of optical pulse can vary, while the parameter β_2 represents dispersion of the group velocity and is responsible for pulse broadening. This phenomenon is known as the *group velocity dispersion* (GVD) and β_2 (ps^2/km) is the GVD parameter. The GVD of a waveguide is more commonly represented by the dispersion parameter, D (ps/nm·km) (Govind, 2013):

$$D = \frac{d\beta_1}{d\lambda} = -\frac{2\pi c}{\lambda^2}\beta_2 \tag{2.14}$$

The coefficient β_3 appearing in that term is called the third-order dispersion should also be included in a thorough treatment of dispersion, especially in cases where both β_2 and *D* at zero dispersion wavelength.

A key parameter for fibers is the zero-dispersion wavelength, as the sign of dispersion *D* determines the nonlinear phenomena that can be observed. When $D > 0$, the fiber is said to exhibit *normal dispersion*. In the normal dispersion regime, low-frequency (long wavelength) of an optical pulse travel faster than high-frequency light. By contrast, the reverse occurs in the *anomalous dispersion* regime in which $D < 0$. The anomalous-dispersion regime is of considerable interest for the study of nonlinear effects because it is in this regime that optical fibers support solitons through a balance between the dispersive and nonlinear effects.

2.3.2 Nonlinear Effects in Optical Fiber

2.3.2.1 Self-Phase Modulation

Self-phase modulation (SPM) arises from the intensity dependence of the refractive index and can lead to both spectral and temporal changes in pulses during propagation in an optical fiber. It is the temporal equivalence of self-focus, which is the spatial-domain consequence of intensity-dependent refractive index. To consider this quantitatively, the real part of the refractive index can be expressed as (G Agrawal, 2007):

$$n(\omega, I) = n_0(\omega) + n_2 I(t) \tag{2.15}$$

where I is the optical intensity, n_0 is the linear index and n_2 is introduced as the nonlinear index, which for silica is accepted as $n_2 = 2.74\times10^{-20}$ m^2 W^{-1} and is almost wavelength-independent (Milam, 1998).

From the NLS equation (2.9), the nonlinear effects included through (G Agrawal, 2007):

$$\gamma = \frac{2\pi n_2}{\lambda A_{eff}} \tag{2.16}$$

where A_{eff} is the effective area of the mode shape in the fiber.

SPM generates new frequency components due to the temporally varying phase induced by the temporally varying intensity profile of optical pulses. Since the original chirp of the pulse sets the initial relative position of the various frequency components of the pulse and the fiber group velocity dispersion (GVD) changes the relative position of the frequency components during propagation, the output pulse spectrum and shape are results of an interplay among SPM, initial chirp of the pulses, and the fiber GVD. It is useful to introduce the concepts of two length scales, dispersion length L_D and nonlinear length L_{NL}, which will help us to identify the various regimes of operation. For optical pulses with width T_0 and peak power P_0, the dispersion length L_D and nonlinear length L_{NL} is defined as (Dong et al., 2016).

$$L_D = \frac{T_0^2}{|\beta_2|} \tag{2.17}$$

$$L_{NL} = \frac{1}{\gamma P_0} \tag{2.18}$$

The dispersion length L_D and nonlinear length L_{NL} are the respective length scales over which effects of dispersion and nonlinear become important. For a fiber with length L, when $L << L_D$ and $L << L_{NL}$, neither dispersion nor nonlinear effects play a significant role in pulse propagation. When $L << L_D$ and $L \approx L_{NL}$, nonlinear effects dominate. When $L \approx L_D$ and $L << L_{NL}$, dispersion dominates. When $L \approx L_D$ and $L \approx L_{NL}$, both effects need to be considered.

The maximum phase shift ϕ_{max} occurs at the pulse center located at T = 0 is given by

$$\phi_{max} = \frac{L_{eff}}{L_{NL}} = \gamma P_0 L_{eff} \tag{2.19}$$

The effective length L_{eff} for a fiber of length L and loss α is defined as

$$L_{eff} = \frac{1 - e^{-\alpha L}}{\alpha} \tag{2.20}$$

Obviously, the nonlinear length is the effective propagation distance when $\phi_{max} = 1$. In dispersion case, the pulse broadening is observed in time domain, whereas SPM induces spectrum broadening. In figure 2.2 a pulse (top curve) propagating through a nonlinear medium undergoes a self-frequency shifting due to SPM. The front of the pulse is shifted to lower frequency and back to higher frequency. For a Gaussian pulse, the SPM-induced chirp $\delta\omega(T)$ is given by

$$\delta\omega(T) = \frac{2m}{T_0}\frac{L_{eff}}{L_{NL}}\left(\frac{T}{T_0}\right)^{2m-1} exp\left[-\left(\frac{T}{T_0}\right)^{2m}\right] \tag{2.21}$$

where m = 1 for a Gaussian pulse.

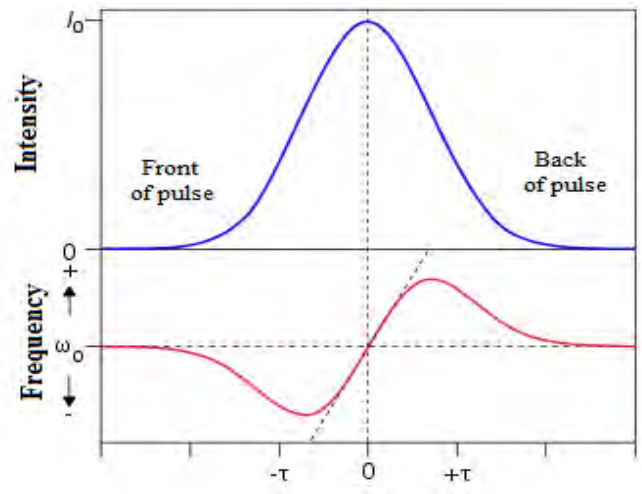

Figure 2.2: SPM-induced chirp in an optical pulse

2.3.2.2 Modulation Instability

Many nonlinear systems exhibit an instability that leads to modulation of the steady state as a result of an interplay between the nonlinear and dispersive effects. This phenomenon is referred to as the *modulation instability*. In the context of optical fibers, modulation instability requires anomalous dispersion regimes and manifests itself as the breakup of the continuous wave (CW) light into a train of ultra-short pulses (Hasegawa, 1984). If we start with NLS equation (2.9), the solution for CW light is simply

$$\bar{A} = \sqrt{P_0}\, exp(i\phi_{NL}) \tag{2.22}$$

where P_0 is the incident power and $\phi_{NL} = \gamma P_0 \zeta$ is the nonlinear phase shift induced by SPM. We can check the stability of the CW light by adding a small perturbation in the amplitude.

$$A = \left(\sqrt{P_0} + a\right) exp(i\phi_{NL}) \tag{2.23}$$

And examine the evolution of the perturbation $a(\zeta, T)$ using a linear stability analysis. Substituting equation (2.23) in NLS equation (2.9) (Govind, 2013), we have

$$i\frac{\partial A}{\partial z} = \frac{\beta_2}{2}\frac{\partial^2 A}{\partial T^2} - \gamma P_0 (a + a^*) \tag{2.24}$$

This linear equation can be solved easily in the frequency domain. However, because of the a^* term, the Fourier components at frequencies Ω and -Ω are coupled. Thus, we should consider its solution in the form

$$a(\zeta, T) = a_1 \exp[i(K\zeta - \Omega T)] + a_2 \exp[-(K\zeta - \Omega T)] \tag{2.25}$$

K and Ω are the wave number and frequency of the perturbation, respectively. Solutions to equations 2.24 and 2.25 are nontrivial only when K and Ω satisfy the following dispersion relation

$$K = \pm\frac{1}{2}|\beta_2\Omega|\sqrt{\Omega^2 + sign(\beta_2)\Omega_c^2} \tag{2.26}$$

where $sign(\beta_2) = \pm 1$ depending on the sign of (β_2),

$$\Omega_c^2 = \frac{4\gamma P_0}{|\beta_2|} = \frac{4}{|\beta_2|L_{NL}} \tag{2.27}$$

The dispersion relation in Eq (2.26) shows that steady-state stability depends critically on whether light experiences normal or anomalous GVD inside the fiber. In the normal dispersion regime where $\beta_2 > 0$, K is always real for all Ω. SPM only affects the phase but not the amplitude of the perturbation. The perturbation will not grow. In the anomalous dispersion regime where $\beta_2 < 0$, K is imaginary when $|\Omega| < \Omega_c$. The amplitude of the perturbation will, therefore, grow exponentially. It is inherently unstable for a CW in the anomalous dispersion regime. The gain is determined by

$$g(\Omega) = |\beta_2\Omega|\sqrt{\Omega_c^2 - \Omega^2} \tag{2.28}$$

2.3.2.3 Cross-Phase Modulation

Cross-phase modulation (XPM) is the phase delay of an optical signal produced by a different wave, which is co-propagating with the signal (Islam et al., 1987). The mechanism is similar to SPM, but the change in refractive index experienced by the signal beam is determined by the intensity of the other wave, which can be expressed as (Govind, 2013):

$$\Delta n_{XPM}(\omega_1) = 2n_2 I(\omega_2) \tag{2.29}$$

where n_2 is the same nonlinear index introduced to describe SPM and $I(\omega_2)$ is the intensity of the second wave. XPM can be practically utilized to synchronize two mode-locked fiber lasers or for pulse diagnostics, but can also cause problems in optical systems such as channel cross-talk in optical fiber communications.

2.3.2.4 Four-Wave Mixing

Four-wave mixing (FWM) is the general term for interactions among four waves through the third-order susceptibility $\chi^{(3)}$, which can be used to generate light at different wavelengths from the pump light. Energy conservation dictates that:

$$\omega_1 + \omega_2 = \omega_3 + \omega_4 \tag{2.30}$$

where ω_i is the angular frequency of the i^{th} wave. The phase-matching requirement for this process is $\Delta k = 0$, where

$$\Delta k = \beta_3 + \beta_4 - \beta_1 - \beta_2 = 0 \tag{2.31}$$

Numerous different mechanisms exist to achieve wavelength conversion, either seeding the FWM process from noise or with a pump or signal inputs to amplify the signal. Generally, the frequencies of the two pump waves do not need to be the same, $\omega_1 \neq \omega_2$. In the more common degenerate case where $\omega_1 = \omega_2$, only one pump is required. In degenerate FWM, higher and lower frequency waves generated around the pump frequency are respectively referred to as *anti-Stokes* and *Stokes* waves. Efficient FWM can only occur in fibers if the process is *phase-matched* – i.e. a fixed phase relationship between the waves must be maintained during propagation.

2.4 Q-Switching Mechanism

Q-switching is a technique for generating optical short pulses on the order of microseconds to nanoseconds by modulating the Q factor (quality factor) of the laser cavity. The Q-factor is defined as the ratio of energy stored in the cavity to energy lost in each oscillation cycle. Q factor modulation is accomplished by embedding an optical loss modulator into the cavity. The Q factor of the resonator can be written in the equivalent form as the following equation:

$$Q = 2\pi v \mathcal{T}_c \tag{2.32}$$

The equation shows that Q can be interpreted physically as 2π times the number of oscillations of the light wave's electric field during a time equal to the cavity lifetime $\mathcal{T}_c$ (Quimby, 2006). The modulator is initially set to yield high losses (low Q factor), which prevents lasing. Energy accumulates in the gain medium as the laser is pumped, increasing the population inversion.

When the cavity loss is then switched to low (high Q factor) as the gain is substantially higher than the loss, the output power rises exponentially. This saturates the gain medium, causing the power to decay and resulting in the formation of a pulse. By cycling the loss modulation, a train of short pulses is produced, as illustrated in Figure 2.3. The loss modulator can be an actively controlled device such as an electronic shutter or a passive element exhibiting intensity-dependent absorption, known as a saturable absorber (SA). Passive Q-switching eliminates the need for complicated electronic systems to drive the modulator, but the repetition rate and pulse duration of the laser are then power-dependent. Q-switched fiber lasers can typically produce microseconds to nanoseconds pulses at kHz repetition rates.

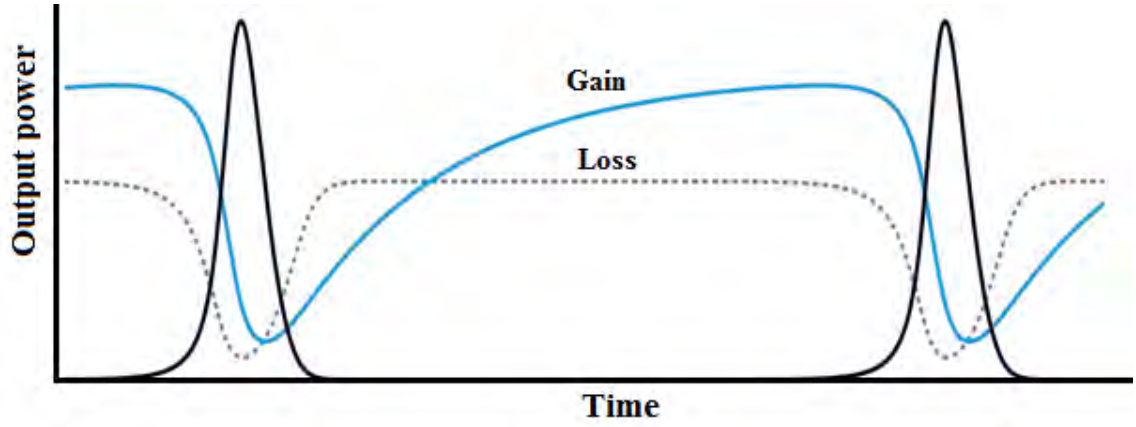

Figure 2.3: Evolution of Q-switched pulse formation, showing the modulation of the cavity gain and loss

2.5 Mode Locking Mechanism

Mode locking is a technique of generating laser pulses with ultrashort duration, particularly within the picoseconds and femtoseconds regimes. In a mode-locked laser, all the longitudinal modes of the cavity are locked to become in phase once every cavity round-trip time. The coherent interference of a large number of longitudinal modes spreading over a wide spectrum leads to a very short pulse formation at every round-trip time. The number of longitudinal modes that can be locked is related to the gain bandwidth of the laser active medium FWHM Δv_g and the frequency separation between adjacent longitudinal modes. Under sufficiently strong pumping, the number of modes oscillating in the cavity is given by

$$M = \frac{\Delta v_g}{c/2L} = \frac{2L}{c}\Delta v_g \tag{2.33}$$

where c is the speed of light and L is the length of a linear cavity. The shortest pulse duration that we can expect to achieve by the mode-locking mechanism is therefore

$$\tau_{min} = \tau_M = \frac{2L}{cM} = \frac{1}{v_g} \tag{2.34}$$

It is found that the shortest pulse duration we can achieve by mode locking is the reciprocal of gain bandwidth (in Hz) (Milonni, 2010).

Mode-locking involves periodic modulation of resonator loss. Once the resonator loss is modulated, all the laser modes phase can easily be fixed. Figure 2.4 shows the difference between continuous wave (*CW)* and mode-locked laser, in which electrical fields of five modes with random phase generated CW as shown in Figure 2.4 (a). On the other hand, when the modes with fixed phase are forced to lock together mode locking pulse train is generated as shown in Figure 2.4(b). Mode locking techniques can be classified as either active or passive mode locking. Active mode-locking can be achieved by applying an external signal to an optical loss modulator using the acousto-optic or electro-optic effect as shown in Figure 2.5. Such an electronically driven loss modulation produces a sinusoidal loss modulation with a period given by the cavity round-trip time T_R. The saturated gain at a steady state then only supports net gain around the minimum of the loss modulation and therefore only supports pulses that are significantly shorter than the cavity round-trip time. On the other hand, passive mode locking can be achieved by integrating an SA with suitable properties into the laser cavity as shown in figure 2.5. Such an absorber introduces some loss to the intra-cavity laser radiation, which is relatively large for low intensities but significantly smaller for a short pulse with high intensity. Generally, with passive mode-locking we can obtain much shorter pulses using SA, because the recovery time of the SA can be very fast, resulting in a fast loss modulation, while the active modulator is significantly slower due to its sinusoidal loss modulation.

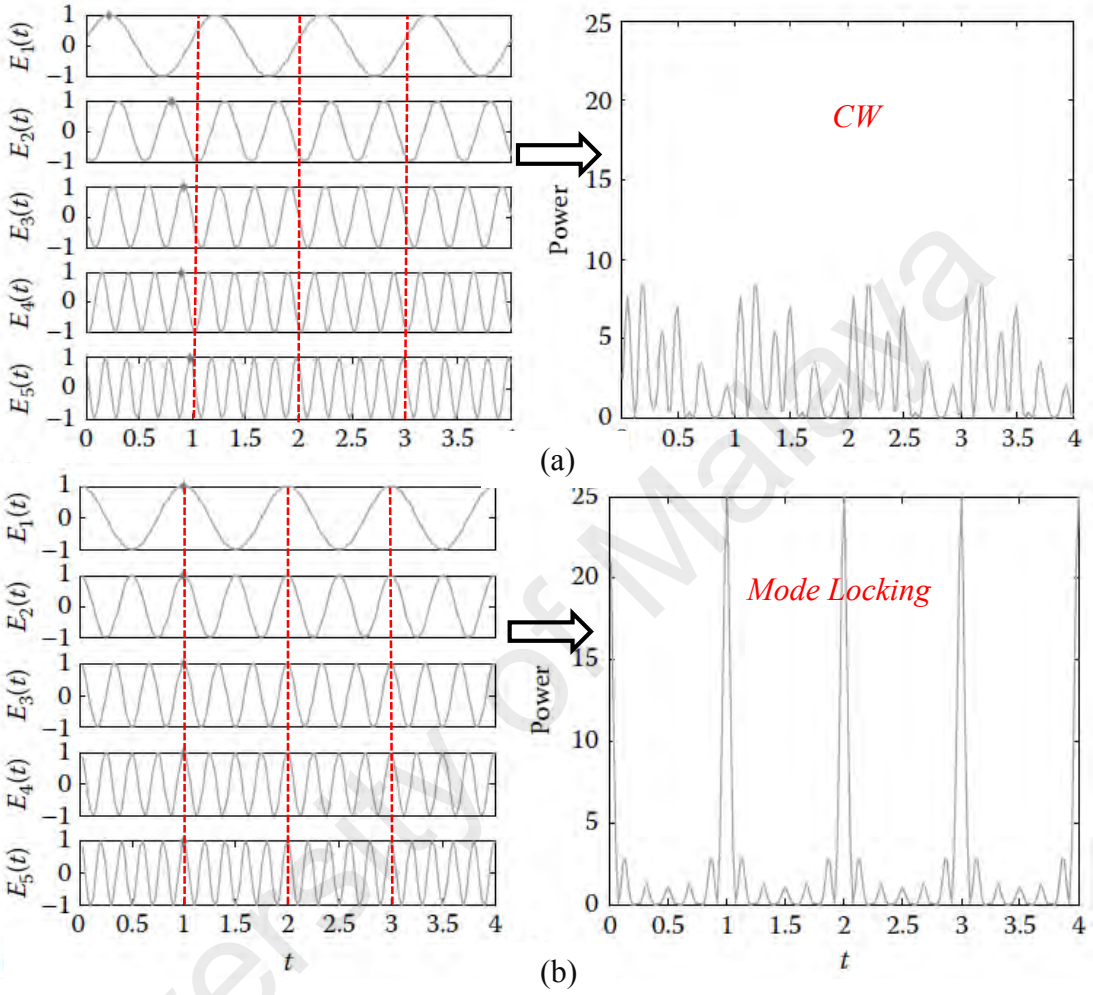

Figure 2.4: Plot of electric field amplitudes of five individual modes of randomly distributed phases and power of the total signal of a multi-longitudinal mode laser, (a) CW, (b) mode locking. (Ngo, 2010)

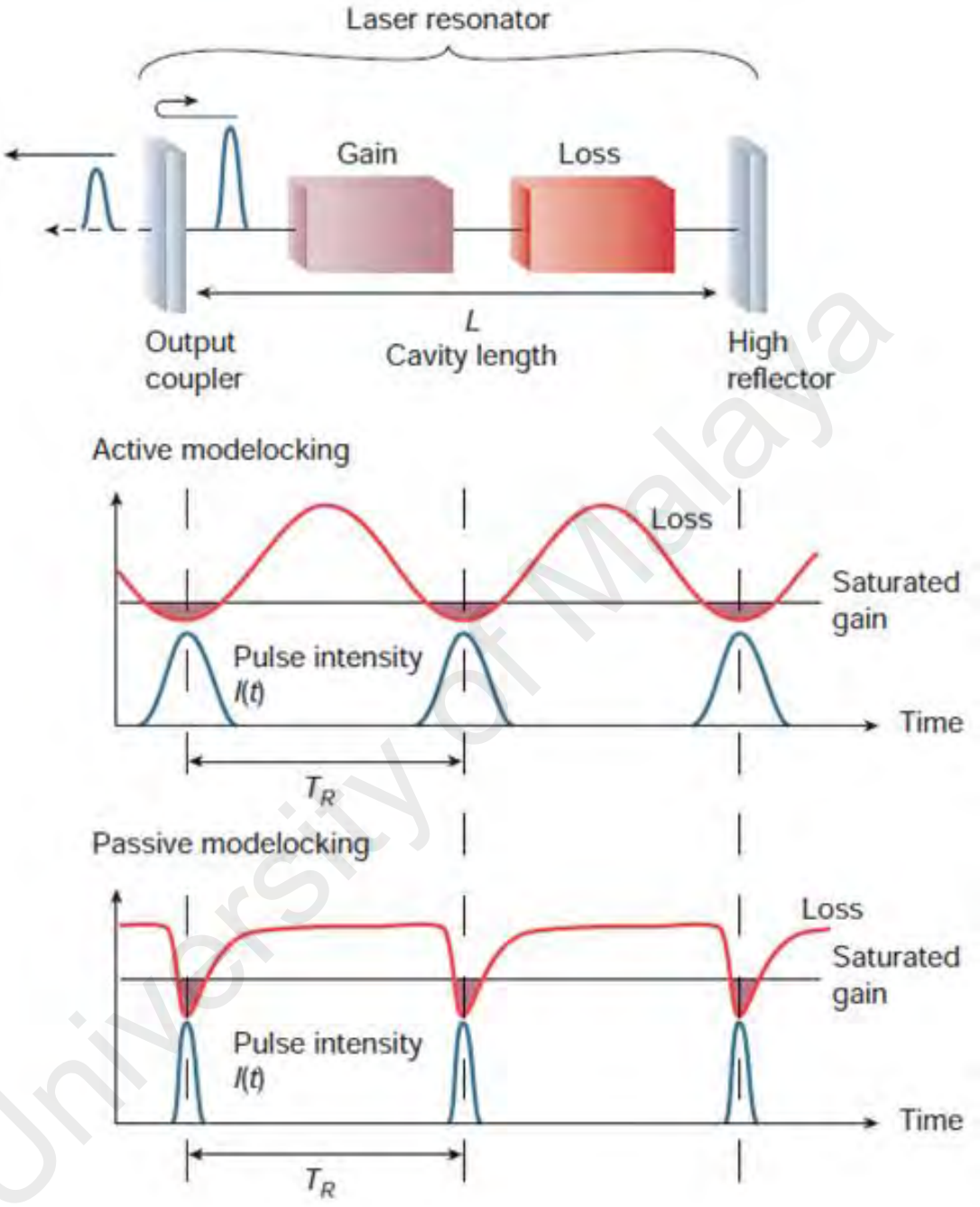

Figure 2.5: Schematic laser cavity setup for active and passive mode-locking (Keller, 2003)

Mode-locked pulses in time and frequency domains are shown in Figure 2.6. In the time domain, the mode-locked laser produces an equidistant pulse train, with a period defined by the round-trip time of a pulse inside the laser cavity T_R and a pulse duration τ_p (Keller, 2003). In the frequency domain, this results in a phase locked frequency comb with a constant mode spacing that is equal to the pulse repetition rate $v_R = 1/T_R$. The spectral width of the envelope of this frequency comb is inversely proportional to the pulse duration. The fundamental repetition rate of a mode lock laser is determined by its cavity length, as shown in the equations below.

$$\text{Repetition rate (for linear cavity)} = \frac{c}{2nL} \tag{2.35}$$

$$\text{Repetition rate (for ring cavity)} = \frac{c}{nL} \tag{2.36}$$

Equations (2.35) and (2.36) can be used to calculate the fundamental repetition rate for linear and ring cavity respectively. Here, *c, n* and *L* represent the speed of light, refractive index and length of the cavity respectively. As the round-trip time, T_R, is the inverse of repetition rate, therefore, T_R is

$$T_R = \frac{2nL \text{ (for linear cavity) or nL (for ring cavity)}}{c} \tag{2.37}$$

depending on the cavity type. Sometimes the repetition rate can be some integer multiple of the fundamental repetition rate. In this case, it is called harmonic mode locking (Becker et al., 1972).

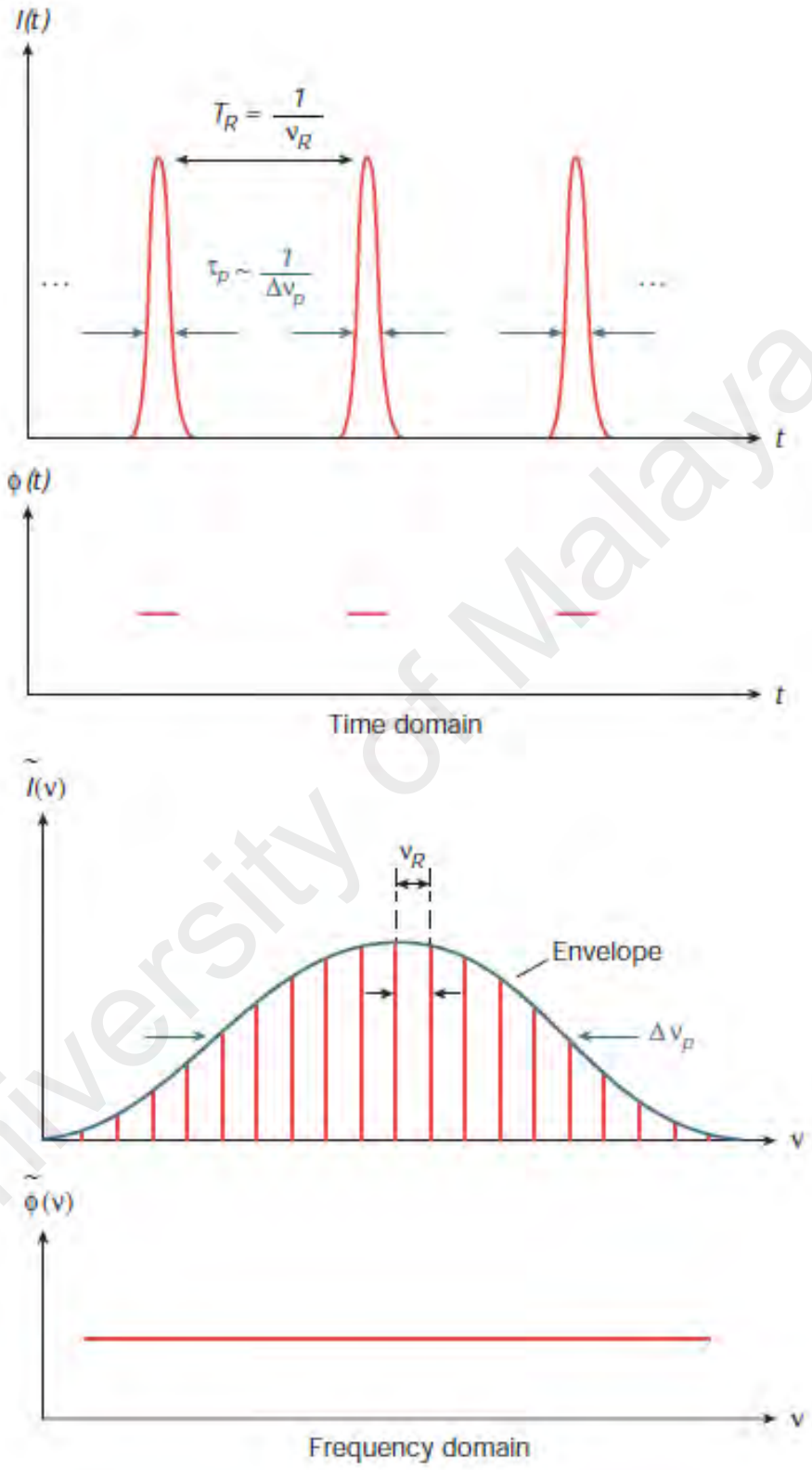

Figure 2.6: Mode-locked pulses in the time and frequency domain (Keller, 2003)

In general, the cavity dispersion and nonlinearity strongly influence the formation and steady-state characteristics of pulses generated in a mode-locked laser (De Silvestri et al., 1984), in addition to contributions from the spectral filtering effect of a finite gain bandwidth, gain saturation and loss (Woodward, 2015). Typically, the interplay between these effects has led to the categorization of laser operation into several distinct regimes as summarized in Figure 2.7, each with different intra-cavity dynamics and output properties.

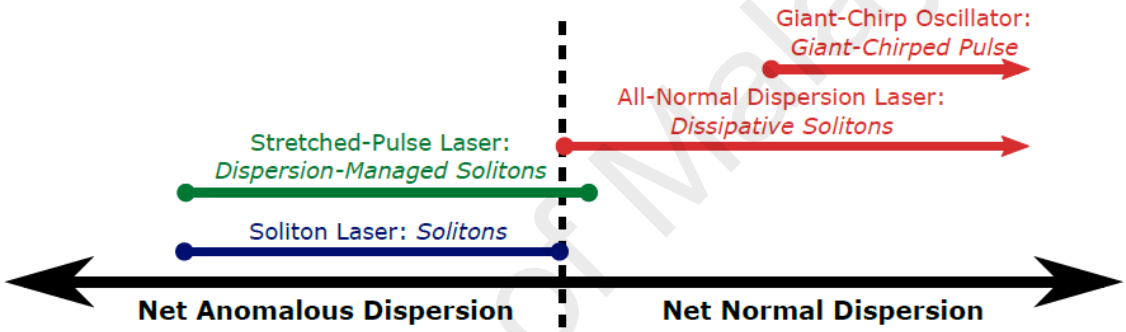

Figure 2.7: Illustration comparing different operating regimes of mode-locked fiber lasers with different dispersion maps, including the laser names and terms for describing the pulses they generate

2.5.1 Historical Perspective of Mode Locking

Mode-locking was first proposed theoretically in the mid-1960s (Lamb Jr, 1964), shortly followed by the first demonstration of active mode-locking using a HeNe laser (L Hargrove et al., 1964). Passively mode-locked lasers were also demonstrated soon after based on a ruby laser (Hans W Mocker et al., 1965), and an Nd:glass laser cavities (DeMaria et al., 1966). However, the development of passively mode-locked laser was plagued by the problem of self-Q-switching instabilities in solid-state lasers. This continued to be a problem for most of the passively mode-locked solid-state lasers until the first intra-cavity saturable absorber was designed correctly in 1992 to prevent self-Q-switching instabilities (U Keller et al., 1992). For some time, in the 1970s and 1980s, the

good progress in passively mode-locking using dye lasers had diverted research interest away from solid-state lasers. Q-switching instabilities are not a problem for dye lasers. The first passive mode-locked dye laser with subpicosecond was demonstrated in 1974 (Shank et al., 1974), followed by sub-100 fs in 1981 (Fork et al., 1981). Kerr lens mode locking of Ti:sapphire laser was discovered in 1991 to produce the shortest laser pulses (Spence et al., 1991; Sutter et al., 1999). In 1992, self-starting and stable passive mode locking was demonstrated for the first time using semiconductor saturable absorber mirrors (SESAMs) as a saturable absorber (U. Keller et al., 1992). Recently, carbon nanotubes and graphene have been used in passively mode-locked lasers as saturable absorbers (Bao et al., 2009; Set et al., 2004). They have the benefits of faster response times than SESAM and can be directly deposited on the fiber end. Further discussion of passive mode locking based on new nanomaterials as saturable absorbers will be presented in the next section.

2.5.2 Soliton Pulse Lasers

The term 'soliton' was introduced by Zabusky and Kruskal in 1965, which was originally used to refer to localized solutions of integrable nonlinear systems (Zabusky et al., 1965). Such solutions are extraordinary because solitons maintain their shape and velocity after interfering with each other, and remain in order when interacting with radiation waves. In optics, integrable conventional solitons result from the interplay between the dispersion and nonlinear effects (Grelu et al., 2012). Also, the word soliton refers to special kinds of wave packets that can propagate undistorted over long distances (GP Agrawal, 2007). Soliton pulses are largely shaped by the GVD and SPM. The saturable absorber does not need to be fast, only to initiate and stabilize the pulses against the broad continuum pulses (Dong et al., 2016). Soliton mode-locking operates in an anomalous dispersion regime with a hyperbolic secant ($sech^2$) intensity profile (Haus, 2000).

2.5.3 Stretched Pulse Lasers

There have been many studies on stretched pulse fiber lasers with periodic identical segments, where each segment consists of anomalous and normal dispersion fiber (Haus et al., 1995; Tamura et al., 1993). It was reported that a stable stretched pulse exists for net anomalous, zero, and small normal dispersion as shown in Figure 2.7. The pulse in the cavity broadens and recompresses during each round trip, so the cavity-averaged peak power is reduced. Therefore, the accumulated nonlinear phase shift is reduced and the pulse energy can be increased before the onset of multiple pulsing operations. These are referred as *dispersion-managed solitons* and by the nature of temporal, periodic 'pulse breathing' in the cavity, the output position from the cavity determines whether the pulses are chirped or transform-limited.

2.5.4 All Normal Dispersion Lasers

The mode-locking theory developed in 1992 predicted that stable mode locking can be achieved in the large normal dispersion regime (Haus et al., 1992). The resulting mode-locked pulses should be broad and strongly chirped. However, Procter et al. (Proctor et al., 1993) have demonstrated the first mode-locking operation in all normal dispersion regime based on a Ti:sapphire laser. The laser produced chirped pulses with sharp spectral edges. In 2006, a mode-locked fiber laser operating in normal-dispersion regime was demonstrated in a simple EDFL cavity consisting a spool of dispersion compensating fiber (DCF) with normal dispersion using a nonlinear polarization rotation mechanism as an artificial SA (Zhao et al., 2006). The resulting pulses are chirped with steep spectral edges. The role of the pulse shaping by spectral gain shape was identified to be responsible for the pulse shaping. In mode-locked fiber laser with normal dispersion regime, the intra-cavity pulse dynamics require dissipative (spectral filtering, gain, and loss) and conservative (dispersive and nonlinear) effects to stabilize the pulse, unlike anomalous dispersion soliton lasers which rely on a balance between dispersion and

nonlinearity alone. These pulses are known as *dissipative solitons* (Grelu et al., 2012). In this case, the interplay between dispersion and nonlinearity in addition to dissipative gain filtering and saturable absorber effects effectively compensate the nonlinear phase shift and stabilizing the pulse (Woodward, 2015).

2.6 Saturable Absorber

Saturable absorbers (SAs) are nonlinear optical devices that exhibit an intensity dependent transmission. The device highly absorbs lower intensity light and the absorption reduces at a higher intensity of light, and thus promoting pulses generation in a laser cavity. The nonlinear absorbers are widely deployed in Q-switched and mode-locked lasers to initiate self-starting and stable short pulse operation (Keller, 2003; M Zhang et al., 2014). The key parameters for SAs are its wavelength range, recovery time, saturation intensity, modulation depth and damage threshold (M Zhang et al., 2014). The absorption wavelength is defining the SA region of operation that has to be synchronized with the gain bandwidth of the corresponding lasing medium. Recovery time sets a limit on the switching speed of the device that can affect the duration of the achievable pulses. The required light intensity in the device to saturate the absorption is referred to the saturation intensity while modulation depth is defined as the maximum possible change of absorption. Damage threshold is the maximum light intensity that a device can tolerate before damage occurs. In addition to these parameters that controlling pulse dynamics, other characteristics are also important in choosing saturable absorbers such as the environmental stability and the ease and cost of fabrication.

2.6.1 Historical Evolution of Saturable Absorber

To date, various types of SAs with different parameters have been investigated and employed to achieve Q-switched and mode-locked lasers. The first demonstration of SA using rhodamine based organic dye was in 1965 by (Hans W. Mocker et al., 1965), which

achieved mode-locked with a pulse width of 10 ns. Figure 2.8 highlights the historical evolution of the SA technologies (RI Woodward et al., 2015). After the initial demonstrations of dyes based mode-locked pulses generation, there are not many developments on SA research until the semiconductor saturable absorber mirror (SESAM) was proposed in the early 1990's (U Keller et al., 1992; Keller et al., 1996). Then, SESAMs have quickly became a highly successful technology for ultrafast mode-locked fiber lasers due to their many advantages (Okhotnikov et al., 2004). However, SESAMs offer only a narrow operating bandwidth, costly to fabricate and require expensive clean room equipment and have low damage threshold and long recovery time. These limitations lead research into novel materials for SA photonics applications. Also, artificial techniques such as nonlinear-optical loop mirror (NOLM) (Doran et al., 1988), nonlinear-amplifying loop mirror (NALM) (Nakazawa et al., 1991) and nonlinear polarization rotation (NPR) (Ippen, 1994; AP Luo et al., 2011) had been widely used as artificial saturable absorbers for fiber lasers.

In the late 1990s, the field of nanomaterial SAs such as one-dimensional (1D) carbon nanotubes (CNTs) have attracted tremendous attention. The nonlinear optical characteristic of single-walled carbon nanotubes (SWCNTs) has also been reported (Kataura et al., 1999; Margulis et al., 1998). Since then, the CNTs with great potential applications have been attracting a considerable attention from the photonics research community. In 2004, (Set et al., 2004) had demonstrated the first mode-locked fiber laser based on SWCNTs. After that, CNTs have been considered as an excellent SAs for their low cost and easy fabrication, but their operating wavelength depends on the diameters of the nanotube (Zhou et al., 2010). Therefore, a strong aspiration to seek new high-performance of broadband operation and low-cost SAs such as graphene has always been at the high demand of laser experts.

Since the first demonstration of graphene based fiber lasers (Bao et al., 2009), graphene has been significantly improved as a promising SA for passive Q-switched and mode-locked fiber lasers (Popa et al., 2010; Sun, Hasan, Torrisi, et al., 2010). The achievement of graphene has greatly encouraged researchers to discover other graphene-like two dimensional (2D) nanomaterials for photonic applications (Bonaccorso et al., 2014). Recently, topological insulators (TIs) with indirect band-gap of 0.35 eV (Chen et al., 2009) and gapless surface states (Haijun Zhang et al., 2009), was extensively investigated as an effective SA for pulse generation in fiber lasers (Chen et al., 2013; Luo et al., 2013; Zhao et al., 2012), but has again the drawback of complicated preparation process (compound with two different elements), which limits its applications in photonics.

Lately, transition-metal dichalcogenides (TMD) like ($MoSe_2$, WSe_2, MoS_2, WS_2) (B Chen et al., 2015; H Li et al., 2015; D Mao et al., 2016; Wang et al., 2013; Robert I. Woodward et al., 2014; H. Zhang et al., 2014), and black phosphorus (BP) (Y Chen et al., 2015; Sotor, Sobon, Macherzynski, et al., 2015; F Xia et al., 2014) have been exploited as SAs for fiber laser applications. In contrast to graphene, which is a semi-metal with zero band-gap, MoS_2 has thickness dependent band-gap (indirect band-gap of 1.29 eV for bulk layers; direct band-gap of 1.9 eV for monolayer) (Wang et al., 2014) and BP has direct band-gap tunable with the number of layer from ~1.5 eV for monolayer to ~0.3 eV for bulk black phosphorus (Tran et al., 2014), which fill up the gap between semi-metallic graphene and wide band-gap TMDs as shown in Table 2.1.

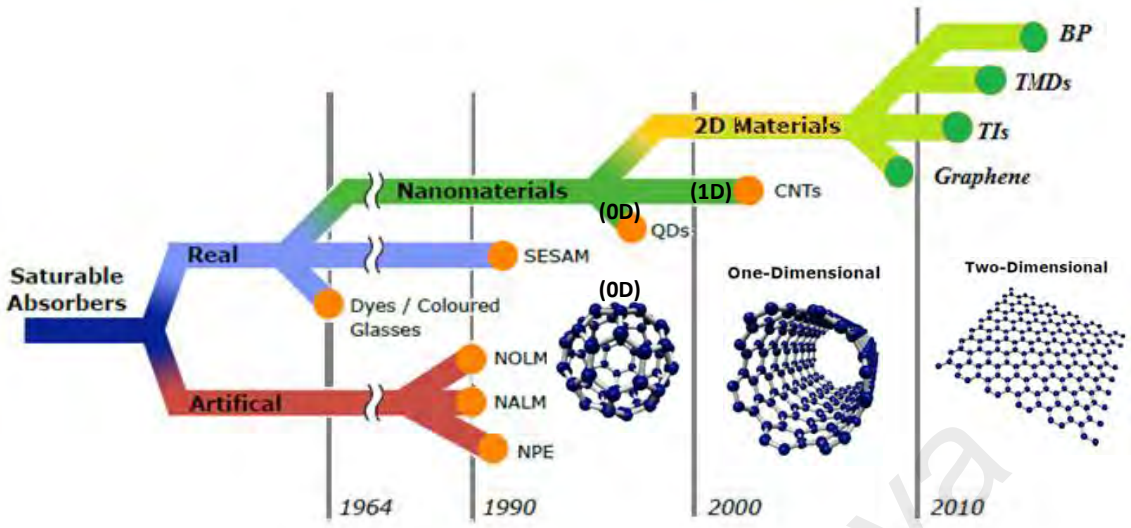

Figure 2.8: The evolution of saturable absorber technologies for fiber lasers; Inset figures show the illustration of atomic arrangements in 0D, 1D, and 2D nanomaterials

Table 2. 1: Summary of the Band Gaps of Typical Layered 2D Nanomaterials

	Materials	Graphene (M Xu et al., 2013)	MoS_2 (R. I. Woodward et al., 2014)	Black Phosphorus (BP) (Churchill et al., 2014)
Bandgap (eV)	**Monolayer**	0	~1.90(direct)	1.5
	Bulk	0	1.29(indirect)	0.3

2.6.2 Two Dimensional (2D) Nanomaterials

The term *nanomaterial* was introduced in the 1970s to describe the low-dimensional nanomaterials structures with size-dependent properties. There are many layered nanomaterials with strong in plan chemical bonds and weak coupling between the layers. The structure of these layers provides the opportunity to be cleaved into individual

freestanding atomic layers. These layers with one dimension precisely restricted to a single layer are called 2D nanomaterial (Gupta et al., 2015). Recently, the fabrication of 2D nanomaterial has become an important field in current materials research due to their physicochemical properties, which are different from the bulk counterpart. Mainly, 2D nanomaterials with certain geometry show unique shape-dependent features and successful applications in nanoelectronic devices (Kim et al., 2009). Also, 2D nanomaterials are developing innovative applications in electronics and optoelectronics (Wang et al., 2012). To this day, 'new' nanomaterials are emerging by exfoliating few-layer forms of existing materials and nanomaterial-enabled optical systems are beginning to transition from laboratories to commercial products. In this section, the fundamental optical properties, production methods and optical characterization methods of three types of 2D nanomaterials will be discussed.

2.6.2.1 Optical Properties of Graphene

Graphene is a single atomic layer of graphite, which was first postulated in 1947 (Wallace, 1947) and poor quality graphene was produced in 1962 (Boehm et al., 1962). Later, high-quality graphene was rediscovered and characterized in 2004 by Konstantin Novoselov and Andre Geim (Novoselov et al., 2004), who was awarded the Nobel Prize for their "groundbreaking experiments regarding the two-dimensional material graphene" (A Geim et al., 2007). Graphene is a two dimensional (2D), a flat monolayer of sp^2 hybridized carbon atoms, arranged in a hexagonal lattice, also known as honeycomb lattice. A 2D graphene can be wrapped up into 0D fullerenes, rolled into 1D nanotubes or stacked into 3D graphite (Figure 2.9).

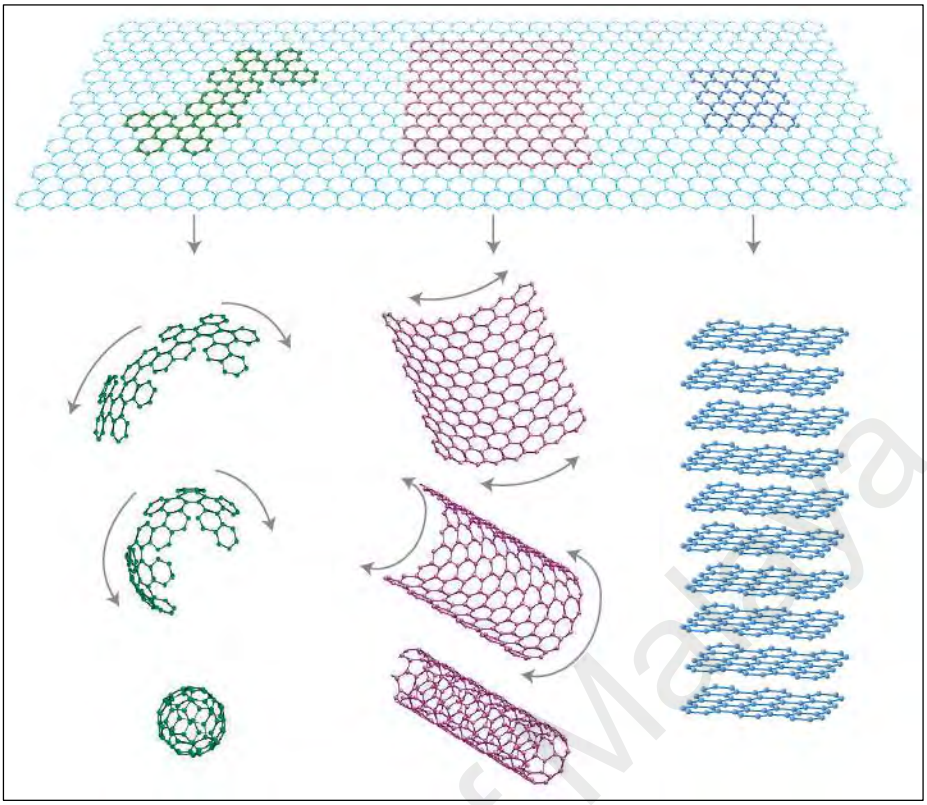

Figure 2.9: Carbon allotropes of graphene: 0D fullerenes, 1D nanotubes and 3D graphite (AK Geim et al., 2007)

The properties of graphene are very unusual (Novoselov, 2011). It was the first example of 2D atomic crystals, which demonstrates unique electronic properties and has promise for many of applications. Also, graphene shows unique and unusual optical properties (Yamashita, 2012). For example, graphene can absorb ~2.3% of incident white light, despite being only a single atom thick (~0.3 nm) (Amos Martinez et al., 2013). The transmittance of a single layer graphene is calculated to be

$$T = (1 - 0.5\pi\alpha)^{-2} \approx 1 - \pi\alpha \approx 97.7\% \qquad (2.38)$$

where $\alpha = e^2/\hbar c \approx 1/137$ is the fine-structure constant. ħ is Plank constant, c is the speed of light and e is the electron charge (Nair et al., 2008). The optical absorption of few-layer graphene is proportional to the number of layers, for each layer absorbing $A \approx 1 - T \approx \pi\alpha \approx 2.3\%$ over the visible spectrum (Nair et al., 2008) (refer to Figure 2.10

(a)). Because of the linear dispersion relation of graphene, graphene absorption is independent of wavelength (refer to Figure 2.10(b)) (Bonaccorso et al., 2010; Yamashita, 2012). In the figure the slightly lower transmittance for $\lambda < 500$ nm is probably due to hydrocarbon contamination. The red line is the transmittance expected for two-dimensional Dirac fermions, whereas the green curve takes into account a nonlinearity and triangular warping of graphene's electronics spectrum. The grey area indicates the standard error of the measurement.

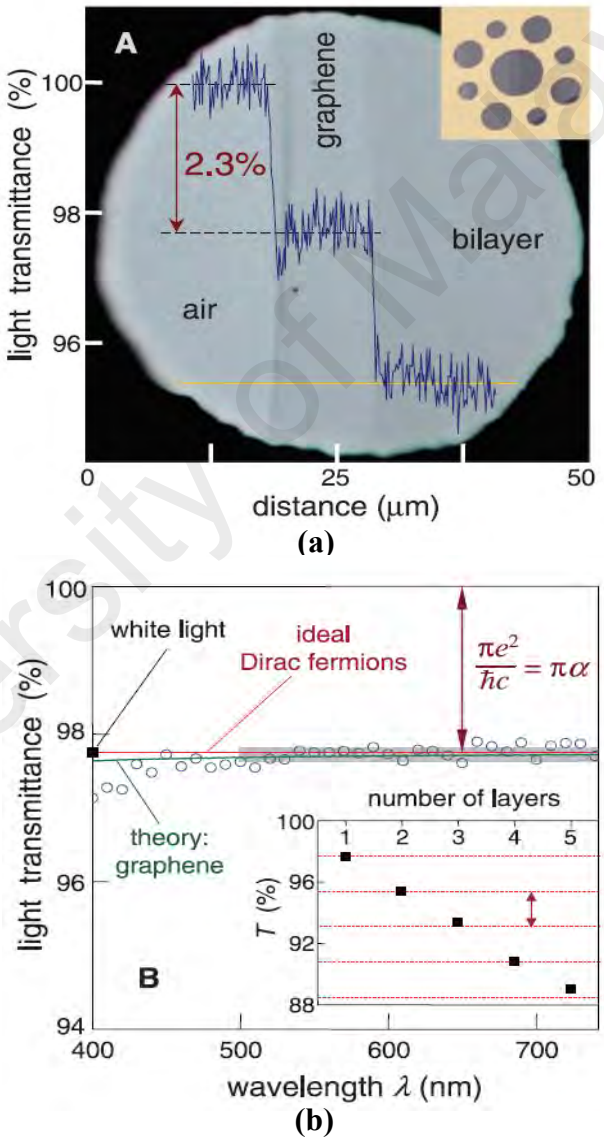

Figure 2.10: The optical properties of graphene. (a) Light transmittance percentage according to graphene layers (inset: sample design), (b) Transmittance spectrum of single-layer graphene (open circles). (Inset) Transmittance of white light as a function of the number of graphene layers (square) (Nair et al., 2008)

Interband excitation in graphene by ultrafast optical pulses produces a non-equilibrium carrier population in the valence and conduction bands. Saturable absorption is observed as a consequence of Pauli blocking. Ultrafast responses down to 100 fs can be observed by different relaxation channels in time-resolved experiments (Bonaccorso et al., 2010). The linear dispersion of the Dirac electrons ensures that, for any excitation, there will always be an electron-hole pair in resonance. As shown in Figure 2.11(a), a few photons can be absorbed by the excitation of the electrons from lower Dirac cone (valence band) to upper one (conduction band). These Dirac-fermions lose energy by coupling with π-plasmons and two-dimensional (2D) phonons in the graphene sheet, thereby the "cooling down" satisfies Fermi-Dirac distribution of the excited carriers in the energy band structure (Castro Neto, 2007). However, as the number of photon increases, the generated carriers fill the energy states to a degree that more electron excitation is not allowed by Pauli blocking of occupying carriers at the edge of the filled band (see Figure 2.11(b)), consequently, the subsequent photons with the specific wavelength can penetrate the graphene layer with no more absorption. Thus, graphene is an ultrafast and ultra-wideband SA material for ultrafast pulse generation. As shown in the figure the energy band structure can be described with Dirac cones in the space formed with 2D momentum plane and energy axis. D(e) is the density of electrons acquired the combination of the Fermi-Dirac distribution function and density of states. The gray areas represent the filled states.

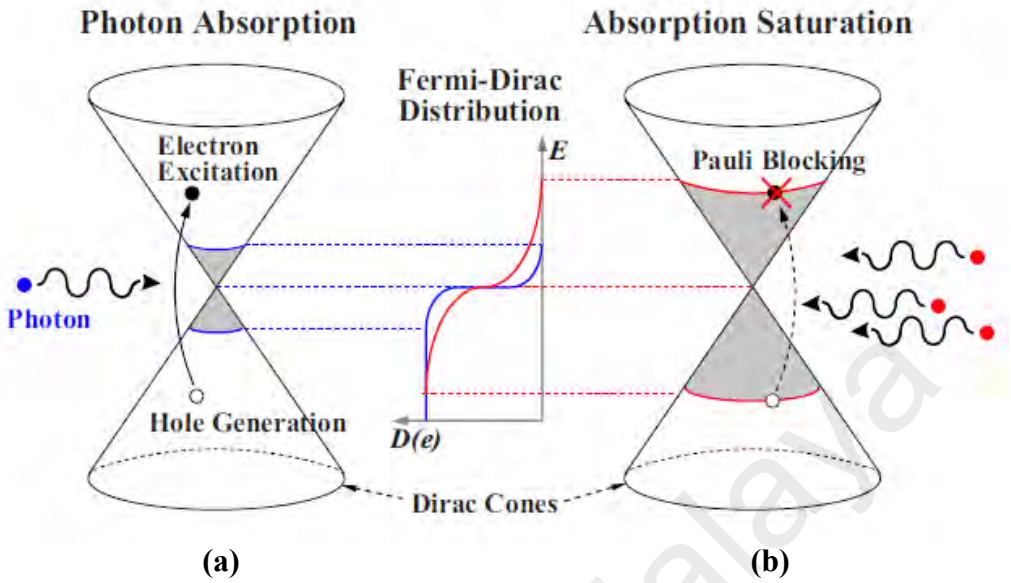

Figure 2.11: Illustration of (a) linear photon absorption and (b) nonlinear saturable absorption in graphene with a point band gap structure. (Song et al., 2010)

2.6.2.2 Optical Properties of MoS_2

Transition metal dichalcogenides (TMDs) are layered nanomaterials with the formula MX_2 stoichiometry (Wilson et al., 1969), where M is a transition metal atom (e.g., Mo, W) and X is a chalcogen atom (e.g., S, Se) (Wang et al., 2012). These nanomaterials form layered structures of the form X-M-X, with the transition metal atoms held between two hexagonal planes of chalcogen atoms by strong covalent bonds (refer to Figure 2.12 (a)). TMDs can either be semiconducting or metallic in nature depending on the coordination and oxidation states of the transition metal atoms (Wang et al., 2012). In bulk form, individual MX_2 layers are held together by relatively weak van der Waals forces (Wilson et al., 1969), which have enabled monolayer and few-layer flakes of TMDs to be exfoliated. Recently TMDs have attracted a great deal of attention, due to their layer-dependent properties. For example, in several semiconducting TMDs there is a range from an indirect bandgap in the bulk to a direct gap in the monolayer: for

molybdenum disulfide (MoS_2) the bulk indirect bandgap of 1.29 eV increases to a direct bandgap of 1.9 eV in monolayer form (refer to Table 2.1). The monolayer MoS_2 direct bandgap also results in photoluminescence, which opens the possibility of many optoelectronic applications (Wang et al., 2012).

Recently, MoS_2 has received particular attention due to its layer-dependent optoelectronic properties (Ganatra et al., 2014). Also, the favorable optoelectronic properties of monolayer and few-layer MoS_2 have been highlighted by recent studies including strong photoluminescence in monolayers (Splendiani et al., 2010), and a nonlinear optical response stronger than that of graphene (Wang et al., 2013), which paving the way for the development of new photonic devices such as SAs for pulsed laser technology.

The first report of monolayer MoS_2 and observation of their thickness-dependent properties highlighted in the literature many decades before the graphene-led revival in the 2D material (AK Geim et al., 2007). Earlier, optical properties of thin MoS_2 crystals (<10 nm thick) have been studied by Frindt and Yoffe, where they acknowledged new features in the absorption spectrum of few-layer MoS_2 flakes using mechanically exfoliated with adhesive tape (Frindt et al., 1963). Also, determination of single layer exfoliation using lithium-based intercalation techniques were published (Joensen et al., 1986). However, early studies were limited by the equipment and characterization techniques that would not encounter recent standards for imaging single and few atomic layers, neither the nonlinear optical properties of few-layer MoS_2 nor the technological benefits were exploited. In 2010, Mak *et al.* (Mak et al., 2010) and Splendiani *et al.* (Splendiani et al., 2010) individually discovered the transition in MoS_2 indirect to direct bandgap, when they varying the thickness from bulk to monolayer. Thus, the significant bandgap of the monolayer (1.9 eV) makes MoS_2 a better choice for photonics devices

more than graphene zero bandgap. In 2012, the valley selective optical excitation and luminescence in monolayer MoS_2 have been reported (Mak et al., 2012). Also, the measurements of the stiffness and breaking strength of monolayer MoS_2 have been reported (Bertolazzi et al., 2011).

A variety of production techniques are being employed to produce monolayer and few-layer MoS_2 flakes, consummated by a range of flexible integration platforms for including flakes in practical devices for target applications (Wang et al., 2012). Techniques like mechanical exfoliation (Frindt, 1965), chemical vapor deposition (CVD) (Zhan et al., 2012), pulsed laser deposition (PLD) (Wang et al., 2014), and liquid phase exfoliation (LPE) (Coleman et al., 2011), have been used to achieve MoS_2 films.

To understand the optical properties of MoS_2, it is necessary to consider the role of excitons (Woodward, 2015). In a semiconductor, photoexcitation places an electron into the conduction band, leaving a hole in the valence band. The attraction force between the electron and hole can create a bound-state quasiparticle known as an exciton. If the electron-hole interaction is weak (e.g. due to long-distance separation or dielectric screening) or if the photoexcitation energy is great, this attraction can be overcome, resulting in free carriers (unbound electrons and holes). Therefore excitons can be considered as the lowest energy electronic excitation in a semiconductor: the energy required to create an exciton by optical absorption is less than the threshold for creating free carriers. Hence, excitons can be represented as an energy level just below the conduction band as shown in Figure 2.12(b). This leads to two definitions of the bandgap: the electronic bandgap (or transport bandgap) Eg, which defines the energy needed to inject free electrons and holes into the material, and the optical bandgap Eo, which is the required energy for a photon to be absorbed. The energy difference is known as the exciton binding energy: $E_b = E_g - E_o$ (Kasap et al., 2006).

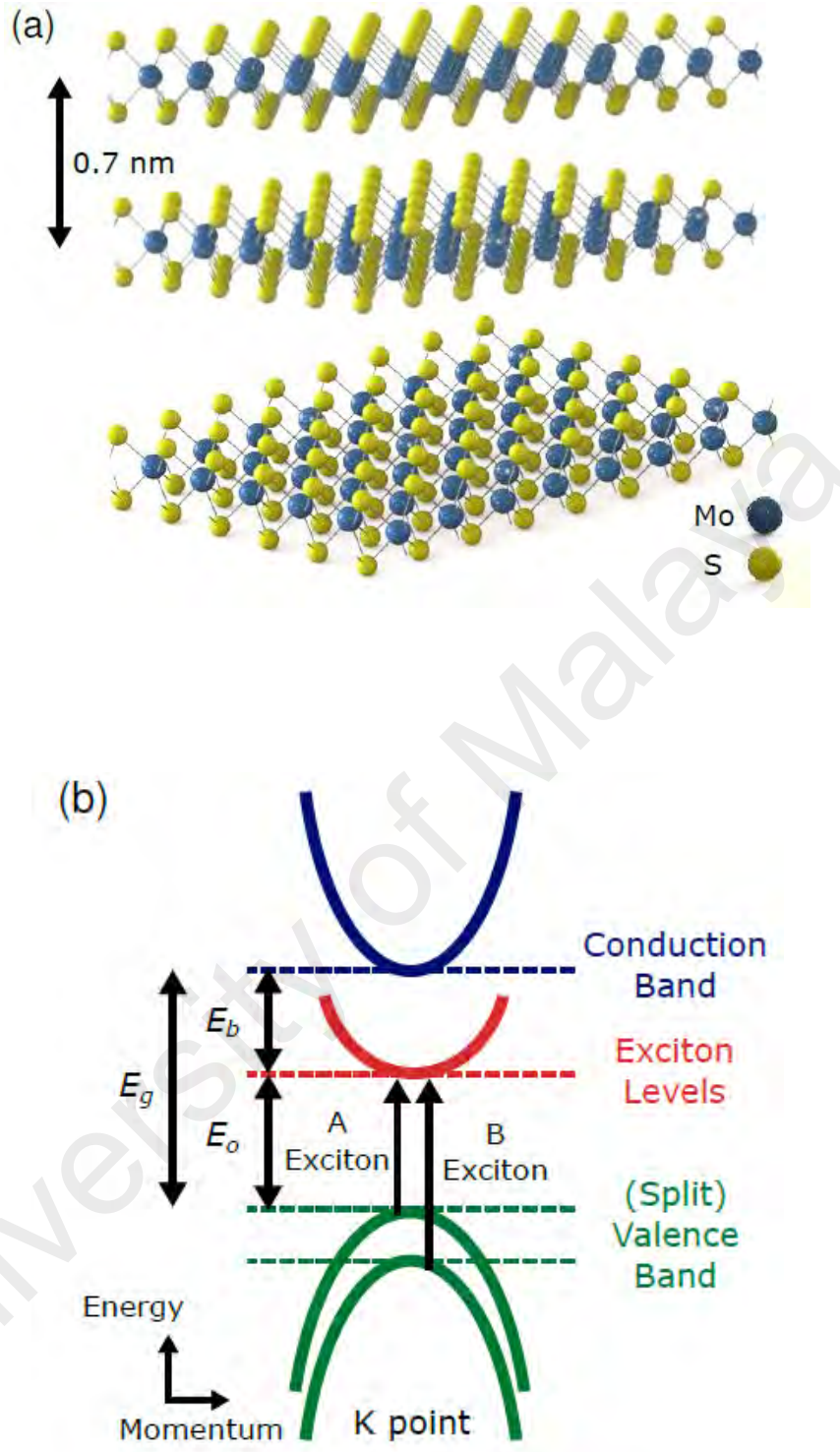

Figure 2.12: MoS_2 structure: (a) Visualization of three-layer MoS_2; (b) Simplified energy structure for monolayer MoS_2 showing the relationship between the electronic bandgap E_g, the excitonic binding energy E_b and the optical bandgap E_o (Woodward, 2015)

2.6.2.3 Optical Properties of Black Phosphorus

Black phosphorus (BP) is a single-elemental layered crystalline material consisting of only phosphorus atoms arranged in a puckered honeycomb lattice, where each phosphorus atom is bonded with three neighboring atoms through sp^3 hybridized orbitals, unlike the sp^2 hybridized carbon atoms in graphene, as shown in Figure 2.13 (Druffel, 1997), where the corresponding x, y, and z directions are indicated in both (a) and (b). x and y correspond to the armchair and zigzag directions of BP, respectively. Recently, BP has been rediscovered as a new and interesting two-dimensional nanomaterial due to its unique electronic and optical properties (F Xia et al., 2014). In contrast to graphene and TMDs, BP has its own unique properties (Churchill et al., 2014). For example, its direct electronic band gap can be tuned from ~0.3 to ~2 eV (corresponding to the wavelength range from ~4 to ~0.6 μ m), depending on the film thickness (Low et al., 2014; Tran et al., 2014). This is particularly interesting for photonics, as it can offer a broadly tunable bandgap with a number of layers for the near and mid-infrared photonics and optoelectronics, and thus bridge the present gap between the zero bandgap graphene and the relatively large band-gap TMDs (Ling et al., 2015).

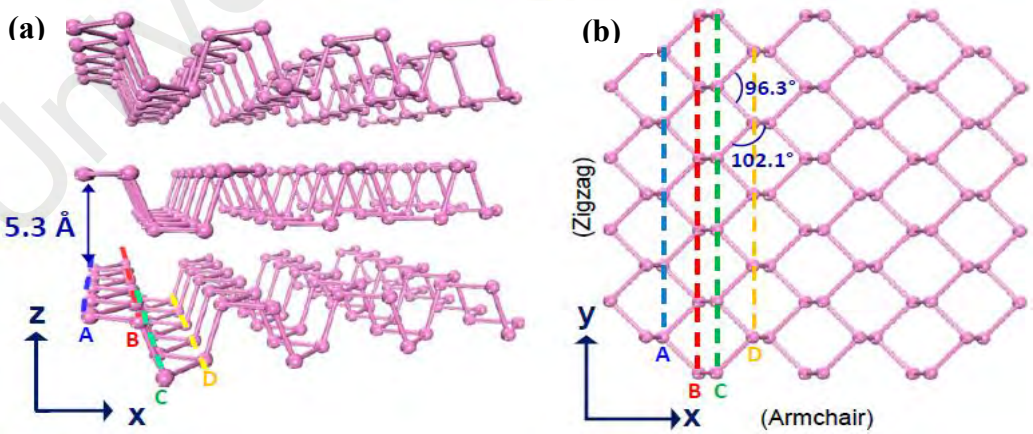

Figure 2.13: Crystal structure and band structure of BP. (a) Side view of the BP crystal lattice. The interlayer spacing is 0.53 nm. (b) Top view of the lattice of single-layer BP. The bond angles are shown. (Ling et al., 2015)

Early work on BP can be traced back to the first decade of the last century (Bridgman, 1914). In 1946, Bridgman was awarded the Nobel Prize for "the invention of an apparatus to produce extremely high pressures, as well as the discoveries he made therewith in the field of high pressure physics". The research on fundamental physical properties of bulk BP has made steady progress in the decades that followed, including the study of crystal structures (Jamieson, 1963) and electrical transport and optical properties (Warschauer, 1963), optical phonon (Ikezawa et al., 1983), and superconducting properties (Wittig et al., 1968). In the 1980s, a significant portion of work was performed by a few Japanese groups that reported a series of key results on BP's fundamental characteristics, including electrical and optical properties (Morita, 1986). However, these early research on BP as a bulk material did not attract much attention from the semiconductor research community, due to the dominant role of silicon at that time. Until 2014, stimulated by the successful studies of graphene and few-layer TMDs, BP has been rediscovered from the perspective of 2D nanomaterials. The BP research has mainly focused on the material in its monolayer and few-layer, where new properties and novel applications have arisen and may be developed.

Then a few reports experimentally demonstrated the optical properties of BP thin films in the visible and near-IR range. Mao et al. measured the reflection spectra of thin BP samples in the visible regime (450–800 nm) (N Mao et al., 2016), where they found that optical anisotropy in the thin samples is less pronounced, which agrees well with the theoretical simulation (Low et al., 2014). The static characteristic of BP's saturable absorption was first studied by Li et al., which measured the nonlinear absorption under a power amplified ultrafast 1550 nm fiber laser (D Li et al., 2015). The authors summarized the transmittance changes for BP simples with different thickness as a function of input light pulse fluence as shown in Figures 2.14 (a) and (b). As shown in both figures, a clear nonlinear increased absorption is observed when incident light

fluence is larger than ~100 μJ/cm^2. Due to the layer-number-tunable anisotropic band structure, BP also exhibits strong polarization and thickness-dependent nonlinear absorption properties. On the one hand, absorption displays a maximum value for incident light polarized along the x-direction (about 3 times higher than that along the y-direction in the reported paper). On the other hand, thicker samples present higher relative transmittance change than the thinner ones. All of these dependencies suggest the desired tunability of saturable absorption for potential applications.

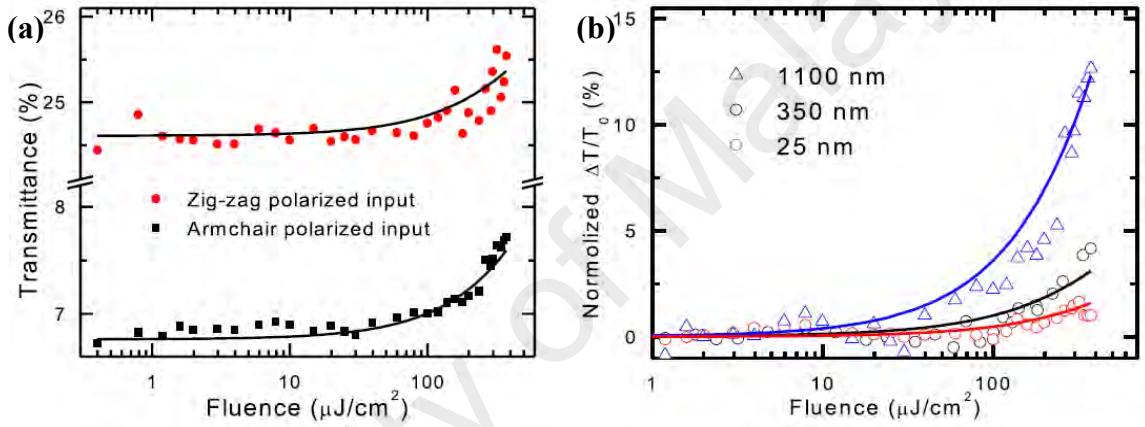

Figure 2.14: (a) Fluence-dependent transmittance of the 1100 nm thick BP film measured with ultrafast pulses at two orthogonal polarized light directions. (b) Relative transmittance change measured from 25-, 350-, and 1100-nm-thick BP films as a function of input pulse fluence. (D Li et al., 2015)

2.6.2.4 Nanomaterials Production Methods

Several production methods exist for obtaining monolayer and few-layer graphene and 2D nanomaterials (Bonaccorso et al., 2012). Among these methods, mechanical exfoliation (ME) and liquid-phase exfoliation (LPE) are purely physical without chemical reactions involved in the fabrication, while others are a chemical such as chemical vapor deposition (CVD). In this subsection, three types of fabrication methods will be discussed.

Mechanical Exfoliation

Mechanical exfoliation is a technique which adopts scotch tape to peel and obtain monolayer or few-layer materials from bulk materials. This technique was first used to exfoliate graphite flakes into single layer graphene by Geim and Novoselov in 2004 (Novoselov et al., 2004) as illustrated in Figure 2.15(a). Mechanical exfoliation technique is easy to carry out and straightforward to obtain only monolayer or few-layer 2D nanomaterials with high completeness and fewer defects, which well maintain the crystal structure and properties. This technique will be used in this thesis to obtain other 2D nanomaterials such as MoS_2 and black phosphorus.

Liquid-Phase Exfoliation

Liquid phase exfoliation (LPE) uses high-strength ultrasound to generate forces in the 2D materials to break the van der Waals force between layers as illustrated in Figure 2.15(b). LPE process generally involves three steps: 1) dispersion of material in a solvent; 2) exfoliation; 3) "purification" (Bonaccorso et al., 2012). In the third step, the exfoliated layered nanosheets separate from un-exfoliated flakes by applying centrifugation after sonication. The un-exfoliated flakes will fall down to the bottom in the dispersions and the nanosheets suspended on the top can be collected. The number of exfoliated layers nanosheets can be roughly controlled by adjusting the time and strength of sonication and centrifugation process. LPE is a simple and low-cost method to produce large amounts of monolayer and few-layer 2D nanomaterials and no post-processing is required compared with chemical solution processing method (Bonaccorso et al., 2012). In this work, this technique will be used to fabricate a free-standing few-layer MoS_2 polymer composite film from pristine MoS_2 crystals.

Chemical Vapor Deposition

Chemical vapor deposition (CVD) is a high-temperature chemical synthesis process by which the desired material is deposited or grown on the substrate as illustrated in Figure 2.15 (c). There are many different types of CVD processes: thermal, plasma enhanced (PECVD), cold wall, hot wall, reactive, and many more. Compared with LPE method, the number of layers of 2D nanomaterials produced by CVD can be controlled with good accuracy by modifying reaction parameters (H Xia et al., 2014). High yields make this method the main method to synthesize commercially available 2D materials. However, cost and process complexity might be high.

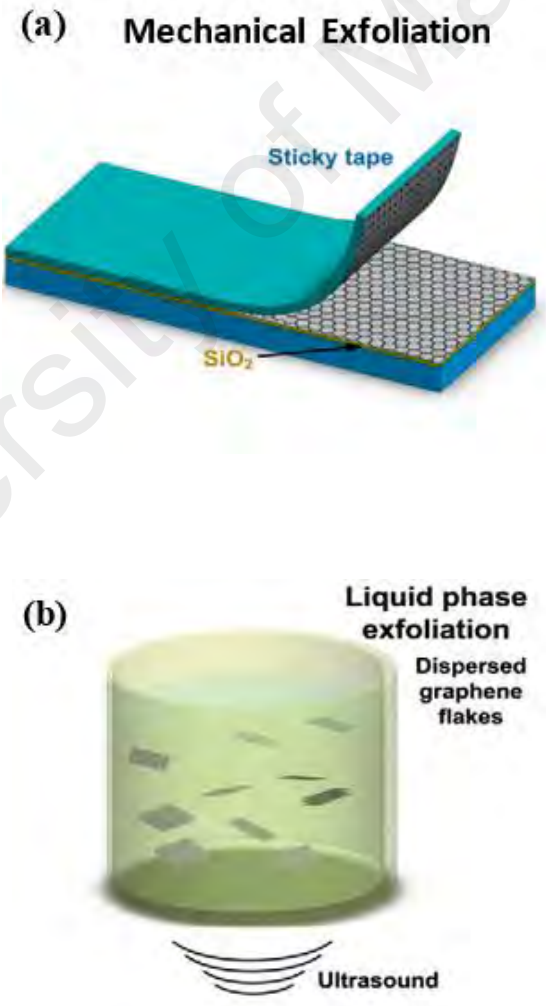

Figure 2.15: Schematic illustration of the main graphene production techniques. (a) Mechanical exfoliation, (b) Liquid phase exfoliation, (c) Chemical vapor deposition (Bonaccorso et al., 2012)

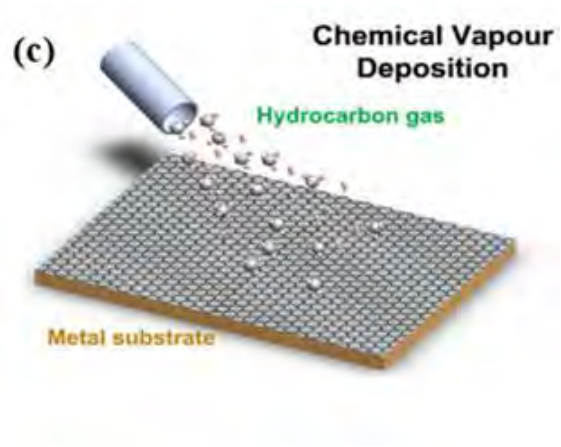

Figure 2.15, continued

2.6.2.5 Optical Characterization Methods

This section will give an overview of the characterization techniques adopted in this work, namely field emission scanning electron microscopy (FESEM), Raman spectroscopy and nonlinear optical absorption.

FESEM is a very useful tool for high-resolution surface imaging in the fields of nanomaterials science. It provides topographical and elemental information with the virtually unlimited depth of field of nanomaterials. Compared to the scanning electron microscopy (SEM), FESEM produces clearer and less electrostatically distorted images with spatial resolution down to 1 nanometer. Also, FESEM has the ability to examine smaller area contamination spots at electron accelerating voltages compatible with energy dispersive spectroscopy (EDS).

Raman spectroscopy is a spectroscopic technique used to determine the molecular structures of the materials. The technique involves light source (i.e. laser with suitable intensity) on the material sample, molecular structures vibrating in a certain mode absorb the corresponding energy from the incident photons and emit new photons with lower energy. The energy difference or frequency shift between the incident photons and newly

emitted photons indicate the information of molecular structures (Wu et al., 2017). Different vibration modes relate to the various frequency shift. For some 2D nanomaterials such as TMDs and black phosphorus, the separation between the peaks on the Raman spectrum is related to the layer structure and consequently can be used to estimate the number of layers.

Nonlinear absorption is related to the imaginary part of $\chi^{(3)}$ in Eq (2.8). Many effects can result in saturable absorption. The origin of saturable absorption for 2D is usually believed to be Pauli blocking (Bao et al., 2009). The absorption spectrum and recovery time are two of the parameters that must be considered when choosing an SA. The remaining key parameters can be seen in the SA model equation:

$$\alpha(I) = \frac{\alpha_s}{1 + I/I_{sat}} + \alpha_{ns} \tag{2.39}$$

where *α (I)* represents the absorption of the input light, α_s is the modulation depth, *I* is the input intensity of the incident light, I_{sat} is the saturation intensity, and α_{ns} is the non-saturable absorption. From this equation, the performance of the SA at a given wavelength can be calculated; the α_s indicates the maximum percentage of absorption that can be 'bleached' under high optical intensities; the α_{ns} indicates the extra linear losses of the SA; and I_{sat} indicates the optical intensity required to reduce the total optical absorption to half of the available modulation depth, thus indicating the input optical intensities required to kick-start the bleaching process (A. Martinez et al., 2013). The saturation intensity is described as the following equation:

$$I_{sat} = \frac{h\nu}{\sigma\tau} \tag{2.40}$$

where $h\nu$ is the photon energy, σ is the absorption cross section from ground state to upper state and τ is the recovery time. Recovery time is the return of the atom population

to the ground state. A typical saturable absorption curve calculated with the use of SA model equation is plotted in Figure 2.16 together with indicated parameters. Preferably a SA would have a large modulation depth, low non-saturable absorption and low saturation intensity.

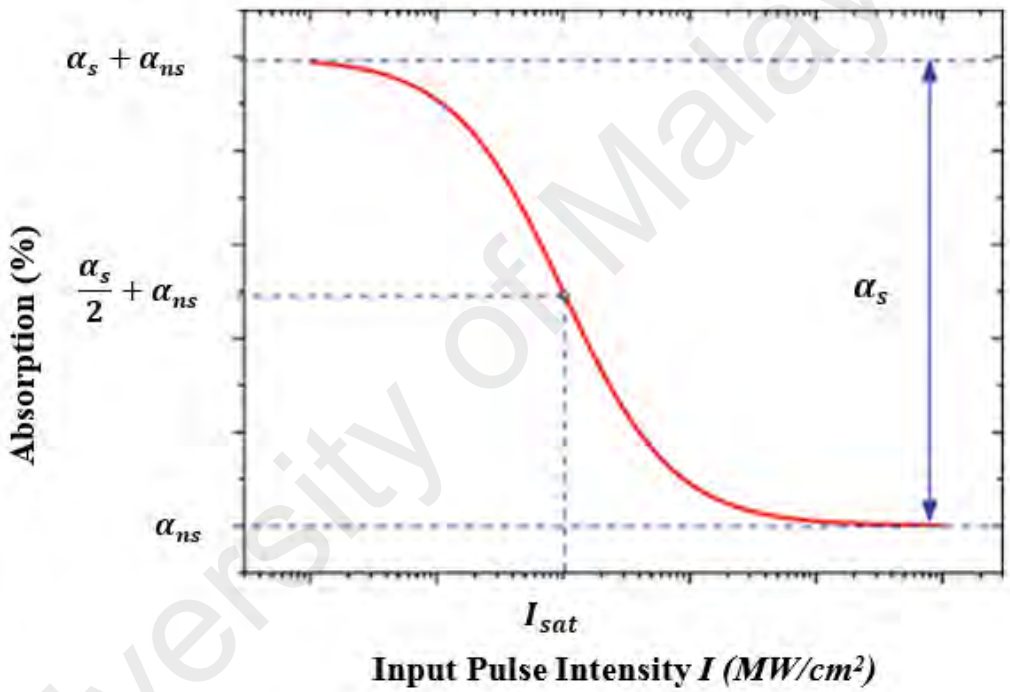

Figure 2.16: Theoretical saturable absorption curve indicated three main parameters of an SA (Sobon, 2016)

2.7 Important Parameters of Pulsed Laser

This section discusses the special parameters of ultrafast fiber laser pulses that are unique and that make them especially useful for a number of applications.

2.7.1 Spectral Bandwidth

Broad spectral bandwidth is an essential property for ultrashort laser pulses. Since the laser was invented, the high spectral purity and extremely narrow spectral linewidths are being the properties that enable lasers to do so many new things that cannot be done with more conventional light sources and considered as the hallmarks of laser technology (Fermann et al., 2002). Not many pulsed lasers applications rely strictly on bandwidth. Usually, the requirement for broad bandwidth occurs in combination with some other desired property. There have been demonstrations of the use of the broad bandwidth of femtosecond lasers for optical communications. For example, ultrafast lasers may well provide an economical solution as transmitters for broadband WDM optical access systems (Collings et al., 2000).

The need for a broad spectral bandwidth as opposed to the usual narrowband output of conventional lasers. The conventional broadband lasers have low brightness, whereas broadband ultrafast lasers have higher brightness by many orders of magnitude. The brightness is absolutely critical to applications that require tight focusing or high spatial resolution along with the good signal to noise ratio (SNR), so that data or image acquisition times remain reasonable (Fermann et al., 2002).

2.7.2 Pulse Repetition Rate

Pulse repetition rate is the number of emitted pulses per second or the inverse temporal pulse spacing. Depending on the pulse generation technique, typical pulse repetition rates can be in MHz for mode-locked or KHz for Q-switched. Theoretically, the fundamental

pulse repetition rate for a passive mode locking in a ring cavity fiber laser can be estimated from the following equation:

$$f_{rep} = \frac{c}{nL} \tag{2.41}$$

where f_{rep} is the pulse repetition rate in Hz, c is the speed of light, n is the refractive index of the medium, which is about 1.5 for silica-based fiber optics and L is the total cavity length.

2.7.3 Pulse Duration

The optical pulse duration (also called pulse width) is defined as the full width at half-maximum (FWHM) of the optical power versus time (Paschotta, 2008). The pulse duration can be varied in a huge range depends on the pulse generation technique. The pulse duration from Q-switched lasers typically varies between few microseconds and hundreds of nanoseconds. Mode-locked lasers can generate pulses with a duration between hundreds of picoseconds and few femtoseconds. In mode-locking, very short output pulse duration can be measured with the fast photodetector in combination with fast sampling oscilloscope or in most cases use optical autocorrelator.

Also, the mode-locked pulse duration τ_P can be mathematically calculate based on the time bandwidth product (TBP) and spectral width of the pulse $\Delta\nu$ in hertz.

$$\tau_P = \frac{K}{\Delta\nu} \tag{2.42}$$

where

$$\Delta\nu = \frac{\Delta\lambda \times c}{(\lambda_0)^2} \tag{2.43}$$

K is a number that depends on the pulse shape, for example, ~0.315 for secant hyperbolic ($sech^2$) shaped pulses and ~0.44 for Gaussian-shaped pulses (Paschotta, 2008). The $\Delta\lambda$ is the spectral bandwidth at FWHM, c is the speed of light and λ_0 is the central wavelength of the spectrum.

2.7.4 Pulse Energy

The pulse energy E_p of ultrashort pulses is in most cases obtained by measuring the average output power (P_{av}) of a pulse train and dividing it by the pulse repetition rate (f_{rep}), as follows:

$$E_p = \frac{P_{av}}{f_{rep}} \tag{2.44}$$

This is accurate as long as the pulse train really consists of single pulses.

2.7.5 Peak Power

Peak power is the maximum optical power of a pulse. For laser pulses of various shapes, the pulse energy E_p, peak power P_p and pulse duration τ_p are approximately related by the very simple equation

$$P_p \approx \frac{E_p}{\tau_p} \tag{2.45}$$

This should be multiplied by a factor that depends on the pulse shape. Thus, the extremely short duration of femtosecond laser pulses implies that very high peak powers can be generated even for moderate pulse energies.

2.7.6 Time-Bandwidth Product

Time-bandwidth product (TBP) is the product of the temporal duration of a pulse and its spectral width. As expressed by the Heisenberg uncertainty principle, the TBP of any pulse cannot fall below a limit *K* (Fermann et al., 2002), which is written as

$$\tau_p \times \Delta\nu \geq K \tag{2.46}$$

K and $\Delta\nu$ are defined in Eq (2.42) and (2.43). The pulse shape can be represented intuitively by a bell-shaped function, depending on the mode locked characteristic, including the output spectrum and the total cavity dispersion. When a pulse has a chirp, its TBP generally becomes larger. During propagation in a medium, the TBP of a pulse can increase, as when a nonlinearity of the medium broadens the spectrum without shortening the pulse or when chromatic dispersion broadens the pulse without decreasing its spectral width (Paschotta, 2008).

2.8 Summary

This chapter has summarized the major historical developments leading to the success of fiber lasers today and introduced the main fundamental and technological concepts that use in this thesis. At first, the pulse generation techniques and the nonlinear effects in optical fiber have been briefly described. Also, the historical evolution of the saturable absorbers technologies has been highlighted and reviewed the fundamental optical properties, production methods and optical characterization methods of 2D nanomaterials, like graphene, MoS_2, and black phosphorus. The following chapters intend to demonstrate, 2D nanomaterials as saturable absorbers for ultrafast pulse generation in erbium-doped fiber lasers.

CHAPTER 3: MODE LOCKING PULSES GENERATIONS WITH GRAPHENE SATURABLE ABSORBER

3.1 Introduction

Atomically thin layered materials, usually referred to as two-dimensional (2D) nanomaterials, have unique electrical and optical properties that open a new field of research in solid state physics and material science (Sobon, 2016). Graphene is the most common example of a 2D nanomaterial, which is composed of a single layer of carbon atoms, forming a 2D honeycomb lattice. Graphene is a fundamental building block of three-dimensional (3D) graphite, which consists of stacked graphene layers held together by weak van der Waals forces (Boehm et al., 1986; Wallace, 1947). Recently, graphene 2D nanomaterials have attracted much attention for ultrafast fiber laser applications as a saturable absorber (SA) due to its unique optical properties, like short recovery time, broadband absorption, nonlinear optical response, low saturation intensity, high-power handling capability, cost-effective and easy fabrication (Bao et al., 2009). Since the first demonstration of graphene-based passively mode-locked fiber lasers (Bao et al., 2009; Hasan et al., 2009), graphene has been used for mode-locked fiber lasers at various wavelength regions including 1 μm, 1.5 μm and 2 μm regions (Fu et al., 2014). According to the demonstrated work, the graphene has an intrinsic property of broadband saturable absorption due to its zero-band gap property, which has been experimentally characterized in passively Q-switched or mode-locked lasers (Bonaccorso et al., 2010).

This chapter demonstrates three mode-locked fiber lasers using graphene SAs. It starts with the demonstration of mode-locked erbium-doped fiber laser (EDFL) using a commercially available nonconductive graphite pencil-core based material as SA. The SA has a simple and low-cost preparation method. Then, the development of two different femtosecond mode-locked EDFLs were reported using another graphene SA by manipulating of net cavity dispersion to produce stretched and soliton pulses trains.

3.2 Mode-Locked Fiber Laser with Graphite Based Saturable Absorber Using Pencil-Core Flakes

The growing interest in graphene started in 2004 after the first demonstration of mechanical exfoliation of graphite using Scotch tape (Novoselov et al., 2004). This approach has provided some advantages such as simple preparation and easier transferring process for graphite nano-particle. Recently, graphite nano-particle has shown its potential as SA to passively mode-locked EDFLs (Lin et al., 2011). Also, Lin et al. confirmed that the graphite nanoparticles possess the saturable absorption effect (Lin et al., 2013; Lin et al., 2015; Lin et al., 2012). Graphite nano-particle or nano-flakes SAs can be obtained by different methods including electrochemical exfoliation (Yang et al., 2013) or mechanical trituration (Lin et al., 2013; Lin et al., 2015; Lin et al., 2012). On the other hand, the graphite can also be exfoliated from pencil-core, which was made of graphite mixed with a clay binder. The various graphite pencil grades are achieved by altering the proportion of graphite to clay; the more the clay, the harder the pencil (Schweizer, 2002). Up to now, graphite pencil-core based SAs have shown their potentials to Q-switched fiber lasers. For instance, Latiff et al. demonstrated Q-switched thulium-doped fiber laser operating at 1940 nm region using a pencil-core as SA (Latiff et al., 2016). Lee et al. also reported graphite SA, which was obtained by using pencil-sketching method for Q-switched EDFL (Lee et al., 2016). In this work, we experimentally demonstrate the generation of mode-locked EDFL using a homemade graphite pencil-core saturable absorber.

3.2.1 Preparation and Characterization of the Graphite-Based SA

In this experiment, graphite pencil-core SA was fabricated using mechanical exfoliation technique, which was very simple and easy as described in Figure 3.1. The pencil-core was 2B grade and made of graphite mixed with a clay binder. It is commercially available from stationery stores and used without further purification. First,

the pencil-core was peeled and crashed into flakes on a clear scotch tape using a metal blade (Figure 3.1(a)). Next, the flakes were repeatedly folded over the flakes and opening it up again so that the flakes stuck on the scotch tape (Figure 3.1(b)). The folding and opening process of the tape was repeated as many times as possible until the graphite fragment became thin enough to transmit light with high efficiency. Then, a small piece of the graphite tape was cut and attached to the end surface of the fiber ferrule with index matching gel. The fiber ferrule with graphite tape was then connected with another fresh FC/PC fiber ferrule using standard flange adapter (Figure 3.1 (c)).

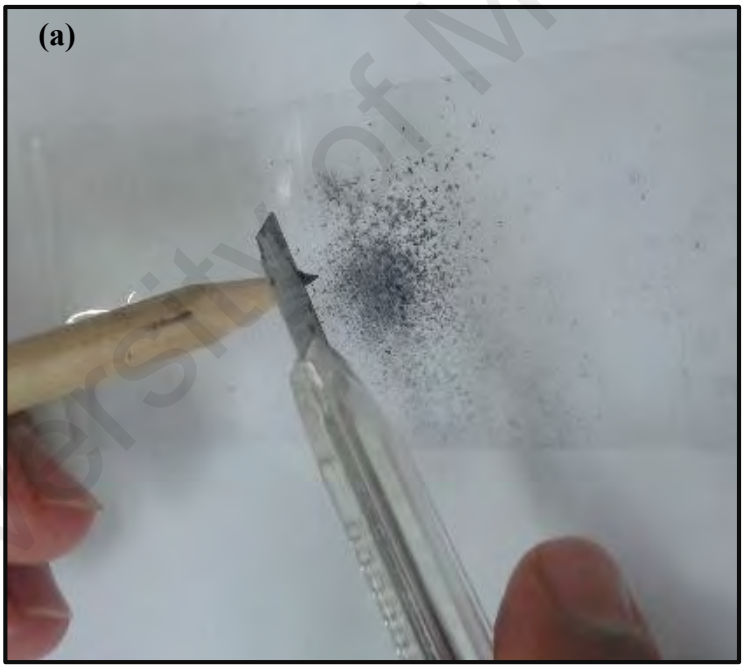

Figure 3.1: Mechanical exfoliation method from pencil core, (a) Peel and crash process, (b) Fold process, (c) Small piece of graphite tape is attached to fiber

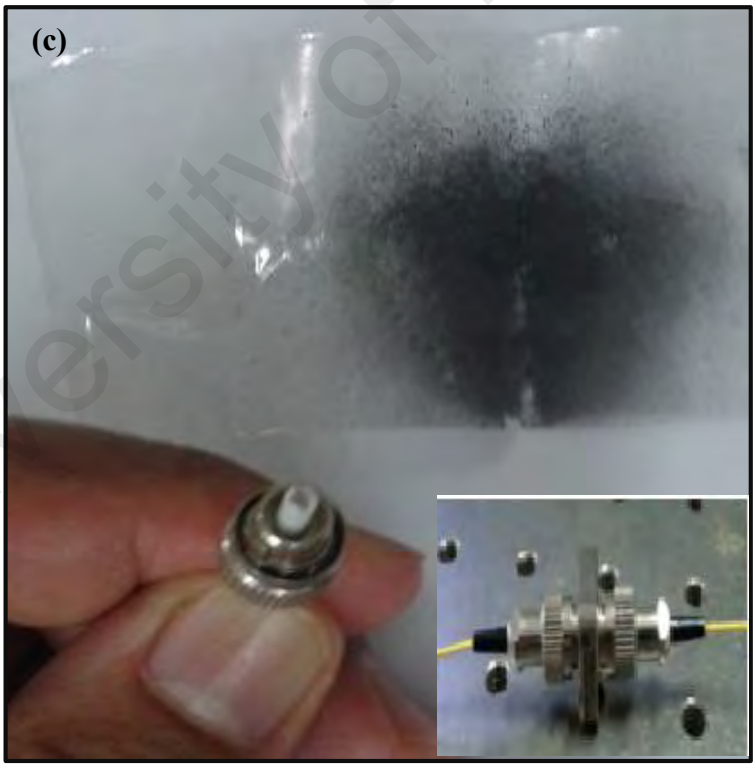

Figure 3.1, continued

Raman spectroscopy (Renishaw in-Via, Raman microscope) was performed to confirm the presence of graphene layer on the surface of the pencil-core tape by using laser excitation at 514 nm with an exposure power of 10 mW. Figure 3.2 shows the Raman spectrum with three prominent peaks; D at 1354.7 cm^{-1}, G at 1579.8 cm^{-1} and 2D at 2723.5 cm^{-1}, which indicates the signature of the graphene layer. The G band contributes to an E_{2g} mode of graphite and is related to the in-plane vibration of the sp^2-bonded carbon atoms, whereas the D band is associated with the vibrations of the carbon atoms with sp^3 electronic configuration of disordered graphite (Reich et al., 2004). The intensity ratio of the D and the G bands of the pencil-core tape is about 0.42 and 0.57 respectively. Thus, this indicates the structural defect is not large since the D peak is not very broad. The intensity ratio between the G and the 2D peak can be used to determine the graphene layer (Ferrari, 2007). It was reported that single-layer graphene has a low-intensity ratio, usually lower than 0.5, whereas multi-layer graphene shows a higher intensity ratio ($\geq$1) (Graf et al., 2007). The shape of the 2D peak can also be used to estimate the number of graphene layers. As the graphene layer increases, the full width half maximum (FWHM) of the 2D peak follows. The Raman spectroscopy reveals a broad 2D peak, which indicates that the graphene has a multi-layer structure. The FWHM of the 2D peak of both areas is obtained at 60 cm^{-1}. From the intensity ratio of the G and the 2D peaks and FWHM, it can be concluded that the number of graphene layers is similar to Highly Oriented Pyrolytic Graphite (HOPG) (Ferrari et al., 2006; Graf et al., 2007).

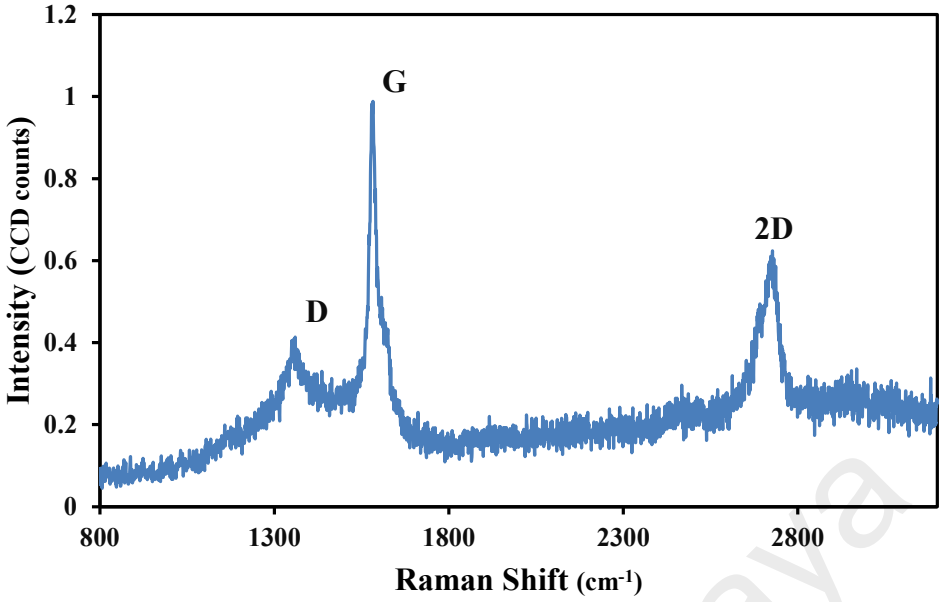

Figure 3.2: Raman spectrum of the fabricated graphite tape

The nonlinear absorption of the graphite-pencil-core was also characterized by using the experimental setup shown in Figure 3.3(a). The setup consists of EDFL cavity that generates mode-locked pulsed laser as the source with a repetition rate of 17.4 MHz and pulse width of 1.2 ps at 1552 nm wavelength. Furthermore, the mode-locked pulses train was amplified using an Erbium-doped fiber amplifier (EDFA) before it was connected to a variable optical attenuator (VOA) to vary the average power of the source that passes through the SA. Through 3 dB coupler, the output of the source was split equally into reference part (R1) and test part (R2) in which graphite-pencil-core tape SA was incorporated. The output of R1 and R2 were connected to a power meter with separate detectors. By varying the power intensity of mode-locked pulses, the absorption of the SA as a function of incident power has been determined by the difference between the output powers of R1and R2. Figure 3.3(b) shows the absorption characterization of graphite-pencil-core SA. The intensity dependent absorption was plotted and the result is well fitted using the following two-level fast SA model (Garmire, 2000);

$$\alpha(I) = \frac{\alpha_s}{1 + I/I_{sat}} + \alpha_{ns} \quad (3.1)$$

where α(I) is the absorption, α_s is the modulation depth, I is the input intensity, I_{sat} is the saturation intensity, and α_{ns} is the non-saturable absorption. As shown in the figure, the absorption curve was relatively flat after the input intensity reached 0.8 MW/cm^2. This shows that the modulation depth is 3% with non-saturable intensity of 22%.

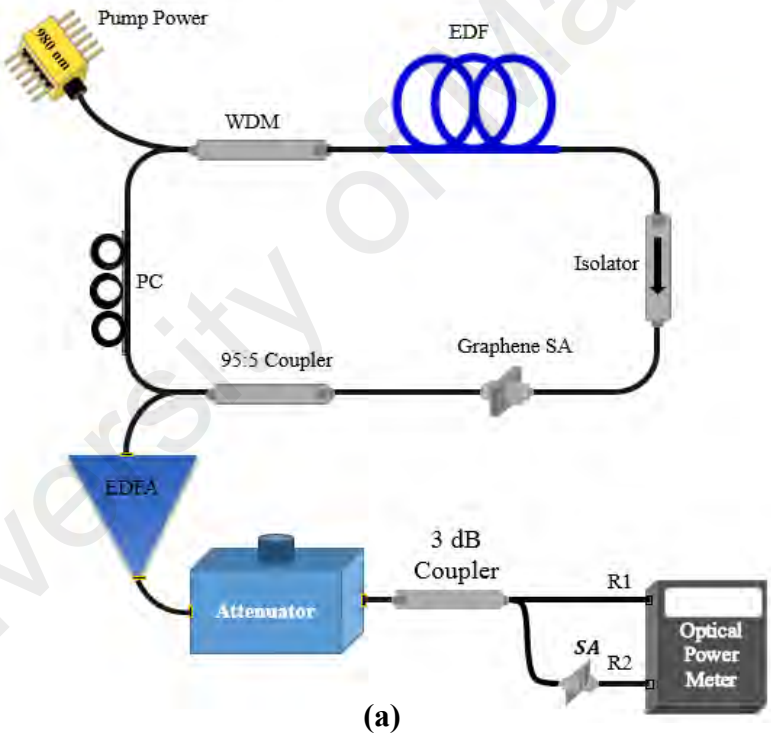

(a)

Figure 3.3: (a) Experimental setup for measuring nonlinear absorption, (b) nonlinear saturable absorption profile for graphite- pencil-core tape

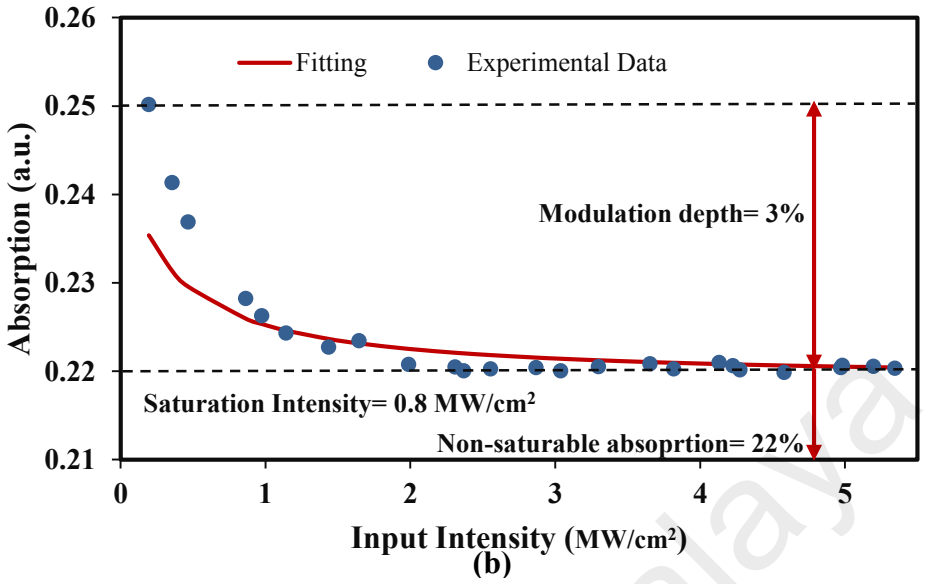

(b)

Figure 3.3, continued

3.2.2 Configuration of the mode-locked laser

The schematic diagram of the mode-locked EDFL with graphite pencil-core SA is shown in Figure 3.4. The graphite SA was inserted into the ring cavity by sandwiching a ~1 mm×1 mm piece of the graphite tape between two ferrules of patch cords as shown in Figure 3.4 (inset). The cavity consists of a 3 m long erbium-doped fiber (EDF) as a gain medium with a core diameter of 4 µm, the numerical aperture (NA) of 0.16, erbium ion absorption of 23 dB m^{-1} at 980 nm and group velocity dispersion (GVD) of 27.6 ps^2km^{-1}. The gain medium was pumped by a 980 nm laser diode via a 980/1550 nm wavelength division multiplexer (WDM). An isolator was used to ensure uni-directionality so that the backward reflection can be significantly reduced to help in initiating mode-locking. The laser output was extracted by a 10% of a 90:10 fiber coupler, which keeps 90% of the light to continue oscillating. A 196 m long of extra single mode fiber (SMF-28) was added to compensate the normal dispersion of EDF so that the cavity dispersion becomes

anomalous (Bao et al., 2009). On the other hand, the long SMF reduced the repetition rate and increase the pulse energy. All the components were made of SMF-28 or patch cord with SMF-28 with a length of 5.5 m and a segment of 0.5 m HI 1060 WDM fiber. The GVD parameters of SMF-28 and HI 1060 fiber at 1550 nm were, -21.7 ps^2 km^{-1} and -48.5 ps^2 km^{-1} respectively, as provided by the fiber producer. The total cavity length of the mode-locked EDFL was 205 m, which operated in anomalous fiber dispersion of -4.3 ps^2. The optical spectrum analyzer (OSA) with a spectral resolution of 0.07 nm was used to analyze the spectrum of the mode-locked laser, an oscilloscope (OSC) via a photo-detector was used to analyze the output pulse train of the mode-locking operation and auto-correlator (AC) for monitoring the pulse duration.

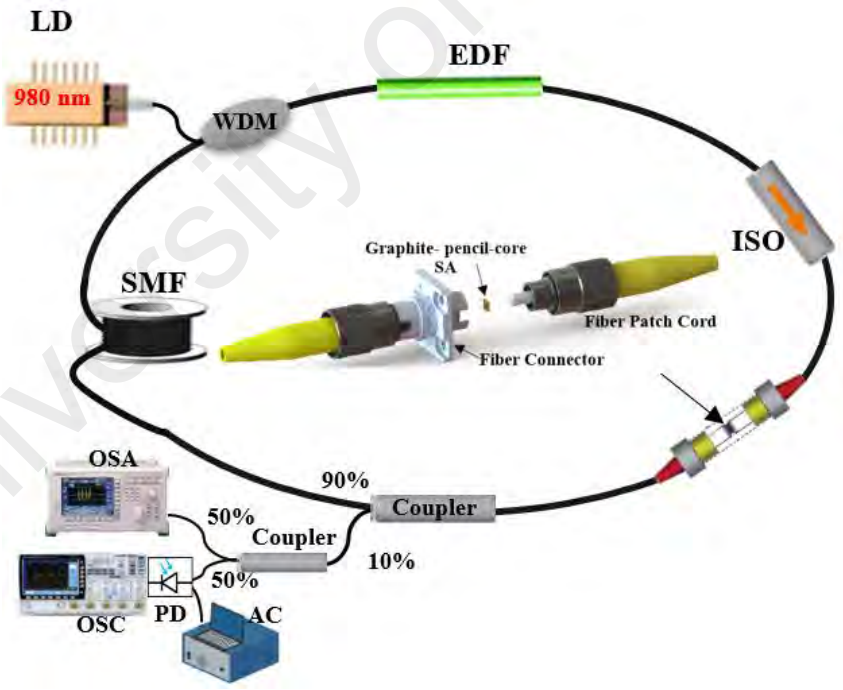

Figure 3.4: Schematic configuration of mode-locked EDFL including a graphite pencil-core SA, Inset: Illustration showing the integration of graphite pencil-core tape into fiber based system by sandwiching a ~1 mm × 1 mm piece of graphite-SA between two fiber patch cords

3.2.3 Mode-locking performance

The mode-locking performance of the laser was investigated as the graphite-SA was integrated into the ring cavity. By varying the 980 nm pump power the continuous wave (CW) laser operation started at a pump power of 90 mW, but as the pump power reached 145 mW, mode locking operation occurred. As the pump power was increased to the maximum power of 170 mW, the output showed a stable mode-locked pulse train and the graphite-SA maintained stably without thermal damage. Figure 3.5 shows the corresponding output spectrum of the soliton mode-locked laser at a pump power of 170 mW with a central wavelength of 1562.0 nm and 3 dB bandwidth of 0.6 nm. As seen in the figure, the spectrum is broadening, due to the SPM effect in the cavity. Although the resultant pulse fiber laser is a soliton mode-locked fiber laser, Kelly sidebands are less prominent due to excessive nonlinearity caused by high pump power and cavity length. The sidebands total power is pulse width dependent. In a relatively long pulse width cavity, the sidebands can be suppressed. This is due to the sideband fractional power, which seems to decrease exponentially with increasing pulse width (Dennis et al., 1994).

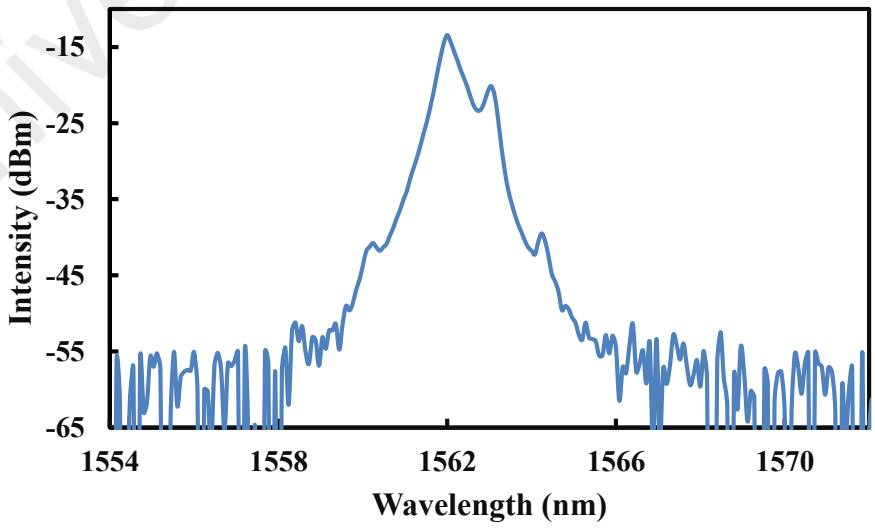

Figure 3.5: Optical spectrum of the mode-locked EDFL at pump power of 170 mW

Figure 3.6 shows the oscilloscope trace of the mode-locked EDFL at a pump power of 170 mW, which produced a regular train of pulses with a period of 1.0246 µs, defined by the fundamental cavity frequency of 976 kHz. The pulse width of the mode-locked EDFL is measured by autocorrelator. The output autocorrelation trace is shown in Figure 3.7, which is well fitted by a $sech^2$ profile with a full width at half maximum (FWHM) of 3.05 ps.

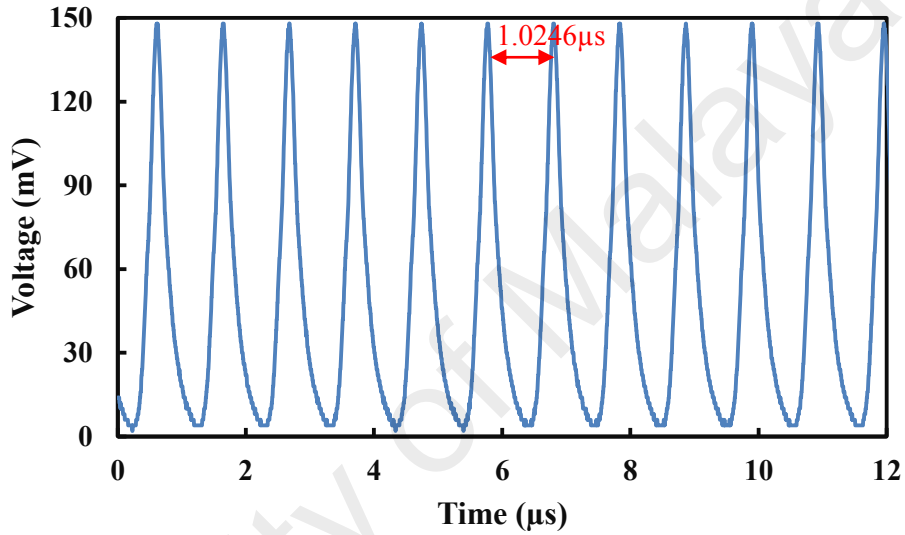

Figure 3.6: Oscilloscope trace of the mode-locked EDFL at pump power of 170 mW

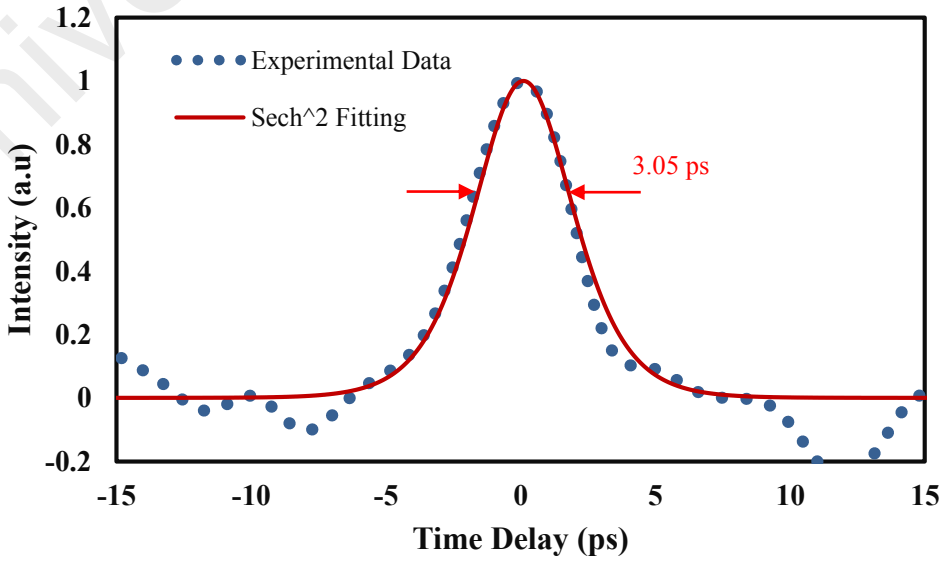

Figure 3.7: Autocorrelation trace of the mode locked EDFL at pump power of 170 mW

The laser stability was also investigated by analyzing the radio frequency (RF) spectrum as proposed by Linde (Linde, 1986). In the experiment, the RF spectrum was measured by using a 1.2 GHz bandwidth photodetector in conjunction with 7.8 GHz RF spectrum analyzer. Figure 3.8 shows the measured RF spectrum with a span of 10 MHz and a resolution bandwidth of 30 kHz. It presented a regular train of harmonics with no Q-switching instabilities. At the fundamental frequency of 976 kHz, the high signal-to-noise ratio (SNR) of 58 dB indicated good pulse train stability. Figure 3.9 shows the average output power and pulse energy in the mode-locked regime at various pump powers. At the maximum pump power of 170 mW, the average output power is 2.07 mW. Therefore, the pulse energy and peak power are estimated at 2.12 nJ and 653 W, respectively. These results indicate that graphite pencil-core with the simple and low-cost method can be very useful for the implementation of practical SAs in the field of ultrafast fiber lasers.

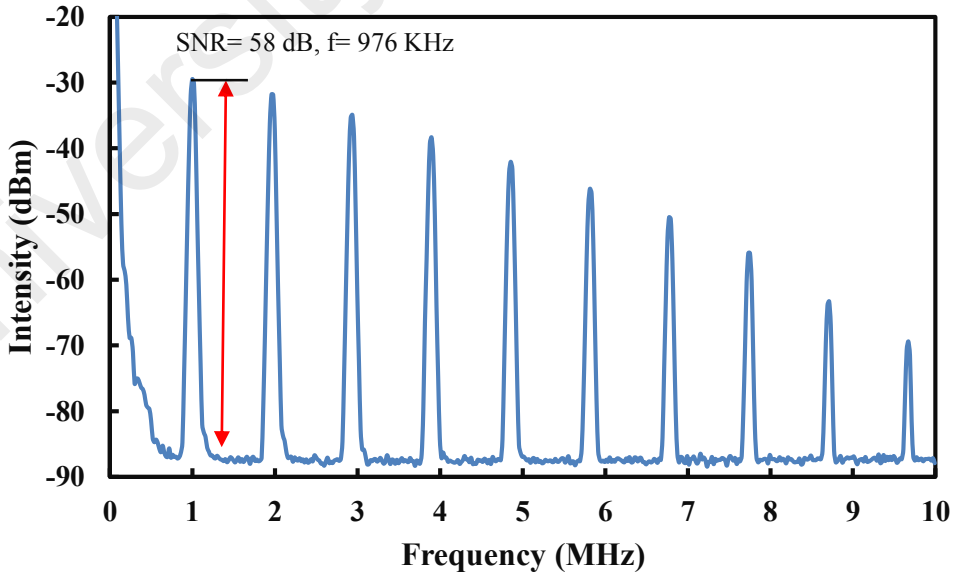

Figure 3.8: RF spectrum of the mode-locked EDFL with a 10 MHz span

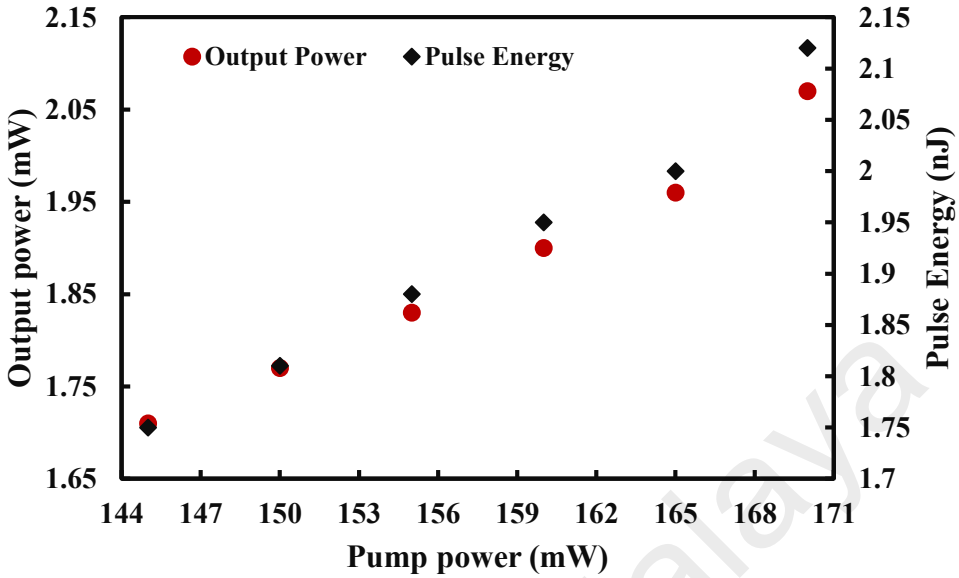

Figure 3.9: Average output power and pulse energy as a function of 980 nm pump power

3.3 Stretched and Soliton Femtosecond Pulses Generation with Graphene Saturable Absorber by Manipulating Cavity Dispersion

The cavity dispersion plays a critical role in the propagation of ultrafast pulses within optical fibers. With the different net dispersion of laser cavity, various pulses including solitons pulses, stretched pulses, and dissipative solitons pulses have been observed experimentally (H Ahmad et al., 2013; Cui et al., 2013; Sotor, Pasternak, et al., 2015). Also, different types of fiber lasers with alternating anomalous and normal group velocity dispersion (GVD) have been proposed (Sun, Hasan, Wang, et al., 2010; Wienke et al., 2012; Xu et al., 2012). When the laser cavity operates with anomalous GVD, solitons with spectral sidebands can be formed by the balance between GVD and fiber nonlinearity (Liu, 2011; Weill et al., 2011). In this work, stretched pulse and soliton mode-locked EDFLs are experimentally demonstrated based on graphene saturable absorber (GSA) with the variation of net cavity dispersion.

3.3.1 Preparation and characterization of graphene

Graphene nano-powder used in this work was purchased from graphene supermarket and it was used as per received. The graphene nano-powder was characterized with specific surface area of 100 m^2/g, purity of 99.9%, average flake thickness of 8 nm (with 20–30 monolayers) and average particle (lateral) size of ~550 nm. To disperse the graphene, 25 mg of graphene nano-powder was mixed with 1% sodium dodecyl sulfate (SDS) in 40 ml deionized (DI) water and undergone bath sonification for 1 h. After sonification process, the dispersed graphene was centrifuged at 1000 rpm to segregate large graphene particles. The host polymer was prepared by dissolving 1 g of polyvinyl alcohol (PVA) (Mw = 89 × 10^3g/mol, Sigma Aldrich) in 120 ml of DI water. The graphene suspension after centrifugation process was mixed with PVA solution at a ratio of 1 and 4 ml of graphene and PVA respectively. Then the graphene-PVA mixture is poured onto Petri dishes and dried at room temperature to obtain a free-standing film with a thickness of about 50 μm.

Figure 3.10 (a) shows the Field Emission Scanning Electron Microscopy (FESEM) image of the fabricated graphene PVA film. As seen in the image, the graphene flakes are clearly well dispersed in the PVA matrix. Raman spectroscopy measurement was also performed on the fabricated Graphene–PVA film sample. Figure 3.10 (b) shows the spectrum recorded by the spectrometer when a 514 nm beam of an Argon-ion laser is radiated on the film. As shown in the figure, the sample exhibits signature peaks at approximately D (1353 cm−1), G (1585 cm−1) and 2D (2724 cm−1) bands. G band contributes to an E_{2g} mode of graphite and is related to the in-plane vibration of sp^2-bonded carbon atoms, while D band is associated with the vibrations of carbon atoms with sp^3 electronic configuration of disordered graphite. The small D peak indicates negligible defects existing in the graphene film. The intensity ratio between G and 2D peak can be used to determine the number of the graphene layer. It was reported that

single-layer graphene has a low-intensity ratio, usually lower than 0.5 while multi-layer graphene shows higher intensity ratio (≥1) (Chen et al., 2011). The shape of the 2D peak can also be used to estimate the number of graphene layers. As seen in the figure, we obtained a G/2D peak ratio of 0.6, which indicates the graphene has a multi-layer structure. As the graphene layer increased, the full-width half maximum (FWHM) of the 2D peak followed (Ferrari et al., 2006). The nonlinear absorption of the graphene-PVA was characterized using the experimental setup in Figure 3.3 (a). The experimental data were well fitted by the equation model (3.1) as shown in Figure 3.10 (c). As presented in the figure, the saturable absorption curve reveals a modulation depth of ~5.9%, the non-saturable intensity of 47% and saturation intensity of 21 MW/cm2. This large modulation depth is expected to suppress wave breaking in the mode-locked fiber laser and thus improves the attainable energy.

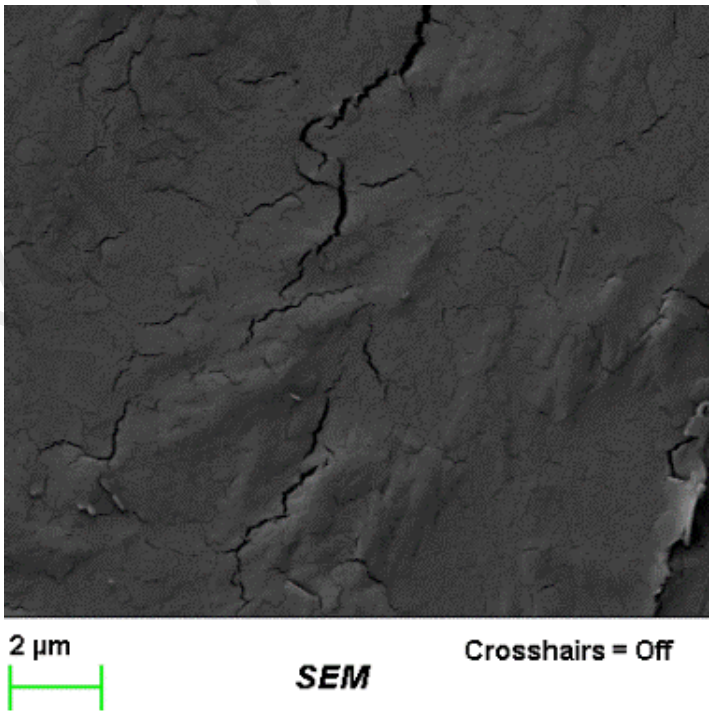

(a)

Figure 3.10: Characterization of the fabricated graphene-PVA film (a) FESAM image (b) Raman spectrum (c) Nonlinear saturable absorption profile showing saturable absorption

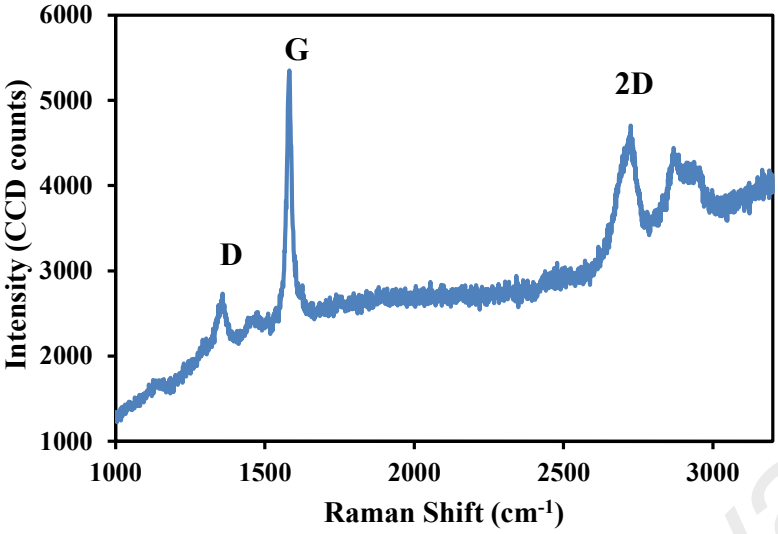

(b)

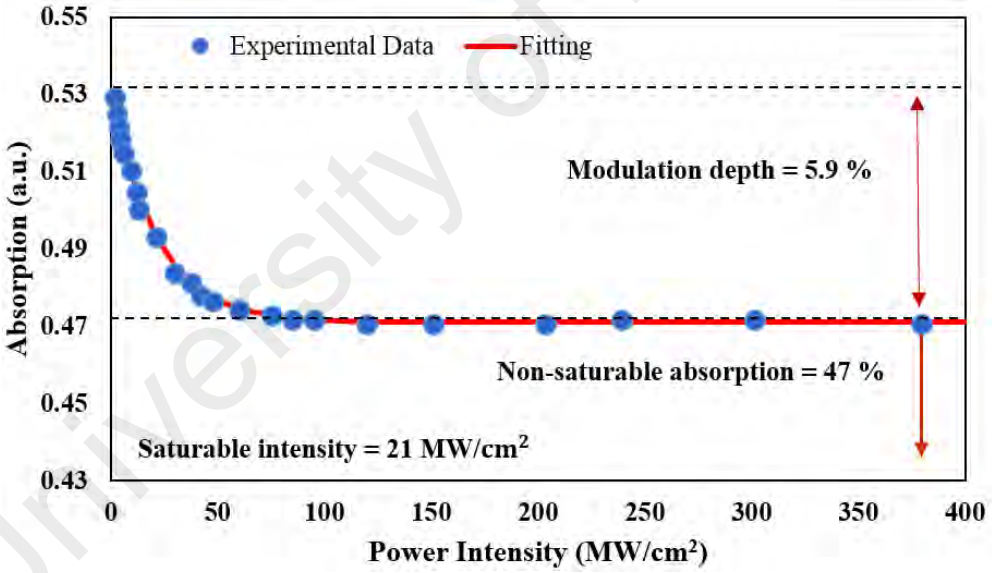

(c)

Figure 3.10, continued

3.3.2 Stretched Pulse Generation in Near Zero Dispersion Cavity

In this section, stretched mode-locked EDFL is demonstrated by adjusting the length of EDF and single mode fiber (SMF) to give near zero round trip group velocity dispersion. The experimental setup of the mode-locked EDFL based on the graphene SA is shown in Figure 3.11. The cavity is designed to operate in near-zero dispersion cavity with the ring resonator consists of a 0.5 m long WDM fiber, a 2.2 m long EDF and 3 m long additional single mode fiber (SMF-28). The EDF, SMF and WDM fiber has group velocity dispersion (GVD) of 27.6, −21.7, and −48.5 ps^2/km, respectively. The cavity length was around 5.7 m, and the net cavity dispersion was estimated to be −0.028 ps^2. The EDF used has a core diameter of 4 μm, a numerical aperture of 0.16 and Erbium ion absorption of 23 dB/m at 980 nm. The graphene SA is obtained by sandwiching the fabricated graphene PVA film in between two fiber ferrules via a fiber adapter. The active fiber or EDF is pumped by a 980 nm laser diode (LD) by a 980/1550 nm WDM. An isolator is incorporated in the ring cavity to prevent backward reflection and ensure unidirectional propagation of the oscillating laser. The output laser is routed out through a 95/5 coupler which keeps the majority of the light oscillating in the ring cavity. An optical spectrum analyzer (OSA) with a spectral resolution of 0.07 nm is used for spectral analysis of the mode-locked laser, an oscilloscope (OSC) is used to analyze the output pulse train of the mode-locking operation via a photo-detector and auto-correlator (AC) for monitoring the pulse duration.

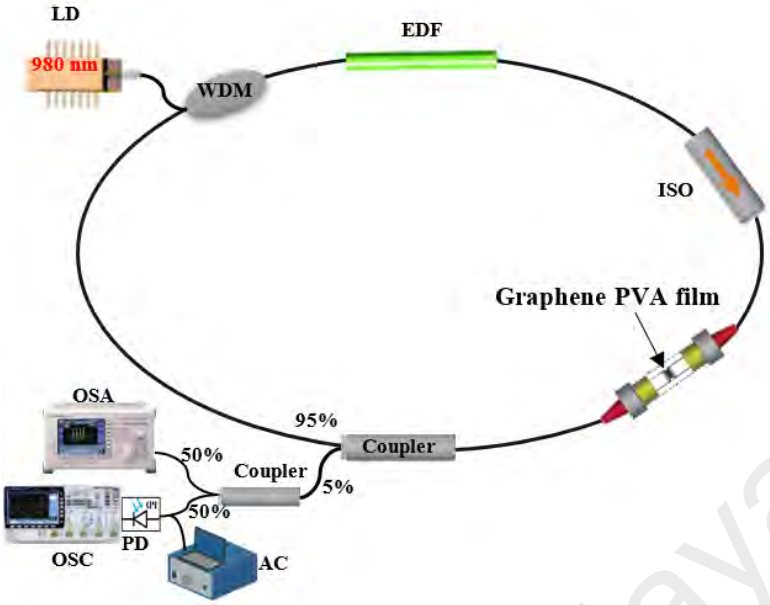

Figure 3.11: Experimental setup of the stretched mode-locked EDFL

It was reported that the net cavity dispersion can be managed by employing different types of fibers with interchanging normal and anomalous GVD (Haus et al., 1995; Sun, Hasan, Wang, et al., 2010; Xu et al., 2012). The stretched mode-locked EDFL was obtained by altering the length of EDF and SMF to give near zero round trip GVD. With the graphene SA, self-started mode locking achieved when the pump power reaches 50 mW. As the pump power increases to 170 mW the stretched pulse achieved at 1575 nm wavelength with 3 dB bandwidth of~15 nm as shown in Figure 3.12. The generation and stability of mode-locked pulse was due to the function of graphene-PVA SA. Figure 3.13 shows the typical stretched mode-locked pulse trains with a pulse period of 28.5 ns at the maximum pump power of 170 mW. The fundamental repetition rate of the mode-locked pulse is 35.1 MHz, which corresponds to the full cavity length of ~5.7 m. Figure 3.14 represents the auto-correlation trace for stretched mode-locked pulses, which indicates the measured pulse duration with a $sech^2$ pulse profile at full-width half maximum (FWHM) of 750 fs. The estimated time-bandwidth product (TBP) corresponding to the

pulse width is ~0.63, larger than the transform-limited prediction of 0.315 for sech^2 profiles.

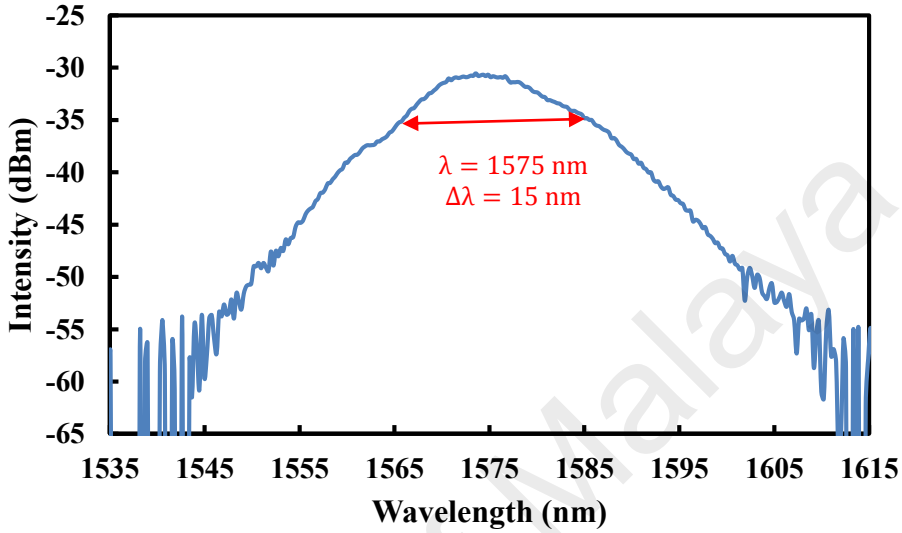

Figure 3.12: The output spectrum of the stretched pulse at pump power of 170 mW

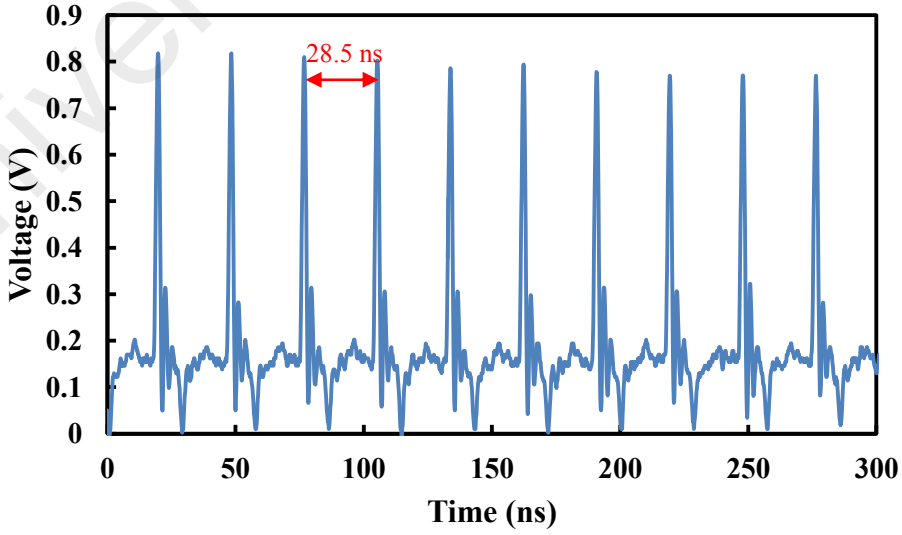

Figure 3.13: Oscilloscope trace of the mode locked EDFL at pump power of 170 mW

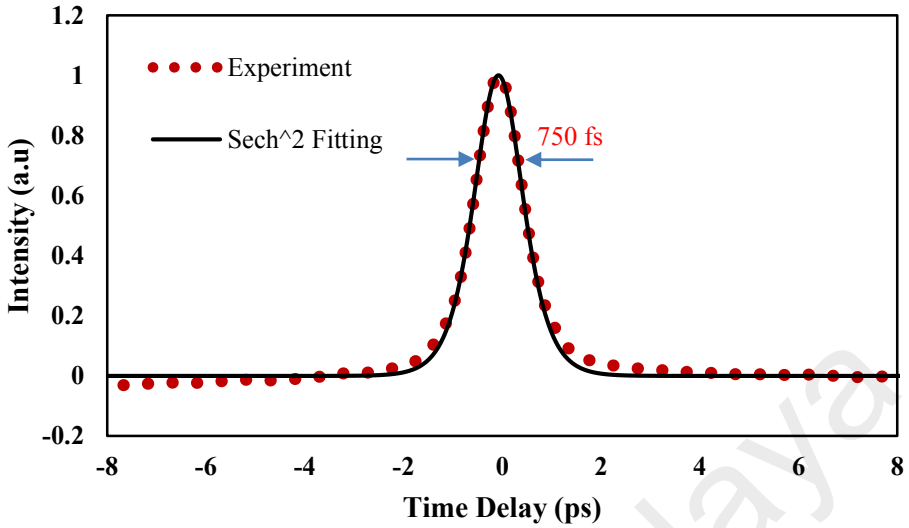

Figure 3.14: Autocorrelator trace of the mode-locked EDFL at pump power of 170 mW

Figure 3.15 shows the average output power and pulse energy of the stretched mode-locked EDFL versus the incident pump power. By increasing the pump power from 50 to 170 mW, we observed that with the increase of the pump power both output power and pulse energy linearly increase. The maximum average output power was 1.9 mW at a pump power of 170 mW, and thus the pulse energy is 54 pJ. The laser stability is characterized by the radio frequency (RF) spectrum. Figure 3.16 shows the RF spectrum for our lasers, which is recorded on a span of 1000 MHz. A high signal to background extinction ratio of ~55 dB is observed at the fundamental frequency of 35.1 MHz. Also, RF spectrum shows higher cavity harmonics, which indicate the good mode-locking performance of the cavity without significant spectra modulation implying no Q-switching instabilities.

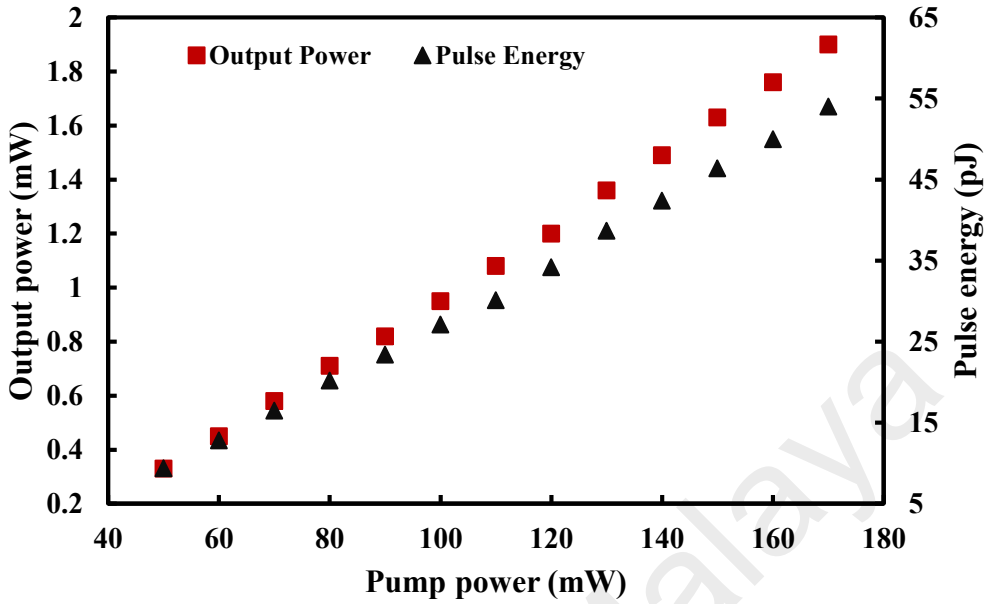

Figure 3.15: Average output power and pulse energy as a function of 980 nm pump power

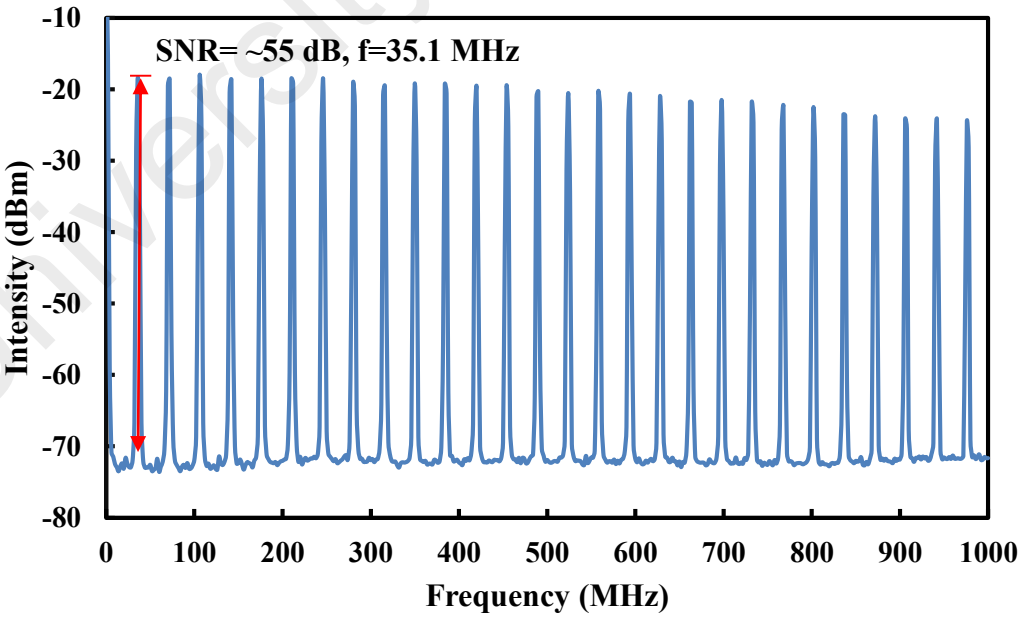

Figure 3.16: RF spectra of the mode-locked EDFL at pump power of 170 mW

3.3.3 Soliton Pulses Generation in Anomalous Dispersion Cavity

Mode-locked EDFL in the anomalous dispersion can be accomplished by adjusting the length of the different fibers that make up the laser cavity. In this experiment, we have obtained mode-locked EDFL in anomalous dispersion by reducing the EDF length from 2.2 to 1.8 m, in order to compensate the negative dispersion. And SMF length was adjusted to be 15 m to get stable pulse trains. The total cavity length of the mode-locked EDFL is 17.3 m, and the net cavity dispersion was estimated to be −0.3 ps^2, which is far from zero than −0.028 ps^2 in the last experiment. In the meantime, 20% output coupler was used to increase the output power. The experimental configuration of the soliton mode-locked EDFL is shown in Figure 3.17. A polarization controller (PC) was used to adjust the polarization state within the cavity, but is not essential to the mode-locking.

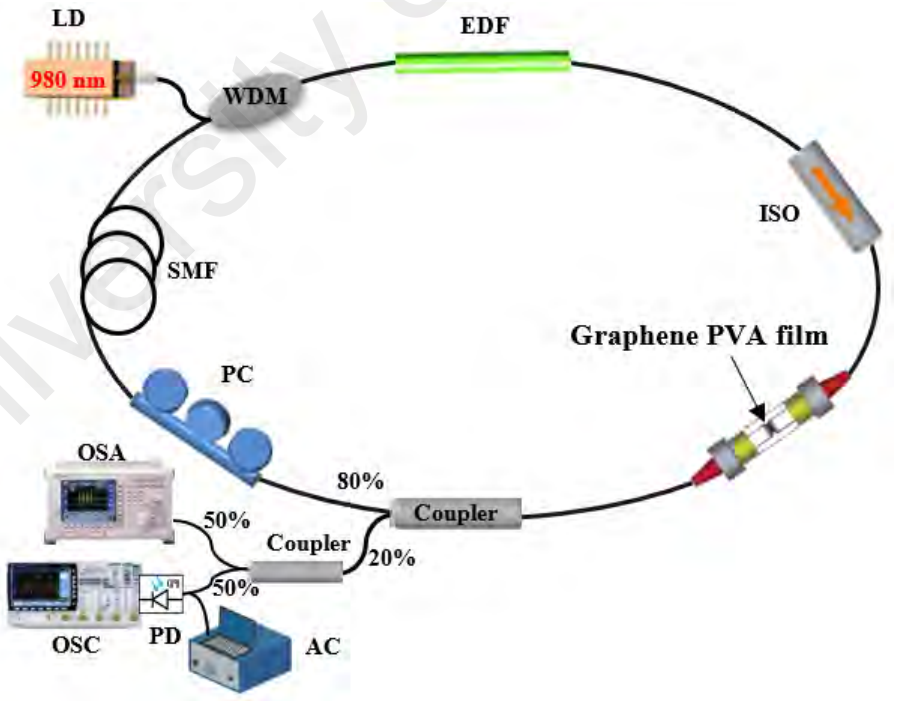

Figure 3.17: Experimental setup of the soliton mode-locked EDFL

In the proposed laser cavity, the net cavity GVD is changed to the anomalous regime, which evolving the pulse train to soliton pulse due to the combined effect of anomalous GVD and Kerr effect induced self-phase modulation (SPM). Figure 3.18 shows the optical spectrum of the soliton pulse with visible Kelly sidebands to the left and right of the spectrum. The sidebands perform due to resonant coupling interaction between soliton and dispersive wave components emitted after soliton perturbations. The soliton mode-locked pulse operates when the 980 nm pump power varying from 40 mW to 130 mW. The output spectra of the soliton mode-locked centered at 1557.7 nm with a 3 dB bandwidth of ~6 nm, which was obtained at a pump power of 130 mW. The separation of the sidebands from the center of soliton spectrum is measured at ~7 nm.

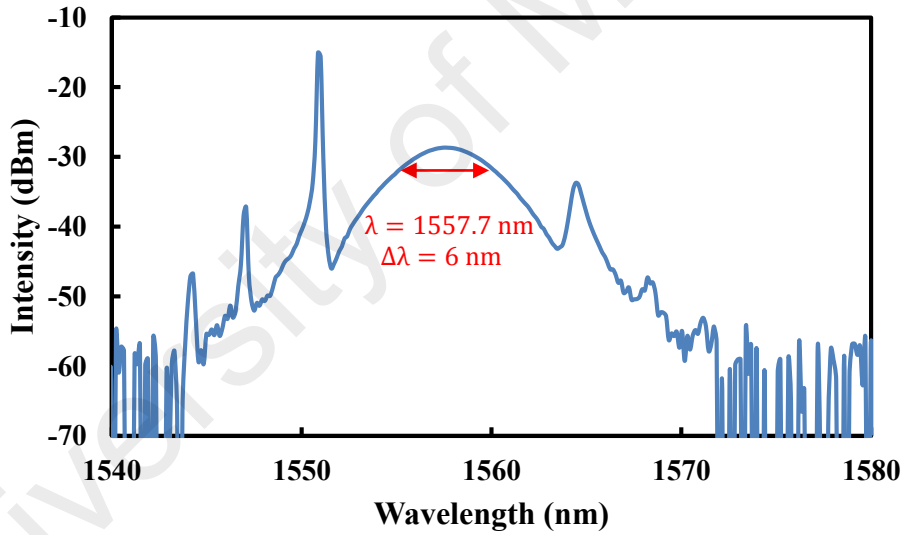

Figure 3.18: The output spectrum of the soliton pulse at pump power of 130 mW

According to sideband separation (Smith et al., 1992), the actual total dispersion can be calculated using Eq (3.2).

$$\Delta\lambda = \frac{1.763\lambda^2}{2\pi c\tau_p}\sqrt{\frac{m4\tau_p^2}{L|\beta_2|} - 1} \tag{3.2}$$

Where c is the speed of light, $\Delta\lambda$ is the sideband separation, λ is the center wavelength, m is the sideband order, τ_p is the pulse width, β_2 is the GVD dispersion and L is the cavity length. From the equation the actual GVD (β_2) is calculated to be -0.76 ps^2, which is contributed by the different types of fibers dispersions that make up the laser cavity and graphene SA dispersion.

Figure 3.19 shows the typical pulse train of the soliton mode-locked EDFL at a pump power of 130 mW. The pulse spacing is approximately ~87 ns, which is corresponding to the fundamental repetition rate of 11.5 MHz. Also, the fundamental repetition rate of the pulse corresponds to the calculated value taking into account the length of the different fibers that make up the laser cavity. As seen in the figure the pulse shape is different from the previous experiment because we have employed another photo-detector with lower bandwidth. An autocorrelator is used to measure the mode-locked pulse duration as shown in Figure 3.20. By fitting the autocorrelation trace with sech^2 pulse profile, the pulse duration was measured with the full width half maximum (FWHM) of 820 fs. By using this pulse width value and spectral width, a time-bandwidth product (TBP) of ~0.71 is attained. Figure 3.21 shows the average output power and pulse energy of the soliton mode-locked EDFL at various pump power. Both output power and pulse energy are seen to increase linearly against the increasing pump power. At a pump power of 130 mW, the average output power of the soliton mode-locked is 4.85 mW. Therefore, the pulse energy and peak power are estimated at 0.42 nJ and 483 W respectively. Figure 3.22 exhibits the laser stability, which indicated from the radio frequency (RF) spectra with a span of 200 MHz. The fundamental frequency of 11.5 MHz, shows a high signal to noise ratio (SNR) of ~45 dB. The RF spectrum also shows higher cavity harmonics, which indicate good mode-locking performance without any noticeable sign of Q-switching instabilities.

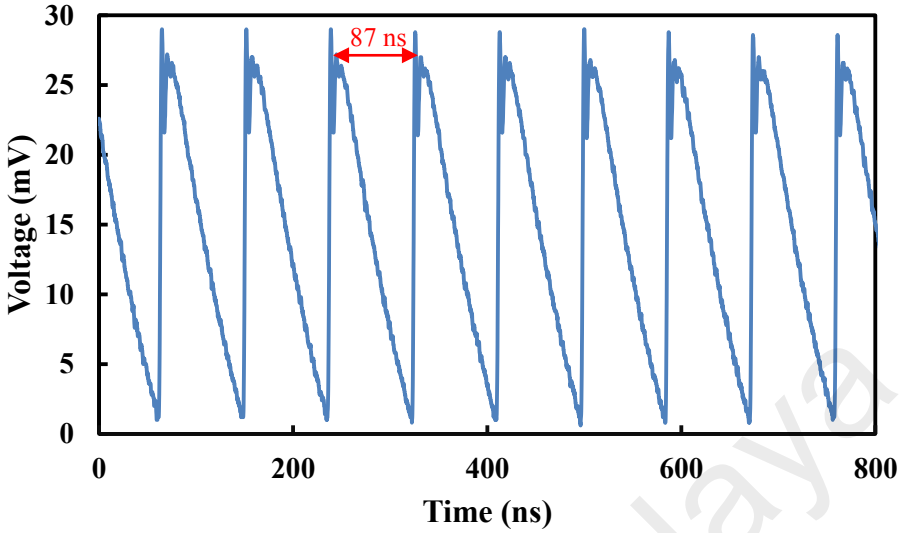

Figure 3.19: Oscilloscope trace of the mode-locked EDFL at pump power of 130 mW

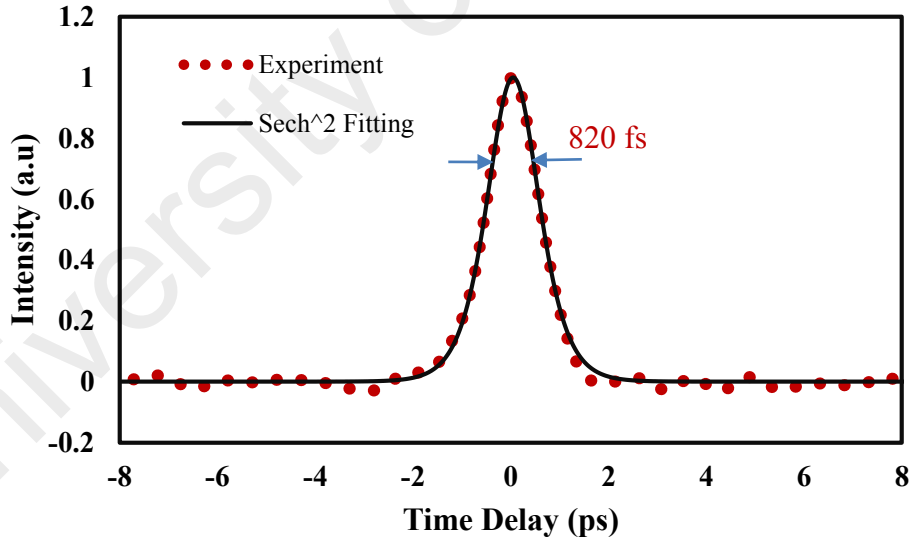

Figure 3.20: Autocorrelator trace of the mode-locked EDFL at pump power of 130 mW

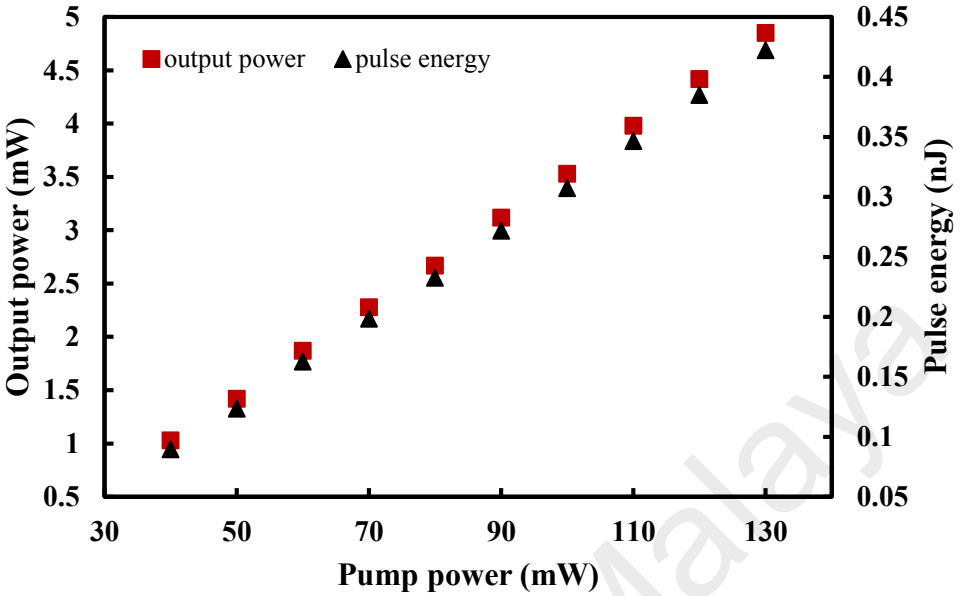

Figure 3.21: Average output power and pulse energy as a function of 980 nm pump power

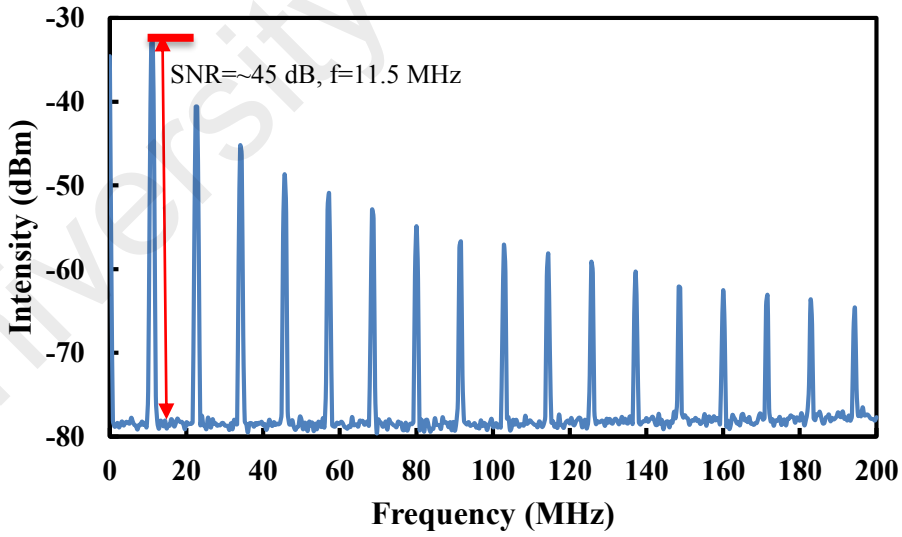

Figure 3.22: RF spectra of the mode-locked EDFL at pump power of 130 mW

3.4 Summary

Three simple and compact mode-locked EDFLs are successfully demonstrated using graphene based SA as a mode-locker. At first, I have successfully demonstrated a mode-locked EDFL using nonconductive graphite pencil-core based SA. The SA is prepared by exfoliating a low-cost graphite pencil-core flakes on adhesive tape surface, then repeatedly folded over the tape until the flakes homogenously deposited on the tape. Then a small piece of the tape is sandwiched between two ferrules and integrate into EDFL ring cavity to realize a self-started mode-locked pulse train at 1562 nm wavelength. The mode-locked pulse has a repetition rate of 976 KHz with a pulse width of 3.05 ps. Next, two different femtosecond mode-locked EDFLs are also successfully demonstrated by using graphene embedded into PVA film as an SA. With dispersion management, the net cavity total dispersion can be decreased to -0.028 ps^2, where we obtained stretched pulse with pulse width of 750 fs at a repetition rate of 35.1 MHz and pulse energy of 0.054 nJ at a maximum output power of 1.9 mW. By varying the net cavity dispersion to -0.3 ps^2, the anomalous dispersion has been achieved, where soliton mode-locked pulse generated with a pulse width of 820 fs at a repetition rate of 11.5 MHz and pulse energy of 0.42 nJ at an output power of 4.85 mW. The proposed mode-locked EDFLs with pulse length, quality and energy can meet the requirements for many applications, such as optical communications, metrology, environmental sensing, and biomedical diagnostics.

CHAPTER 4: MODE LOCKING PULSES GENERATIONS WITH MOS_2 SATURABLE ABSORBER IN BOTH ANOMALOUS AND NORMAL DISPERSION REGIMES

4.1 Introduction

Ultrafast fiber lasers have potential applications in many fields such as industry, medicine, remote sensing and optical communication (Fermann et al., 2013; Grelu et al., 2012). Therefore, the tremendous increase in research interest on developing new saturable absorbers (SAs) for passive mode locking was observed in recent years because of their advantages of excellent mechanical stability, easy implementation and low cost (Keller, 2003; Liu et al., 2015).

To date, various type of SAs have been intensively investigated and implemented to realize passive mode-locked pulses (Amos Martinez et al., 2013; Wang et al., 2016). Recently, graphene has been extensively used for generating passive Q-switching and mode locking applications (Fu et al., 2014; Liu et al., 2016). In Chapter 3, three different mode-locked Erbium-doped fiber lasers (EDFLs) were successfully demonstrated using graphene based mode-lockers, which have the advantages of ultra-fast recovery time and broadband saturable absorption. But the absence of band-gap and the low absorption co-efficiency (2.3%/layer) of graphene have also restraint its applications. These limitations lead to the intensive research on other two-dimensional (2D) materials which can complement the graphene.

Currently, transition-metal dichalcogenides (TMDs), molybdenum disulfide (MoS_2) has also attracted much attention of fiber laser research as an SA for ultrafast laser applications, due to their thickness dependent band-gap and optical properties (Ren et al., 2015; H Xia et al., 2014). It was reported that MoS_2 nano-sheets in dispersions have stronger saturable absorption response than graphene dispersions (Ren et al., 2015). To

date, there are only a few reported works on using few layer of MoS_2 as SA (Du et al., 2014; Liu et al., 2014; Ren et al., 2015; H Xia et al., 2014; H Zhang et al., 2014). For instance, Du et al. demonstrated dissipative solitons by using few-layer MoS_2-SA based on evanescent field interaction in ytterbium-doped fiber laser (YDFL) cavity. The laser operated at 1042.6 nm with pulse duration of 656 ps (Du et al., 2014). Liu, et al. reported the generation of ~710 fs pulse with a repetition rate of 12.09 MHz centered at 1569.5 nm wavelength by MoS_2-based SA fabricated by solution processed using intercalation (Liu et al., 2014). Xia et al. proposed multilayer MoS_2 prepared by chemical vapor deposition (CVD), which resultant output soliton pulses have a central wavelength, pulse width, and repetition rate of 1568.9 nm, 1.28 ps, and 8.288 MHz, respectively (H Xia et al., 2014). Also, Zhang, et al. used MoS_2 for demonstrating a mode-locked laser with a pulse width of 960 fs (Zhang et al., 2015).

In this chapter, several passively mode-locked EDFLs are demonstrated using MoS_2 based SA, which was obtained by different techniques. Firstly, the MoS_2 is obtained via mechanical exfoliation method to generate soliton mode locking pulses with pulse width of 830 fs. Then, few-layer MoS_2-PVA thin film is fabricated for mode-locked EDFL to achieve the shortest pulse width of 630 fs. Finally, the MoS_2-PVA based SA used for generating another mode locking pulse in ultra-long normal dispersion regime.

4.2 Soliton Laser with Mechanically Exfoliated MoS_2 SA

In this section, MoS_2 based SA is prepared by using mechanical exfoliation method to experimentally demonstrate ultrafast fiber laser. Using scotch tape, 2D thin layers can be peeled off from a bulk MoS_2, attached to the end-facet of a fiber ferrule, and turning it into an SA device. By placing this device inside an EDFLs cavity, soliton mode-locking pulses with pulse width of 830 fs is obtained.

4.2.1 Preparation and characterization of mechanically exfoliated MoS_2 based SA

In this work, the MoS_2-SA was prepared by mechanical exfoliation method, which has been widely used in graphene based ultra-fast fiber laser applications (Chang et al., 2010; Martinez et al., 2011). Mechanical exfoliation is advantageous mainly because of its simplicity and reliability, where the entire fabrication process is free from complicated chemical procedures and costly instruments. As shown in Figure 4.1 (a), relatively thin flakes were peeled off a big block of commercially available MoS_2 crystal using scotch tape. Then, we repeatedly pressed the flakes stuck on the scotch tape so that the MoS_2 flakes become thin enough to transmit light with high efficiency. Then we cut a small piece of the MoS_2 tape and attached it onto a standard FC/PC fiber ferrule end surface with index matching gel as shown in Figure 4.1 (b). After connecting it with another FC/PC fiber ferrule with a standard flange adapter, the all-fiber MoS_2 SA was finally ready.

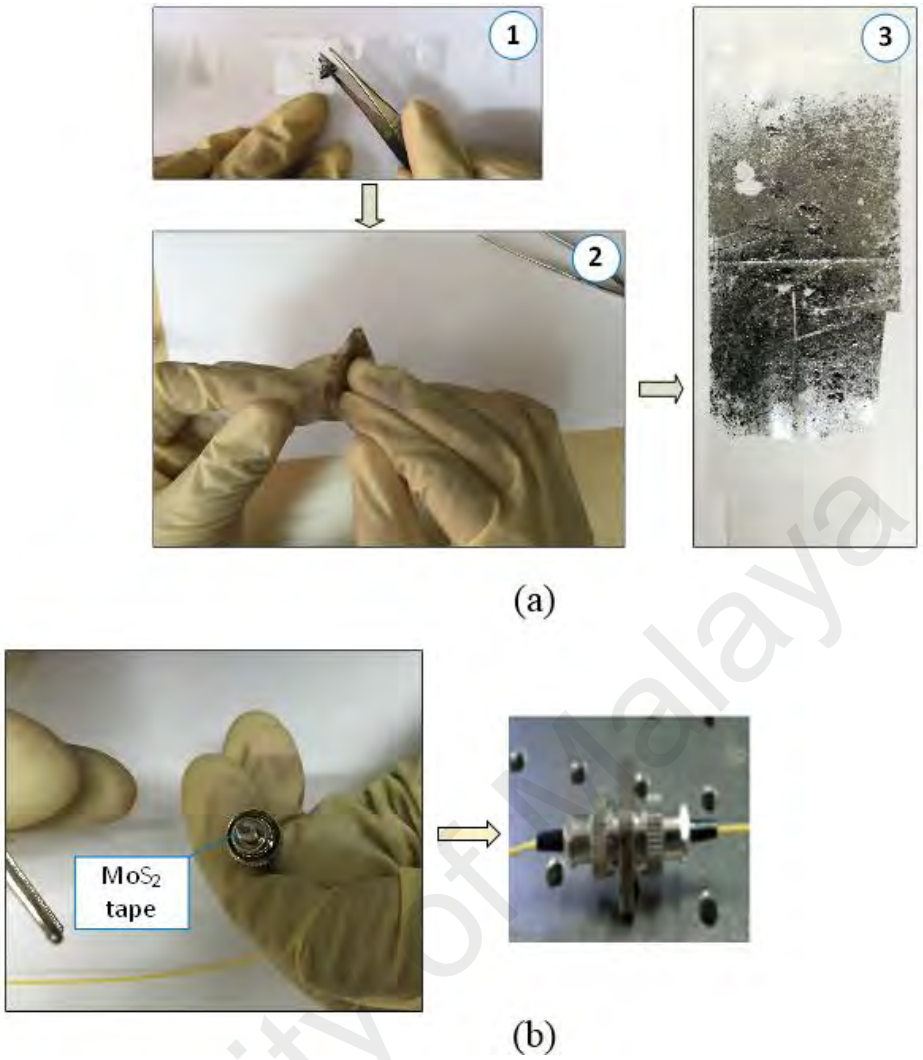

Figure 4.1: Mechanical exfoliation method; (a) Simple peeling process, and (b) MoS_2 tape at standard FC/PC fiber end surface

After the preparation process, the fabricated MoS_2-SA tape sample was characterized by performing Raman spectroscopy. Figure 4.2 (a) shows the Raman spectrum, which is recorded by a spectrometer when a 514 nm beam of an Argon ion laser is radiated on the tape for 10 seconds with an exposure power of 10 mW. As shown in the figure, the sample exhibits two characteristic peaks, in parallel with two phonon modes; out of plane vibration of Sulfide atoms at 408 cm^{-1}, and in plane vibration of Molybdenum and Sulfide atoms at 383 cm^{-1}, with a frequency difference of 25 cm^{-1}. It is observed that the E_{2g}^1 mode due to the in-plane motion red shifts after complete exfoliation, indicating that the few

layer MoS_2 with thicknesses in the range of 2-5 layers had been successfully fabricated (Li et al., 2012). The full-width-half-maximum (FWHM) of as E_{2g}^1 and A_{1g} bands are calculated to be 5.0 and 5.5 cm^{-1}, respectively, which agree with other reported results (Wu et al., 2015). The linear absorption of the SA for a broadband amplified spontaneous emission (ASE) light source is in the range from 1520 to 1600 nm. As shown in Figure 4.2 (b), the linear absorption is at the level of about 35 % and is characterized by a flat profile.

The nonlinear optical response property for the MoS_2-SA tape is then investigated to confirm its saturable absorption via a transmission technique. A self-constructed mode-locked fiber laser (1558 nm wavelength, 1.5 ps pulse width, 17.5 MHz repetition rate) is used as the input pulse source. The transmitted power is recorded as a function of incident intensity on the device by varying the input laser power. The experimental data for transmission are fitted according to a simple two-level SA model of

$$T(I) = 1 - \alpha_s * exp\,(-I/I_{sat}) - \alpha_{ns} \tag{4.1}$$

where $T(I)$ is the transmission, α_s is the modulation depth, I is the input intensity, I_{sat} is the saturation intensity, and α_{ns} is the non-saturable absorption. The nonlinear transmission of the multilayer MoS_2 on the scotch tape is shown in Figure 4.2 (c). As shown in the figure, the modulation depth, non-saturable absorption, and saturation intensity are obtained at 11.3 %, 23.0 %, and 23.5 MW/cm^2, respectively. This large modulation depth of 11.3 % is expected to be able to suppress wave breaking in the mode-locked fiber laser, and thus improves the attainable pulse energy.

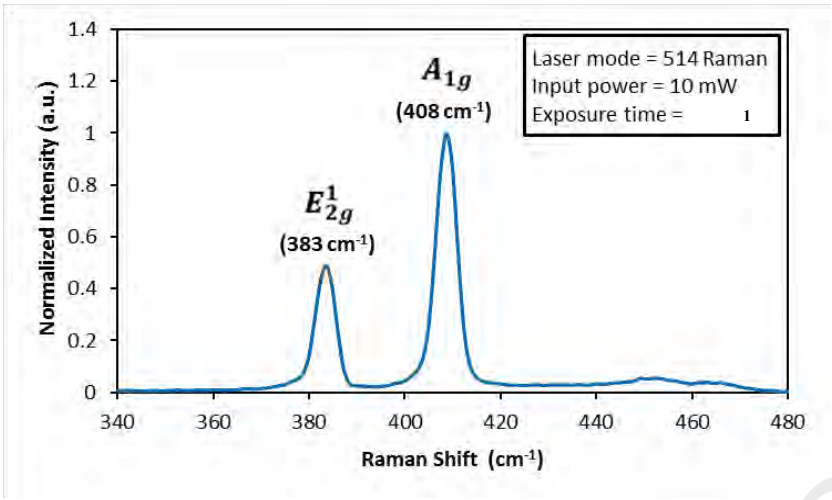

(a)

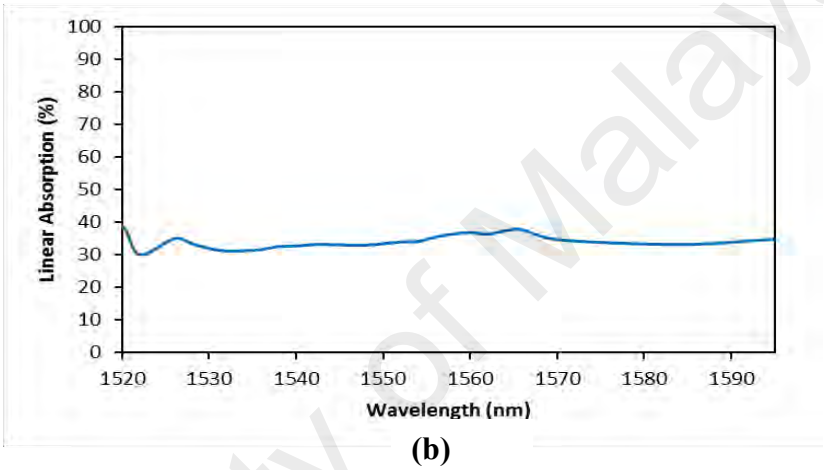

(b)

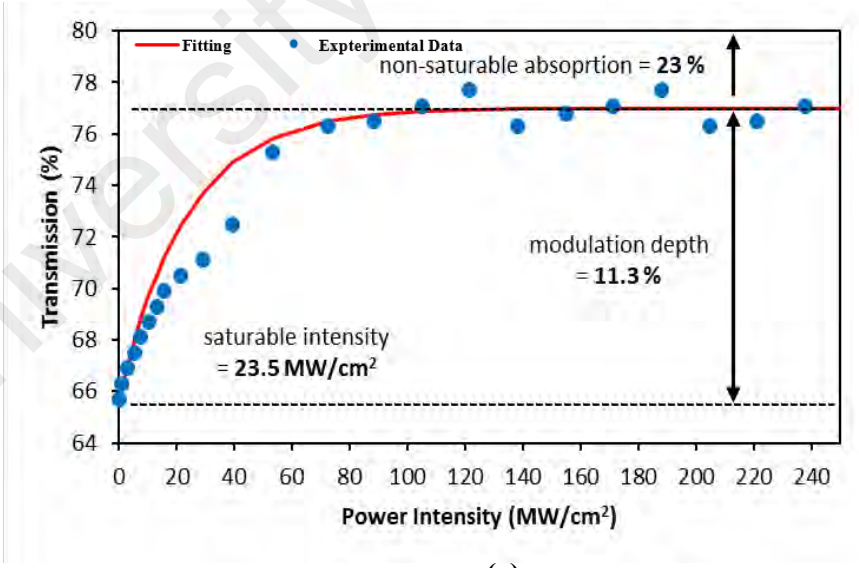

(c)

Figure 4.2: Optical characteristic of the MoS_2 tape; (a) Raman spectrum, (b) Linear absorption, and (c) Nonlinear transmission

4.2.2 Laser configuration

Figure 4.3 shows the experimental setup of the mode-locked EDFL using the fabricated MoS_2 based SA as the mode locker. The MoS_2 SA is integrated into the fiber laser cavity by sandwiching a ~1 mm × 1 mm piece of the composite tape between two fiber connectors, adhered with index matching gel. The mode-locked EDFL has total cavity length of 11.5 m which operates in anomalous fiber dispersion of -0.1151 ps^2. The cavity length consists of a 3 m long Erbium-doped fiber (EDF), 8.0 m long standard single mode fiber (SMF-28), and a segment of 0.5 m HI 1060 wavelength division multiplexer (WDM) fiber with group velocity dispersion (GVD) of 27.6, -21.7, and -48.5 ps^2/km, respectively. The EDF has core and cladding diameters of 4 μm and 125 μm respectively, a numerical aperture of 0.16 and Erbium ion absorption of 23 dB/m at 980 nm. It is pumped by a 980 nm laser diode (LD) via a 980/1550 nm WDM. An isolator is used in the laser setup to avoid backward reflection and ensure unidirectional propagation of the oscillating laser. The output laser is delivered through a 95/5 coupler which keeps 95% of the light oscillating in the ring cavity for both spectral and temporal diagnostics. The addition of a polarization controller (PC) enables adjustment of the polarization state within the cavity, but is not fundamental to the mode-locking. The optical spectrum analyzer (OSA) with a spectral resolution of 0.07 nm is used for spectral analysis of the mode-locked laser and an oscilloscope (OSC) is used to analyze the output pulse train of the mode-locking operation via a photo-detector.

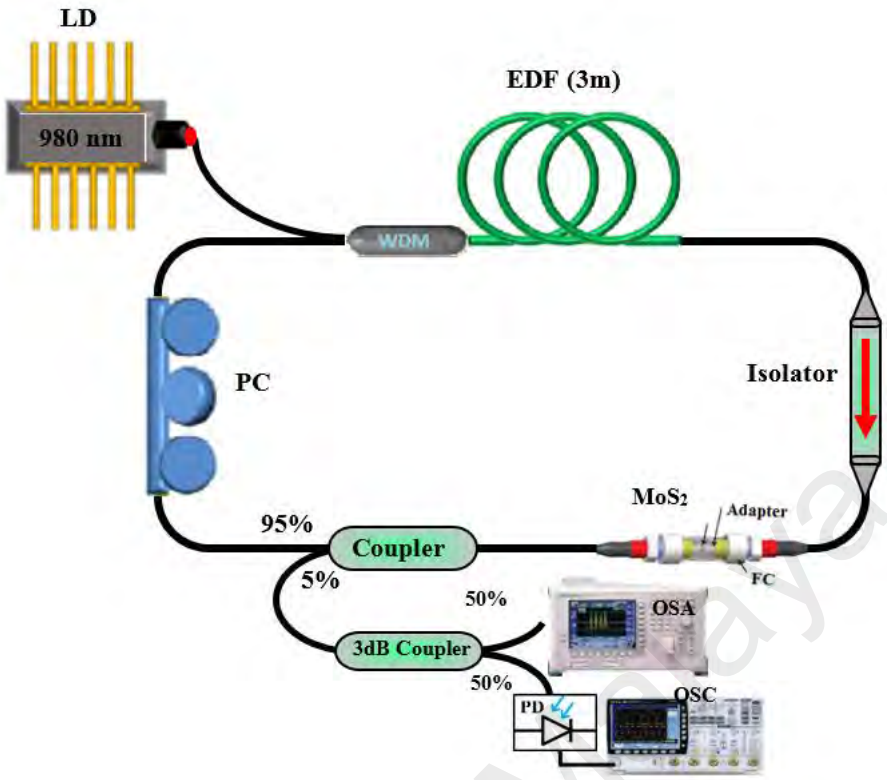

Figure 4.3: Schematic diagram of the proposed mode-locked EDFL with MoS_2 SA

4.2.3 Mode-locking performance

When the laser operation was initiated with pump power over threshold 36 mW, the laser first went into continuous wave (CW) operation. As the pump power was increased gradually to over 50 mW, the self-started soliton pulse was easily produced by carefully controlling the rotation of the PC. The MoS_2 SA was maintained stably without thermal damage with a stable repetition rate as the pump power was further raised to the maximum pump power of 110 mW. The pulse repetition rate was 17.1 MHz. The mode-locking pulse generation was due to the multilayer MoS_2 tape, which functioned as SA. The SA preferentially transmitted higher power and promoted the formation of a pulse from noise. We believe that in spite of operating at below the material bandgap, our MoS_2 SA initiated mode-locking because of saturable absorption from the edge-related sub-bandgap states (Zhang et al., 2015). Figure 4.4 shows the output spectrum of the soliton pulse, which

was obtained at a pump power of 110 mW. As shown in the figure, the soliton mode-locked pulse operates at a central wavelength of 1598.94 nm with a peak power of -26.5 dBm and 3 dB bandwidth of about 5.4 nm. The net cavity GVD in the laser cavity is anomalous, facilitating soliton pulse shaping through the interplay of GVD and self-phase modulation (SPM). This is confirmed by the observation of Kelly sidebands in the output spectrum, which appears due to resonant coupling interaction between soliton and dispersive wave components emitted after soliton perturbations. As shown in the figure, the Kelly sidebands are visible to the left and right within the center of soliton spectrum. Sidebands on the shorter wavelength from the center wavelength are indicated by '-1' (1588.5 nm, -17.3 dBm), whereas '+1' (1609.2 nm, -26.7 dBm) represents the sidebands on the longer wavelength. The Kelly sideband separation from the center of soliton spectrum is measured at approximately ± 10.26 nm. Based on the sideband separation (Nelson et al., 1997), Eq (3.2) the actual total dispersion is estimated to be -0.2016 ps^2, which is contributed by the three types of fiber used (EDF, SMF-28, HI 1060) and SA (MoS_2) dispersions. Based on this total dispersion value, the MoS_2 SA dispersion is calculated to be around – 0.0865 ps^2.

Figure 4.5 shows the corresponding pulse train at the maximum pump power of 110 mW, which shows the generation of soliton pulse train. It can be seen from the figure that the pulse train is quite uniform with a pulse period of 58.5 ns. The measured repetition rate of the pulses is approximately 17.1 MHz, which is about the same as the calculated value, taking into account the length and the refractive indices of the different fibers that make up the laser cavity. Figure 4.6 shows the autocorrelation trace of the soliton pulse, which takes on a $sech^2$ pulse profile with a pulse duration of 830 fs as measured at the full width half maximum (FWHM). This pulse duration, combined with the above mentioned spectral width, gives a time-bandwidth product (TBP) of ~0.526. The small deviation from the transform-limited TBP for $sech^2$ pulses of 0.315, indicates a chirp.

This chirp may partially be due to third-order dispersion. Another factor may be spectral filtering by the non-uniform erbium gain medium (Tamura et al., 1994). The present of third-order dispersion may have a negative impact on the generation of very short pulses and further study is required to investigate to the actual cause of the chirping. It is also observed that a small change of room temperature does not affect the stability of output mode-locking pulse train.

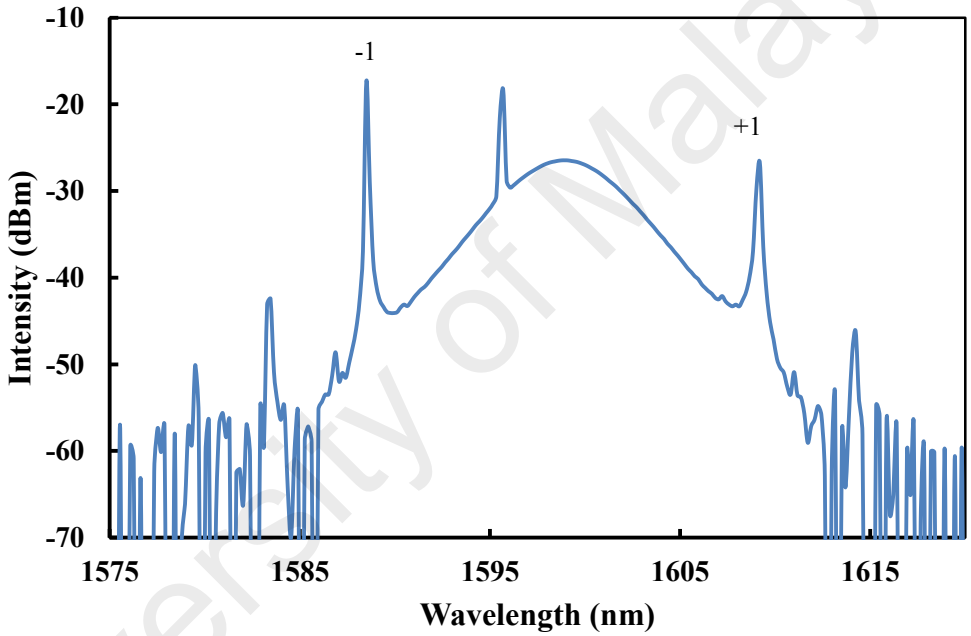

Figure 4.4: Optical spectrum of the soliton mode-locked at pump power of 110 mW

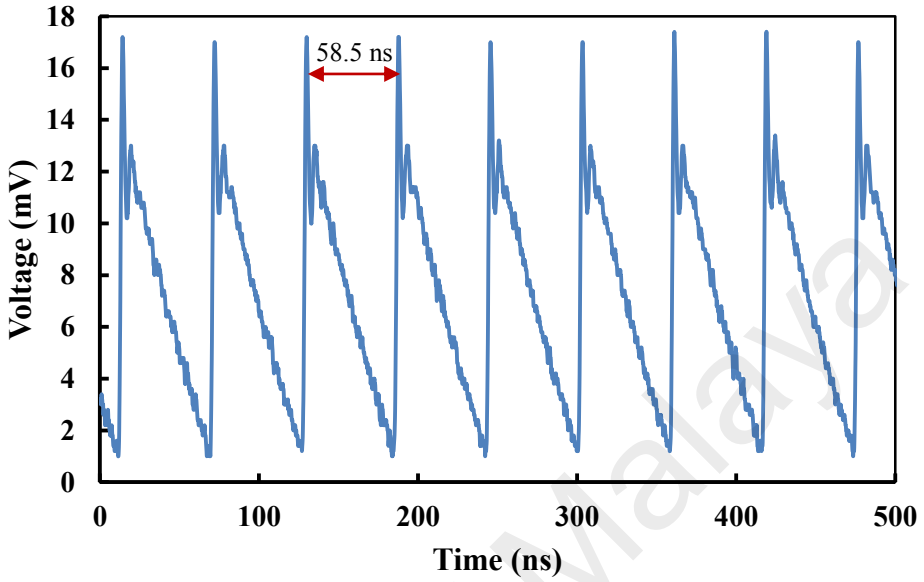

Figure 4.5: Oscilloscope trace of the mode-locked EDFL

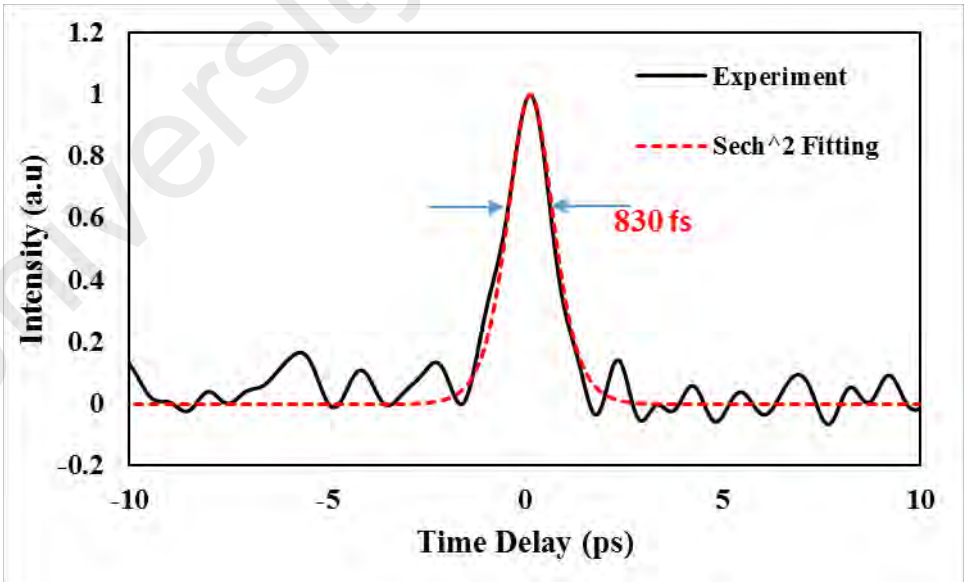

Figure 4.6: Autocorrelation trace of the soliton mode-locked EDFL

Both output power and pulse energy of the proposed mode-locked EDFL show a linear increase with pump power as shown in Figure 4.7. The maximum output power of 1.26 mW and pulse energy of 74 pJ are obtained at the maximum pump power of 110 mW. Laser stability is inferred from the radio frequency (RF) spectra (Peccianti et al., 2012). The RF spectrum for our laser is shown in Figure 4.8, which is recorded on a span of 100 MHz. The fundamental frequency obtained at 17.1 MHz, shows a high signal to background extinction ratio of ~41 dB. The RF spectrum also shows higher cavity harmonics without any noticeable sign of Q-switching instabilities, indicating the good mode-locking performance of the cavity (Zhang et al., 2015). These results show that MoS_2 and other similar 2D TMDs materials such as WS_2, $MoSe_2$, and $MoTe_2$, may have a great potential for applications in ultrafast photonics.

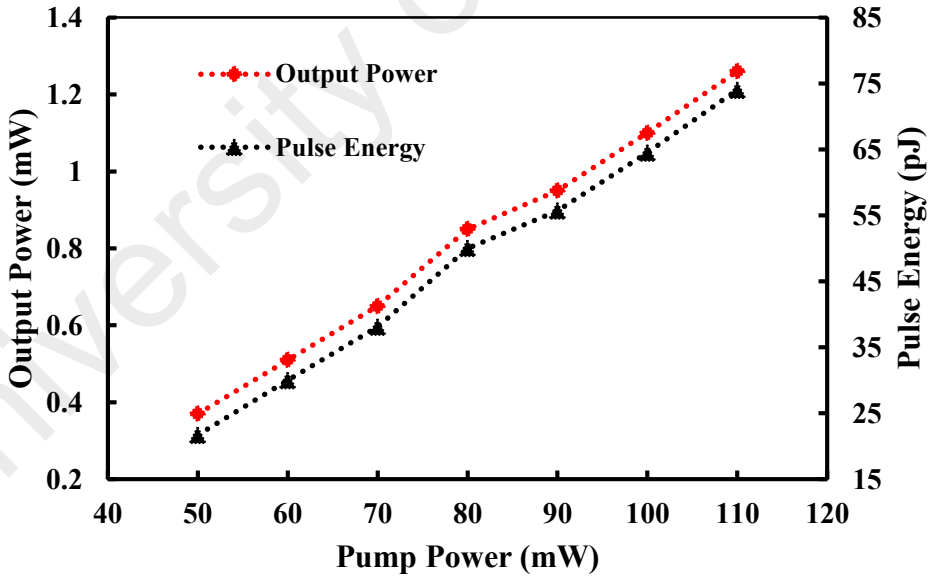

Figure 4.7: Average output power and pulse energy as a function of 980 nm pump power

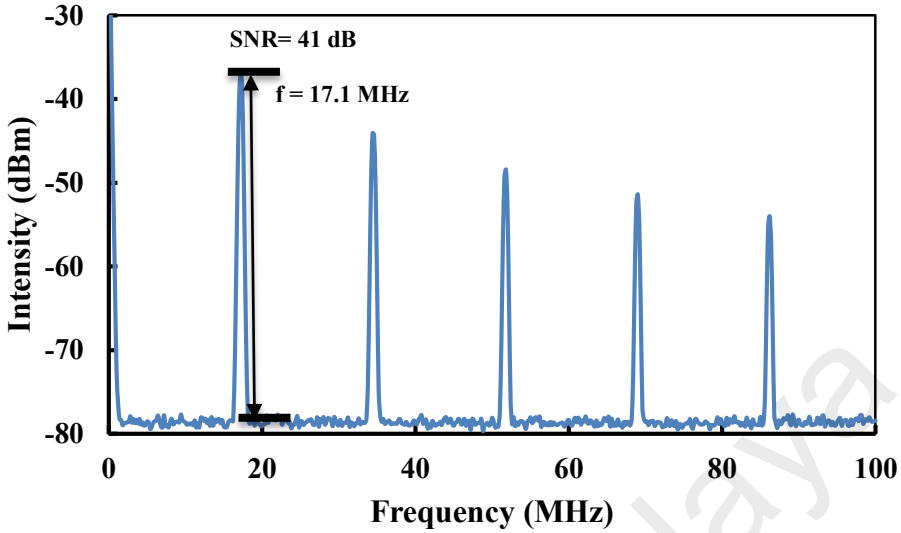

Figure 4.8: RF spectrum of the soliton mode-locked EDFL with a 100 MHz span

4.3 Femtosecond Fiber Laser With a Few-Layer MoS_2–PVA Thin Film SA in anomalous dispersion regime

In this section, a free-standing few-layer MoS_2 – polymer composite film is fabricated by liquid phase exfoliation (LPE) of chemically pristine MoS_2 crystals. The film is then used to demonstrate a soliton mode-locked EDFL. A stable self-started mode-locked soliton pulse is generated by fine-tuning the rotation of the polarization controller at a low threshold pump power of 25 mW. Its solitonic behavior is verified by the presence of Kelly sidebands in the output spectrum. The central wavelength, pulse width, and repetition rate of the laser are 1573.7 nm, 630 fs, and 27.1 MHz, respectively. The maximum pulse energy is 0.141 nJ with peak power of 210 W at a pump power of 170 mW. This result contributes to the growing body of work studying the nonlinear optical properties of TMDs that present new opportunities for ultrafast photonic applications.

4.3.1 Preparation and characteristics of MoS_2-polymer composite film

Liquid phase exfoliation (LPE) is a simple and low-cost method to produce large amounts of monolayer and few-layer 2D nanomaterials and no post-processing is required compared with chemical solution processing method. The LPE process for MoS_2 exfoliation consists of 2 steps as described in Figure 4.9. First, bulk MoS_2 crystals are mixed with a solvent that has a similar surface energy with the MoS_2 (~75 $mJ \cdot m^{-2}$) (Cunningham et al., 2012). In this work, Dimethylformamide (DMF) with an initial concentration of 5 mg/ml was used as the solvent. The second step is to apply ultrasound through a sonication process to exfoliate the material and produces a dispersed solution enriched with few-layer flakes (Hasan et al., 2010). The ultrasound creates local pressure variations that sufficient to overcome the weak van der Waals forces between the atomic layers of the bulk crystal (Coleman et al., 2011; Hasan et al., 2010). The MoS_2 dispersion was obtained by ultra-sonicating the solution for 24 hours. The resultant dispersion is centrifuged for 1 hour at 3000 rpm in a swinging bucket rotor. This process helps to sediment the un-exfoliated material as larger flakes descend more rapidly through the centrifuge cell than the exfoliated few-layer flakes (Bonaccorso et al., 2013). The upper 80 % of the dispersion, which now primarily contains few-layer flakes, is decanted for composite fabrication.

The free-standing MoS_2–polymer composite film is prepared by mixing 10 ml of the few-layer MoS_2 dispersion with 20 ml of aqueous polyvinyl alcohol (PVA) solution with a concentration of 10 mg/ml. The solution was obtained by dissolving 200 mg of PVA in 20 ml of deionized water. The MoS_2-PVA solution mixture, which is now 30 ml, is then stirred using a magnetic stirrer and heated continuously at a temperature of 80 °C till the solution is reduced to approximately 10 ml. This process takes approximately 7 hours to complete. The reduced MoS_2–PVA mixture is then poured into a glass substrate and dried

in an oven at ~80 °C for another 4 hours to form a ~40 µm thick free-standing composite film.

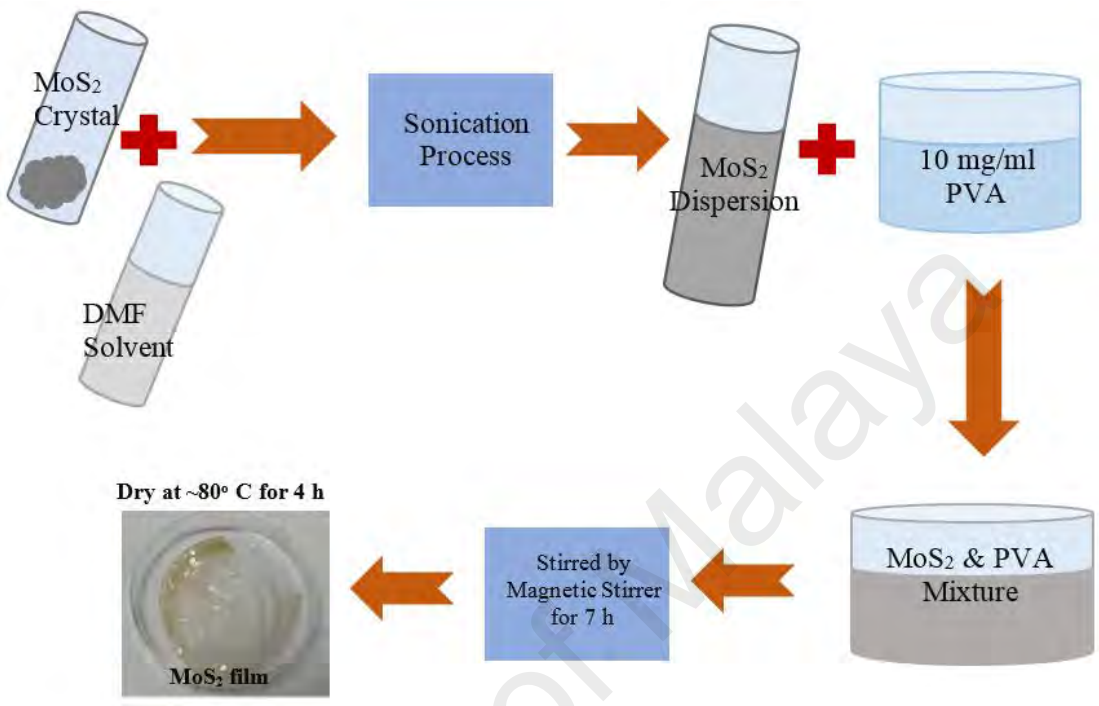

Figure 4.9: Fabrication procedures of MoS_2-PVA film

The field emission scanning electron microscopy (FESEM) in Figure 4.10 (a) can be used to determine the quality of the fabricated MoS_2-PVA film. The FESEM image clearly shows that the MoS_2 flakes were well dispersed in the PVA matrix. Raman spectroscopy was also performed on the 1 x 1 mm^2 piece of the fabricated MoS_2–PVA film and the result is shown in Figure 4.10 (b). The Raman spectrum is recorded by a spectrometer when a 514 nm beam of an Argon ion laser is radiated on the film for 10 seconds with an exposure power of 50 mW. As shown in the figure, the sample exhibits two characteristic peaks, in parallel with two phonon modes; the out-of-plane vibration of Sulfide atoms at 404 cm^{-1}, and in-plane vibration of Molybdenum and Sulfide atoms at 379 cm^{-1}, with a frequency difference of 25 cm^{-1}. It is observed that the A_{1g} mode due to the out-of-plane motion blue shifts after complete exfoliation, indicating that the few

layer MoS_2 with thicknesses in the range of 2~3 layers had been successfully fabricated (Lee et al., 2010; Li et al., 2012). The absence of a noticeable shift in the peak positions from those measured for the mechanically exfoliated MoS_2 indicates that the material structure is unaffected by its inclusion in the composite as shown in Figure 4.2 (a).

In order to further investigate the characteristics of the fabricated MoS_2 thin film, we measured the nonlinear optical response to confirm its saturable absorption via a transmission technique. A self-constructed mode-locked fiber laser (1567 nm wavelength, 0.9 ps pulse width, 15.1 MHz repetition rate) is used as the input pulse source as shown in Figure 4.10 (c). The transmitted power is recorded as a function of incident intensity on the device by varying the input laser power. The experimental data for absorption were prepared depending on the two-levels of SA model:

$$a(I) = \frac{\alpha_s}{1+I/I_{sat}} + \alpha_{ns} \tag{4.2}$$

where $a(I)$, α_s, I, I_{sat} and α_{ns} are stand for absorption, modulation depth, input intensity, saturation intensity, and non-saturation loss respectively. For the MoS_2 sample that was used in this work, the modulation depth, non-saturable intensity, and saturation intensity were measured to be approximately 9.7 %, 10.9 %, and 32 MW/cm^2, respectively.

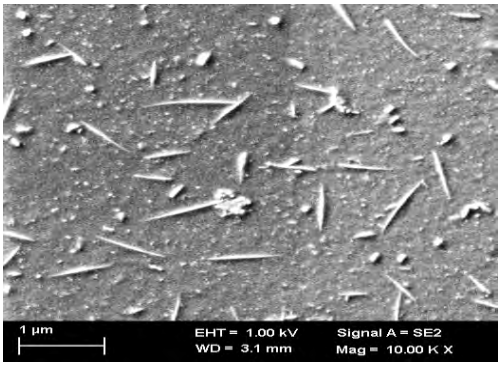

(a)

Figure 4.10: Characterization of the few-layer MoS_2-PVA: (a) FESAM image of the MoS_2-PVA, (b) Raman spectrum, (c) nonlinear saturable absorption profile

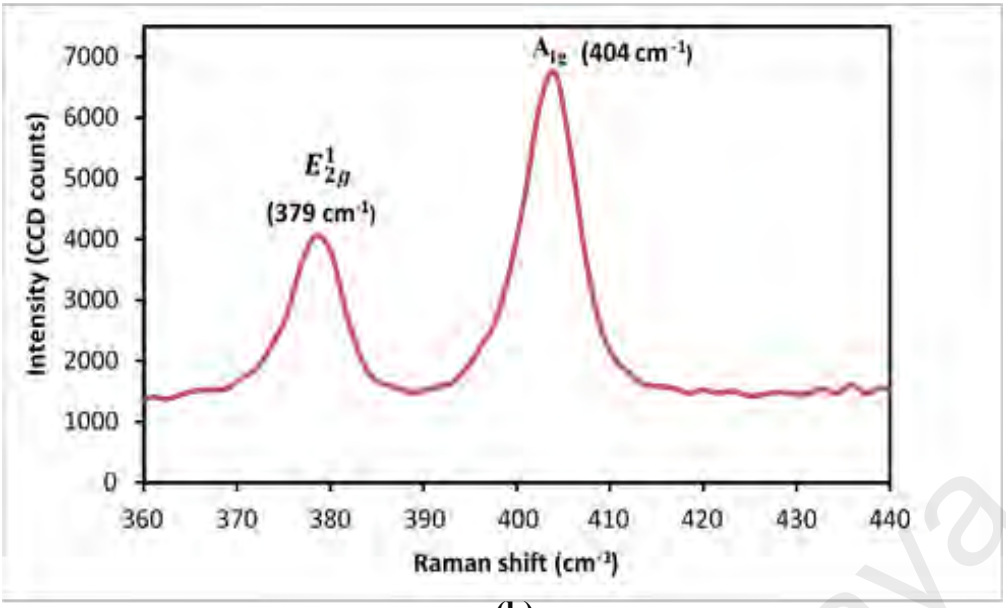

(b)

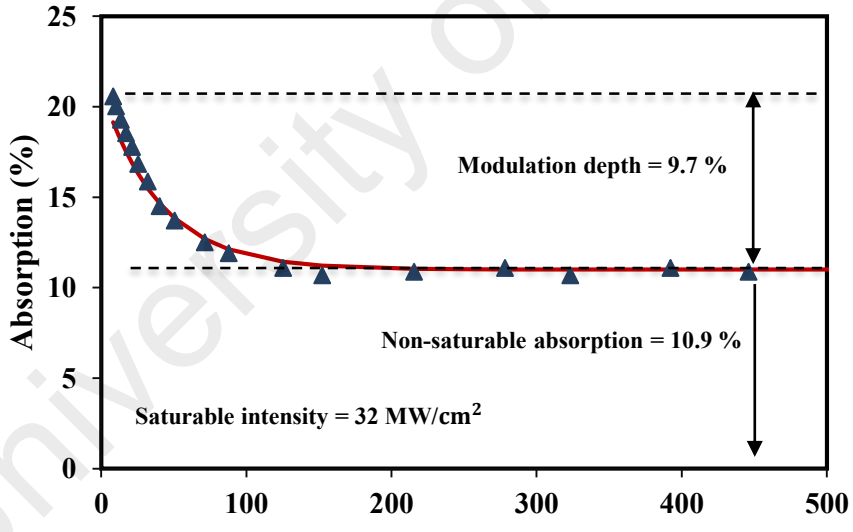

(c)

Figure 4.10, continued

4.3.2 Experimental setup for lasing

The fabricated free-standing MoS_2–PVA composite film was used to build and test an ultrafast laser. A soliton mode-locked EDFL was constructed with a resonator consisting of all-fiber integrated components for an alignment-free and compact system, as shown in Figure 4.11. The MoS_2-PVA SA is integrated into the fiber laser cavity by sandwiching a ~1 × 1 mm^2 piece of the fabricated film between two fiber connectors, adhered with index matching gel. The mode-locked EDFL has total cavity length of 7.3 m which operates in anomalous fiber dispersion of -0.094 ps^2. The cavity length consists of a 1.8 m long EDF, 5 m long standard single mode fiber (SMF-28), and a segment of 0.5 m HI 1060 WDM fiber with GVD of 27.6, -21.7, and -48.5 ps^2/km, respectively. The EDF has core and cladding diameters of 4 μm and 125 μm respectively, a numerical aperture of 0.16 and Erbium ion absorption of 23 dB/m at 980 nm. It is pumped by a 980 nm laser diode (LD) via a 980/1550 nm WDM. An isolator is used in the laser setup to avoid backward reflection and ensure unidirectional propagation of the oscillating laser. The output laser is delivered through a 95/5 coupler which keeps 95 % of the light oscillating in the ring cavity for both spectral and temporal diagnostics. The addition of a polarization controller (PC) enables adjustment of the polarization state within the cavity, but is not fundamental to the mode-locking. The 5% output connected to the OSA with a spectral resolution of 0.07 nm is used for spectral analysis of the mode-locked laser and an oscilloscope is used to analyze the output pulse train of the mode-locking operation via a photo-detector.

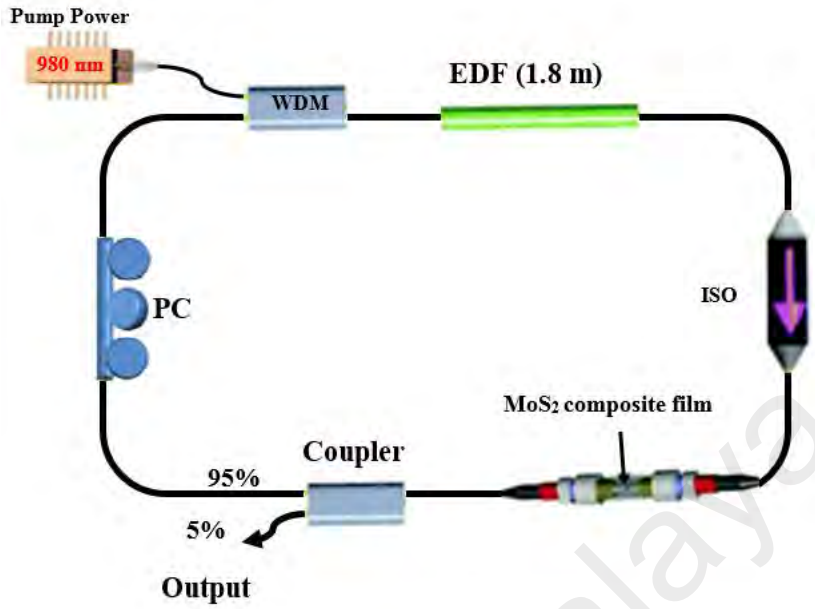

Figure 4.11: Experimental setup of the proposed mode locked EDFL configured with MoS_2-PVA based SA

4.3.3 Lasing performance

Since the MoS_2-PVA film SA has a relatively low insertion loss of ~1.05 dB, the laser operation was initiated at pump power threshold of 17 mW. At first, the laser went into continuous wave (CW) operation. As the pump power was increased gradually to over 25 mW, the self-started soliton pulse was easily produced by carefully controlling the rotation of the PC. The MoS_2-PVA SA was maintained stably without thermal damage with a stable repetition rate as the pump power was further raised to the available maximum pump power of 170 mW. The pulse repetition rate was 27.1 MHz, which was determined by the 7.3 m cavity length. The stable femtosecond mode-locked pulse generation was due to the MoS_2 composite film, which functioned as SA. The SA preferentially transmitted higher power and promoted the formation of a pulse from noise. I believe that in spite of operating at below the material bandgap, the developed MoS_2 SA initiated mode-locking because of saturable absorption from the edge-related sub-bandgap states (R Woodward et al., 2014).

Figure 4.12 shows the output spectrum of the mode-locked soliton pulse centered at 1573.7 nm with a peak power of -20.1 dBm and 3dB bandwidth of about 7.3 nm, which was obtained at a pump power of 170 mW. The net cavity GVD in the laser cavity is anomalous, facilitating soliton pulse shaping through the interplay of GVD and self-phase modulation (SPM). This is confirmed by the observation of Kelly sidebands in the output spectrum, which appears due to resonant coupling interaction between soliton and dispersive wave components emitted after soliton perturbations. As shown in the figure, the Kelly sidebands are visible to the left and right within the center of soliton spectrum. Sidebands on the shorter wavelength from the center wavelength are indicated by '-1' (1560.2 nm, -23 dBm), whereas '+1' (1586.3 nm, -17.7 dBm) represents the sidebands on the longer wavelength. It is also noticed that the presence of additional peaks around 1570 nm due to the phase difference between soliton pulse and dispersive waves, where the soliton pulse interferes constructively with the dispersive waves (Nelson et al., 1997). The Kelly sideband separation from the center of soliton spectrum is measured at approximately ± 13 nm. Based on the sideband separation (Smith et al., 1992), and Eq (3.2) the actual total dispersion is estimated to be -0.118 ps^2, which is contributed by the three types of fiber used (EDF, SMF-28, HI 1060) and SA (MoS_2) dispersions. Based on this total dispersion value, the MoS_2 SA dispersion is calculated to be around – 0.024 ps^2.

Figure 4.13 shows the oscilloscope trace of the soliton pulse at the maximum pump power of 170 mW. It can be seen from the figure that the pulse train is quite uniform with a pulse period of 36.9 ns. The measured repetition rate of the pulses is approximately 27.1 MHz, which is about the same as the calculated value, taking into account the length and the refractive indices of the different fibers that make up the laser cavity. Figure 4.14 shows the autocorrelation trace of the soliton pulse, which takes on a $sech^2$ pulse profile with a pulse duration of 630 fs as measured at the full width half maximum (FWHM). This pulse duration, combined with the above mentioned spectral width, gives a time-

bandwidth product (TBP) of ~0.557. Compared to the demonstrated MoS_2 mode-locked fiber laser (Liu et al., 2014; R Woodward et al., 2015; H Xia et al., 2014; Zhang et al., 2015), our pulse width is shorter at 25 mW threshold pump power.

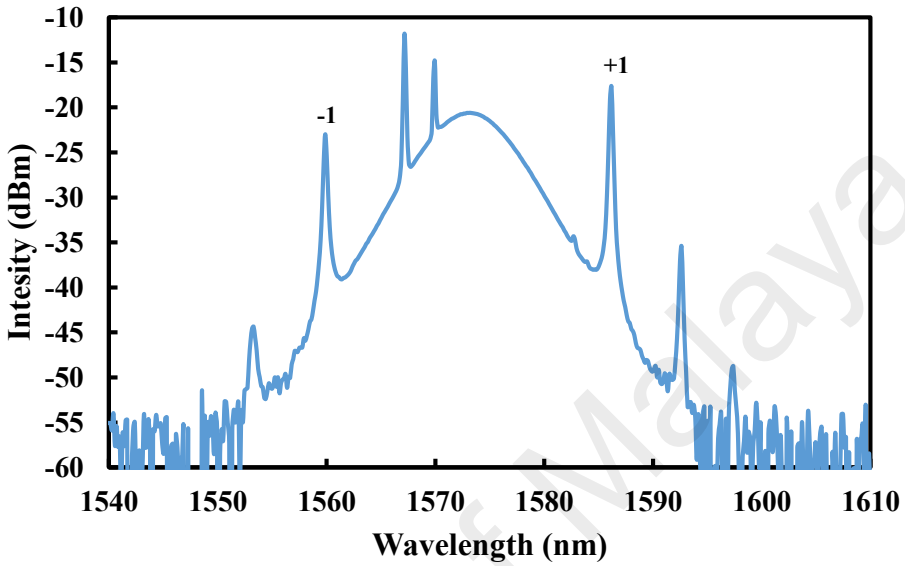

Figure 4.12: Optical spectrum of the proposed mode-locked EDFL at pump power of 170 mW

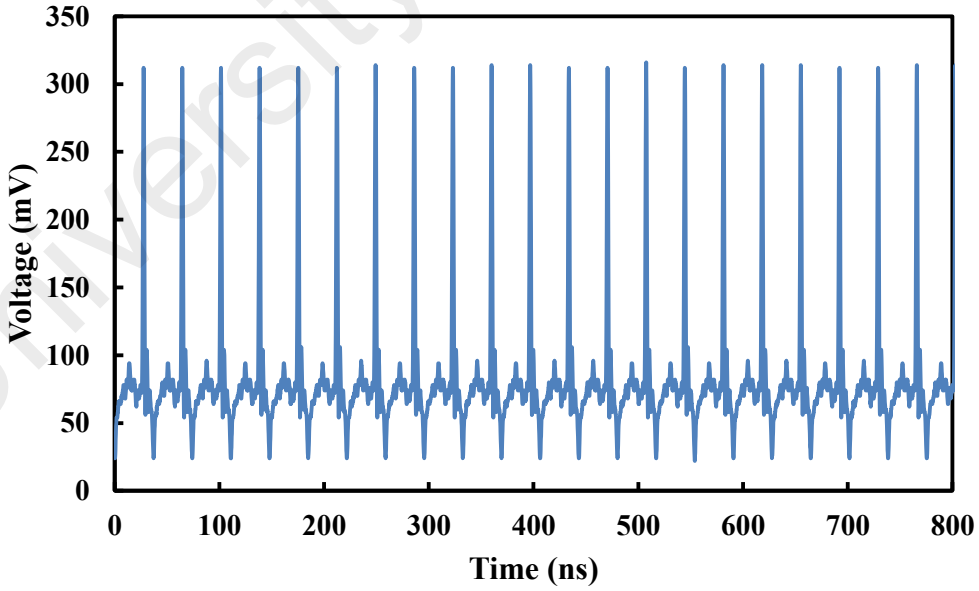

Figure 4.13: Oscilloscope trace of the mode-locked EDFL at pump power of 170 mW

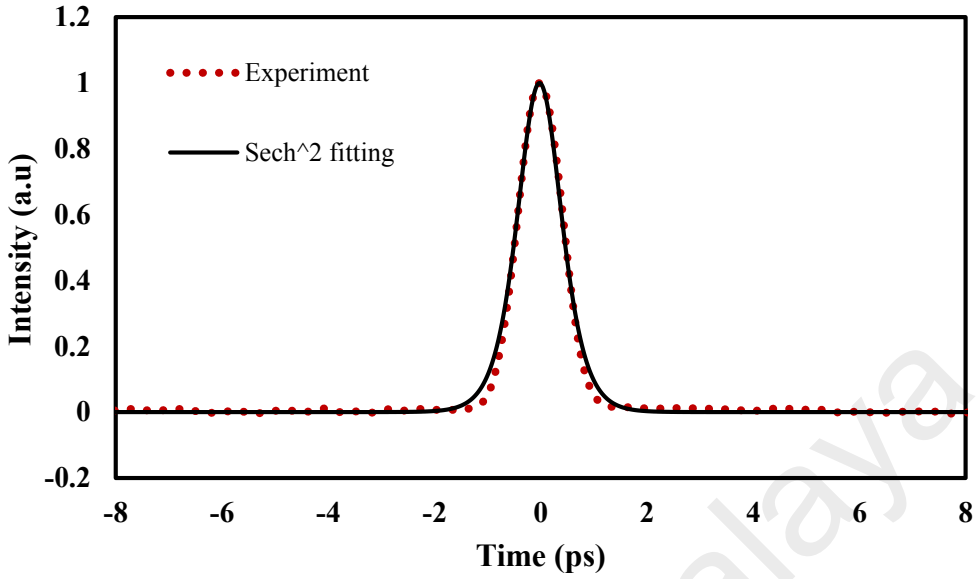

Figure 4.14: Autocorrelation trace of the soliton mode-locked EDFL at pump power of 170 mW

Figure 4.15 shows the average output power and pulse energy of the proposed mode-locked EDFL as a function of pump power. It is observed that both output power and pulse energy linearly increase with the pump power. At the maximum pump power of 170 mW, the average output power is 3.82 mW and thus the pulse energy and peak power are estimated at 0.141 nJ and 210 W respectively. Up to available 170 mW pump power, our MoS_2 film was working in a good condition. Laser stability is inferred from the radio frequency (RF) spectra. The RF spectrum for our laser is shown in Figure 4.16, which is recorded on a span of 200 MHz. The fundamental frequency obtained at 27.1 MHz, shows a high signal to background extinction ratio of ~61 dB which confirms the long-term stability of pulse for at least 24 hours. The RF spectrum also shows higher cavity harmonics without any noticeable sign of Q-switching instabilities, indicating the good mode-locking performance of the cavity. These results show that MoS_2 and other similar

2D TMDs materials such as WS_2, $MoSe_2$, and $MoTe_2$, may have a great potential for applications in ultrafast fiber lasers.

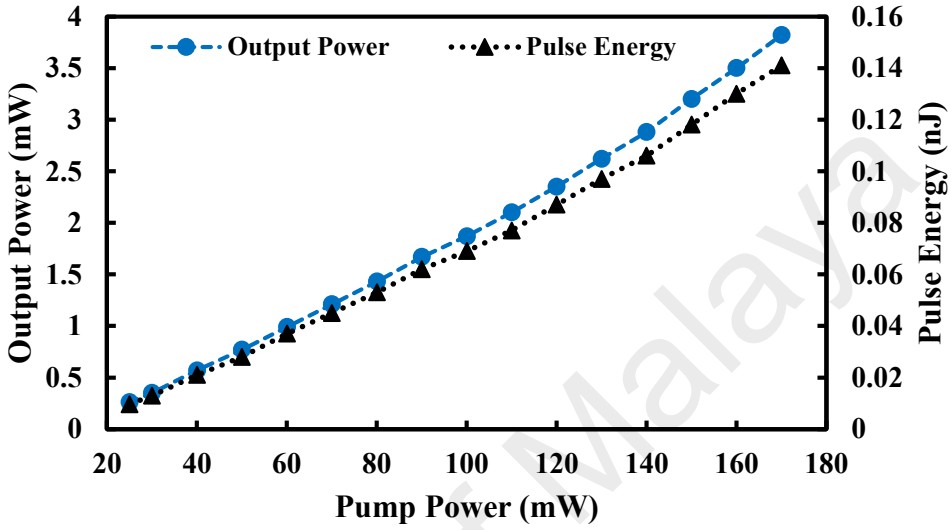

Figure 4.15: Average output power and pulse energy as a function of 980 nm pump power

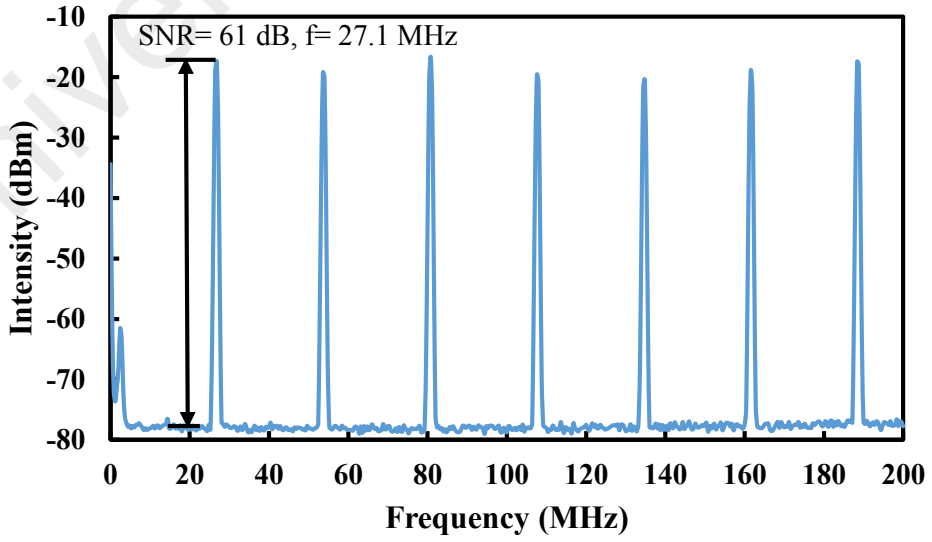

Figure 4.16: RF spectrum of the mode-locked EDFL with a 200 MHz span

4.4 Mode-Locking Pulse Generation with MoS_2-PVA Film SA in Ultra-Long Normal Dispersion Regime

As discussed in the previous section, the fabricated MoS_2-composite film has enabled the generation of self-started stable soliton mode-locked EDFL. In this section, we used the same MoS_2-PVA SA to achieve dissipative soliton mode-locked with a square pulse by adding a dispersion shifted fiber (DSF) in the cavity. By incorporating 850 m of DSF in the cavity, the dispersion is shifted from anomalous to the normal operating region. Stable dissipative soliton pulses with 90 ns pulse width are generated at the repetition rate of 231.5 kHz with a broad spectral width of 19.68 nm.

4.4.1 Experimental setup

The configuration of the proposed mode-locked EDFL is shown in Figure 4.17. The fabricated passive MoS_2-PVA SA is integrated into the laser cavity by sandwiching a ~1 × 1 mm^2 piece of the fabricated film between two fiber ferrules via a connector with an assistance of index matching gel. The cavity length consists of a 1.8 m long EDF, 4.5 m long standard single mode fiber (SMF-28), a segment of 0.5 m HI 1060 WDM fiber, and 850 m of DSF with a GVD of 27.6, -21.7, -48.5 ps^2/km and 5.1 ps^2/km respectively. The normal dispersion regime was achieved by adding 850 m of DSF in the cavity. The mode-locked EDFL has a total cavity length of 856.8 m which operates in normal fiber dispersion of 4.26 ps^2. The EDF used has a core diameter of 4 μm, numerical aperture (NA) of 0.16 and Erbium ion absorption of 23 dB/m at 980 nm. The active fiber is pumped by a 980 nm laser diode via a 980/1550 nm WDM. An isolator is incorporated in the ring cavity to prevent backward reflection so that unidirectional propagation of the oscillating laser is ensured. A PC is employed to adjust the polarization state of the oscillating light within the cavity. The output laser is routed out via a 95/5 coupler which keeps the majority of the light to continue oscillating. An optical spectrum analyzer (OSA) and an oscilloscope (OSC) are used for spectral and temporal measurement respectively. The

OSA has a spectral resolution of 0.07 nm while a fast photodetector is used to convert the optical into an electrical signal for the oscilloscope.

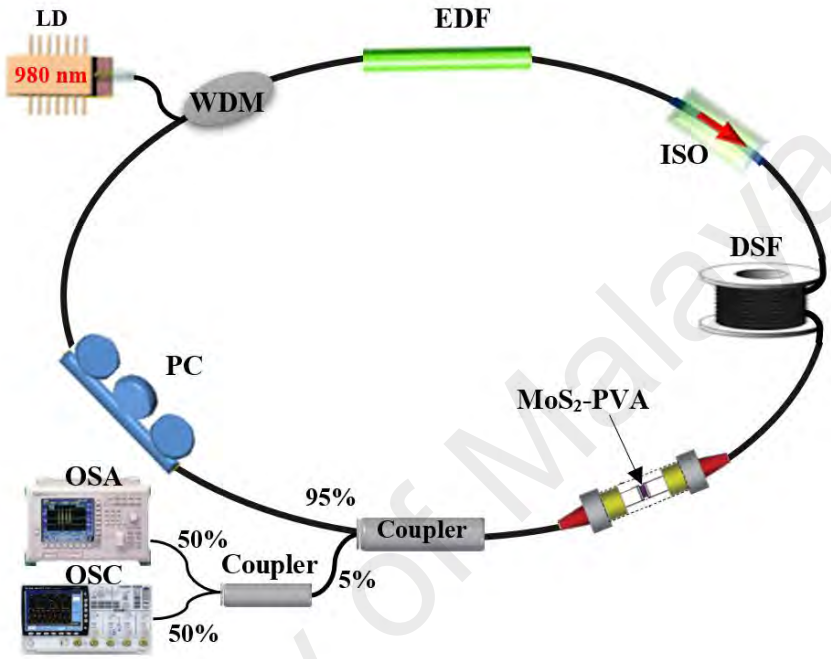

Figure 4.17: Experimental setup of the proposed mode-locked EDFL configured with MoS_2-PVA based SA and DSF

4.4.2 Lasing performance

Self-starting mode-locked pulse train was obtained with the use of the MoS_2-PVA composite film SA. The SA preferentially passed the light through at higher power to promote the formation of a mode-locking pulse from noise. The MoS_2 SA initiated mode-locking based on the saturable absorption characteristics of the edge-related sub-bandgap states. The laser started to operate at a pump power threshold of 42 mW due to the additional length of DSF, which caused insertion loss in the cavity compared to the pump power threshold for soliton mode-locked in section 4.3. Initially, the laser went into continuous wave (CW) operation but as the pump power increased above 50 mW, it

transformed into the self-started dissipative soliton pulse after carefully controlling the rotation of the PC. The MoS_2-PVA SA maintained a stable operation without thermal damage as the pump power was further increased to the maximum power of 170 mW. Figure 4.18 shows the optical spectra of the mode-locked EDFL at a pump power of 170 mW. Compare to the soliton mode-locked in the last experiment, a piece of 850 m DSF was added in this experiment to change the net dispersion of the cavity from anomalous to the normal regime. The laser generated mode-locked dissipative soliton pulses where the spectrum obtained is centered at 1567.44 nm with a 3 dB bandwidth of 19.68 nm. The pulse broadening in dissipative soliton spectrum is caused by self-phase modulation effect, which becomes pronounced with the incorporation of DSF.

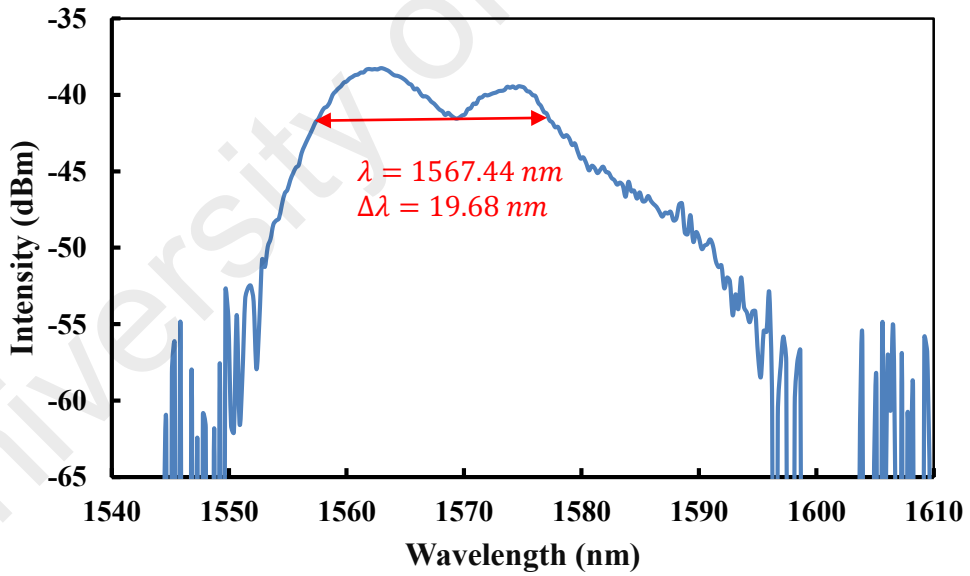

Figure 4.18: Optical spectra of the mode-locked EDFL with DSF at pump power of 170 mW

Figure 4.19 illustrates the dissipative soliton pulse characteristics. Figure 4.19 (a) shows a typical oscilloscope trace of the square pulse train at a lower repetition rate of 231.5 kHz as the DSF increases the cavity length. However, the pulse train is not uniform due to the fluctuation of the pulse peak power. Figure 4.19 (b) focuses on a single pulse with a pulse duration of 90 ns. As seen in the figure, at the maximum pump power of 170 mW, the square pulse holds a distinct square characteristic where its pulse width is maintained constantly. The square shape of the pulse is still maintained from the pump power of 50 mW to 170 mW. However, the ripple is observed at the top of the square pulse. This is due to the fluctuation of gain in the ultra-long cavity needed to compensate for the loss. In order to check the internal structure of the generated square pulse, an auto-correlator was used to measure the pulse profile. No pulse is observed in picosecond region which indicates that there is no internal structure in the square pulse. We believe the square pulse is due to the dissipative soliton resonance phenomenon which normally occurs in the long cavity fiber laser (Chang et al., 2008).

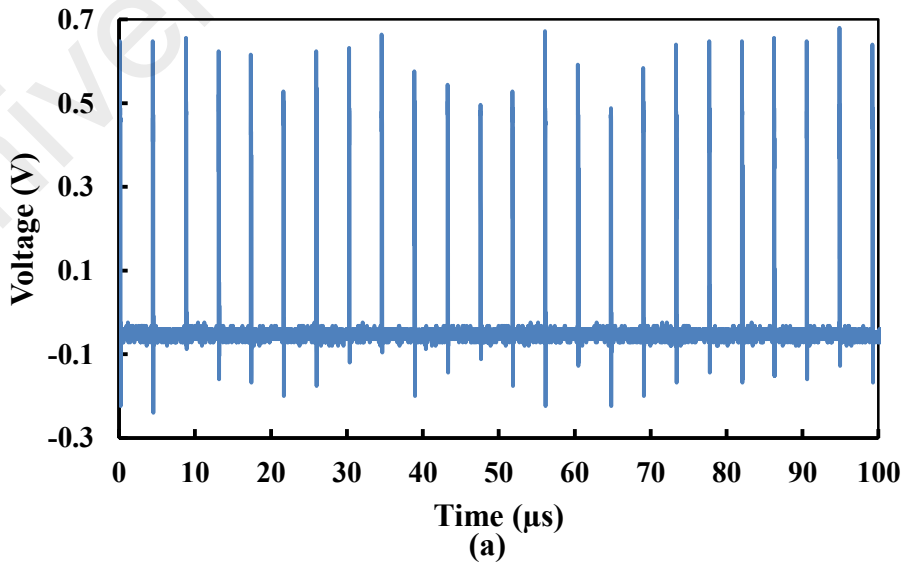

Figure 4.19: Dissipative soliton pulse characteristics: (a) Typical pulse train at pump power of 170 mW, (b) single square pulse envelop

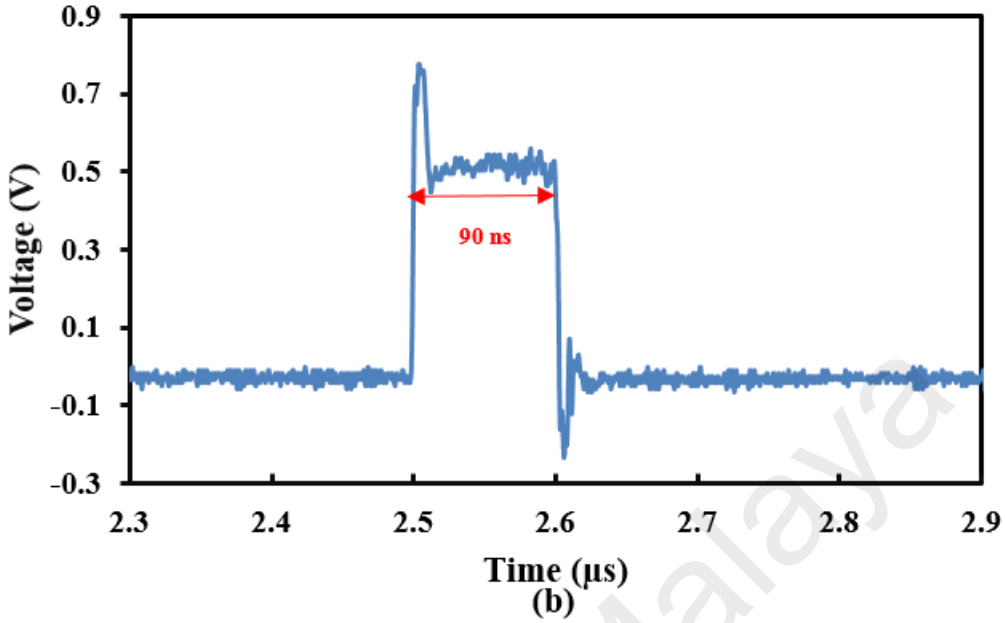

Figure 4.19, continued

Figure 4.20 exhibits the radio frequency (RF) spectrum of the dissipative pulse soliton with a resolution bandwidth of 30 kHz. The fundamental frequency of 231.5 kHz and a signal to noise ratio (SNR) of ~35 dB confirm the long-term stability of the pulse for at least 24 hours. It is observed that the SNR of the dissipative soliton laser is lower compared to the normal soliton. This is attributed to the longer cavity used which significantly increases the noise. However, the RF spectrum indicates a stable operation of the laser without showing Q-switching instability. Figure 4.21 shows the average output power and pulse energy of the dissipative soliton mode-locked EDFL at various pump power. We can observe that the output power and pulse energy are linearly related with the pump power. An average output power of 0.58 mW and the pulse energy of 2.5 nJ are obtained at the maximum pump power of 170 mW. These results affirm that the MoS_2-PVA SA enables the generation of highly stable self-started dissipative soliton

mode-locking EDFL. This type of mode locked lasers have widespread applications in many fields, e.g., laser spectroscopy, biomedical diagnostics.

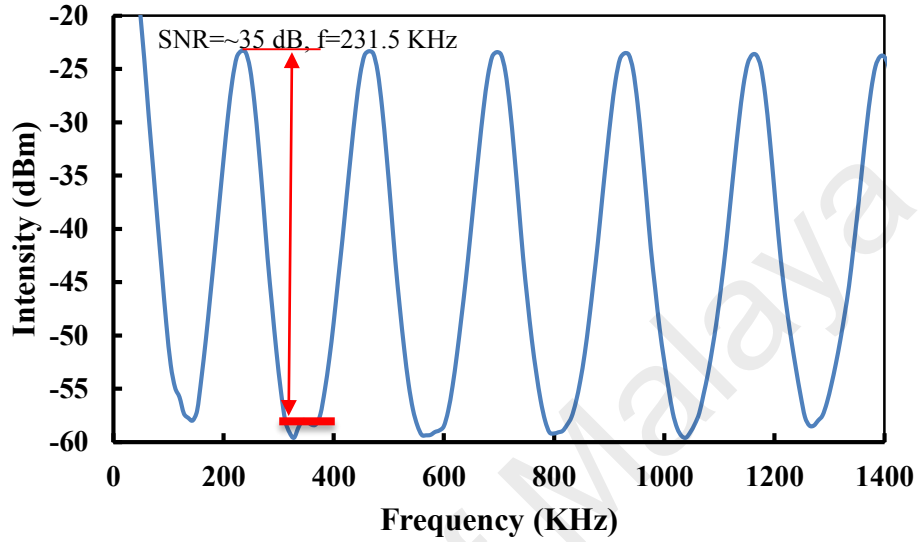

Figure 4.20: RF spectrum of the dissipative soliton mode-locked EDFL

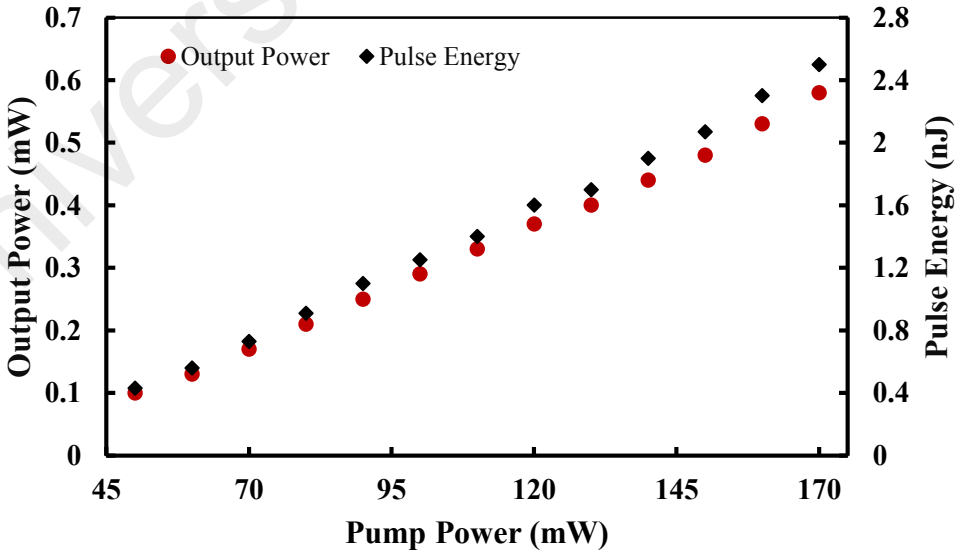

Figure 4.21: Average output power and pulse energy as a function of 980 nm pump power

4.5 Summary

In this chapter, various types of mode locking operations have been demonstrated based on MoS_2 with different fabrication techniques, which included soliton and dissipative soliton mode-locked EDFLs. First, the MoS_2 SA is prepared by mechanical exfoliation technique. The exfoliated acquired MoS_2 flakes are fixed onto the end surface of a standard FC/PC fiber connector. A soliton mode-locked EDFL pulse is generated in an anomalous regime with estimated net dispersion of -0.1151 ps^2 at 1598.94 nm wavelength with a repetition rate of 17.1 MHz and pulse width of 830 fs. Second, a free-standing few-layer MoS_2 polymer composite is fabricated by liquid phase exfoliation of chemically pristine MoS_2 crystals. By using the MoS_2-SA film based EDFL, a stable 630 fs pulse operates at 1573.7 nm wavelength with fundamental repetition of 27.1 MHz was achieved in anomalous dispersion regime with a net dispersion of -0.094 ps^2. On the other hand, by inserting a 850 m long dispersion shifted fiber (DSF) in the cavity, a dissipative soliton with square pulse train is obtained in the normal dispersion regime with net dispersion of 4.26 ps^2, where the operating wavelength is centered at 1567.44 nm with a 3dB bandwidth of 19.68 nm, repetition rate of 231.5 KHz and pulse width of 90 ns. These results indicated that the MoS_2-SA could be used as a simple, low cost, low insertion loss, ultrafast saturable absorption device for ultrafast photonic applications.

CHAPTER 5: BLACK PHOSPHORUS SATURABLE ABSORBER

5.1 Introduction

The up growth of graphene, which is a typically two-dimensional (2D) material has pointed out another group of nanomaterials with extraordinary physical properties, and afterward refreshed our typical perspectives on nanotechnology, and even opened up another field with novel possibilities for testing and acknowledging conceptually new optoelectronic devices (Bonaccorso et al., 2010; AK Geim et al., 2007). At first, research in 2D nanomaterials concentrates on graphene, a topological insulator (Bi_2Te_3, Bi_2Se_3) and the wide band-gap transition metal dichalcogenides (TMDs) materials (MoS_2, $MoSe_2$) (Castro Neto et al., 2011; Mas-Balleste et al., 2011; Sobon et al., 2012; Wang et al., 2012). Each type of 2D nanomaterials has some essential advantages for specific applications. However, the absence of band-gab nature in graphene has limited its intrinsic interest for photonic and electronics applications. Various solutions have been applied to open the bandgap in graphene using complicated techniques which make them less attractive for particular applications (Balog et al., 2010; Y Zhang et al., 2009). These restrictions lead to the comprehensive research on other 2D nanomaterials which can complement graphene. For instance, TMDs have been demonstrated for photonic applications as SAs. In the previous chapter, various mode-locked EDFLs have been demonstrated using MoS_2 based SA.

Recently black phosphorus (BP) has been rediscovered as a new promising material for various optoelectronics and electronics applications (F Xia et al., 2014). BP is a layered material consisting of only phosphorus atoms, which is the most thermodynamically stable allotrope and its structure is like graphite where the phosphorene monolayers are bound with van der Walls interactions to form layered crystals of BP (Nishii et al., 1987). It has recently joined the family of 2D materials same as graphene and TMDs such as MoS_2 which was investigated and applied in ultrafast fiber

lasers as SAs (Churchill et al., 2014; Du et al., 2014; Lu et al., 2015; Sotor, Sobon, Macherzynski, et al., 2015; H. Zhang et al., 2014). Its band-gap relies on the number of layers from 0.3 eV (bulk) to 2.0 eV (single layer) (Tran et al., 2014). Compared to graphene which has zero band-gap and MoS_2 which owns indirect band-gap at multilayer form, BP has the direct transition for all thicknesses, which shows a significant benefit for optoelectronic applications, especially at the long wavelength range. In addition, it can offer a broad tuning range of band-gap with a number of layers, and bridge nearly the entire range of between the zero band-gap of graphene and the large band-gap of TMDs. The broadband nonlinear optical response in multi-layer BPs has also been verified (Lu et al., 2015).

This chapter demonstrates Q-switched and mode-locked erbium-doped fiber laser (EDFLs) using a multi-layer BP based SA, which is obtained by mechanical exfoliation method. Since the BP consists of only the elemental phosphorus, it could be easy to peel off by using mechanical exfoliation technique. In this work, the SA is prepared by peeling bulk-structured BP 2D thin layers using a scotch tape. By inserting a small piece of the BP-SA tape into the different EDFL cavities, either Q-switching or mode locking pulses are obtained. Mechanical exfoliation is advantageous mainly because of its simplicity and reliability, where the entire fabrication process is free from complicated chemical procedures and costly instruments.

5.2 Preparation and Characterization of Black Phosphorus

In this work, the BP-SA was prepared by mechanical exfoliation method, which has been extensively developed for graphene and other 2D nanomaterials based ultra-fast fiber laser applications (Martinez et al., 2011; Sotor et al., 2014). Mechanical exfoliation method has advantages of simplicity and reliability, where the entire fabrication process is free from complicated chemical procedures and costly instruments. Figure 5.1 describes the preparation of BP based SA using mechanical exfoliation method. As shown in the figure, relatively thin flakes were peeled off from a big block of commercially available BP crystal (purity of 99.995 %) using a clear scotch tape. Then, we repeatedly pressed the flakes stuck on the scotch tape so that the BP flakes become thin enough to transmit light with high efficiency. Then we cut a small piece of the BP tape and attached it onto a standard FC/PC fiber ferrule end surface with index matching gel. The complete preparation process was done very fast in less than 2 minutes. After connecting it with another FC/PC fiber ferrule with a standard flange adapter, the all-fiber BP based SA was finally ready.

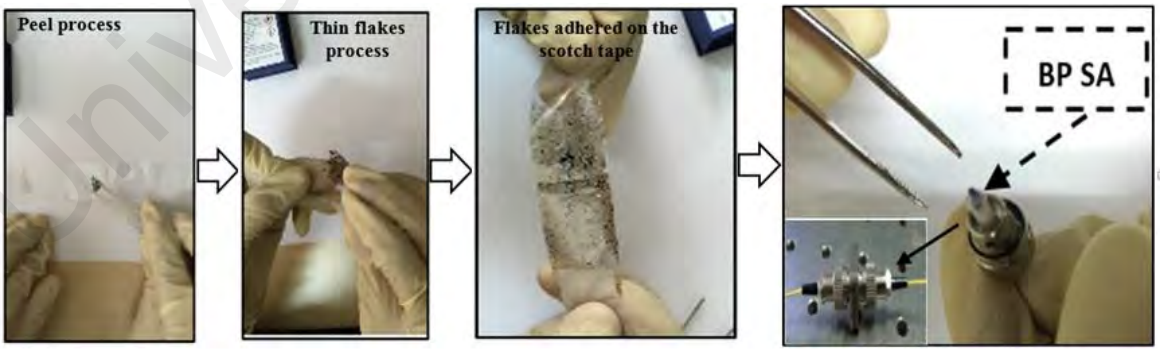

Figure 5.1: The preparation flow of BP-SA using mechanical exfoliation method

BP-SAs have been prepared with different thicknesses while the quality of the BP tape was verified by using Field Emission Scanning Electron Microscopy (FESEM). Figure 5.2 (a) shows the FESEM image, which indicates the existence of the uniform layers and confirms the absence of > 1μm aggregates or voids in the composite SA. These microscopic aggregates may increase the non-saturable scattering losses. We also performed Raman spectroscopy on the fabricated BP tape sample. Figure 5.2 (b) shows the Raman spectrum, which is recorded by a spectrometer when a 514 nm beam of an Argon ion laser is radiated on the tape for 10 s with an exposure power of 10 mW. As shown in the figure, the sample exhibits three distinct Raman peaks at 359 cm^{-1}, 437 cm^{-1} and 465 cm^{-1}, corresponding to A_g^1, B_{2g} and A_g^2 vibration modes of layered BP (Sugai et al., 1985). While the B_{2g} and A_g^2 modes correspond to the in-plane oscillation of phosphorus atoms in BP layer, the A_g^1 mode corresponds to the out-of-plane vibration. The ratio between A_g^1 peak and silicon (Si) level at 520 cm^{-1} estimates the thickness of BP flake as ~ 200 nm. The thickness for single-layer BP was about 0.8 nm, thus the prepared BP based SA is expected to consist of about 200 to 300 layers (Castellanos-Gomez et al., 2014). The A_g^2 peak at 465 cm^{-1} also confirms the large number of layers (Guo et al., 2015).

(a)

Figure 5.2: Characterization of the exfoliated black phosphorus layers, transferred onto the tape: (a) FESAM image of the BP tape, (b) Raman spectrum of the multi-layered BP tape

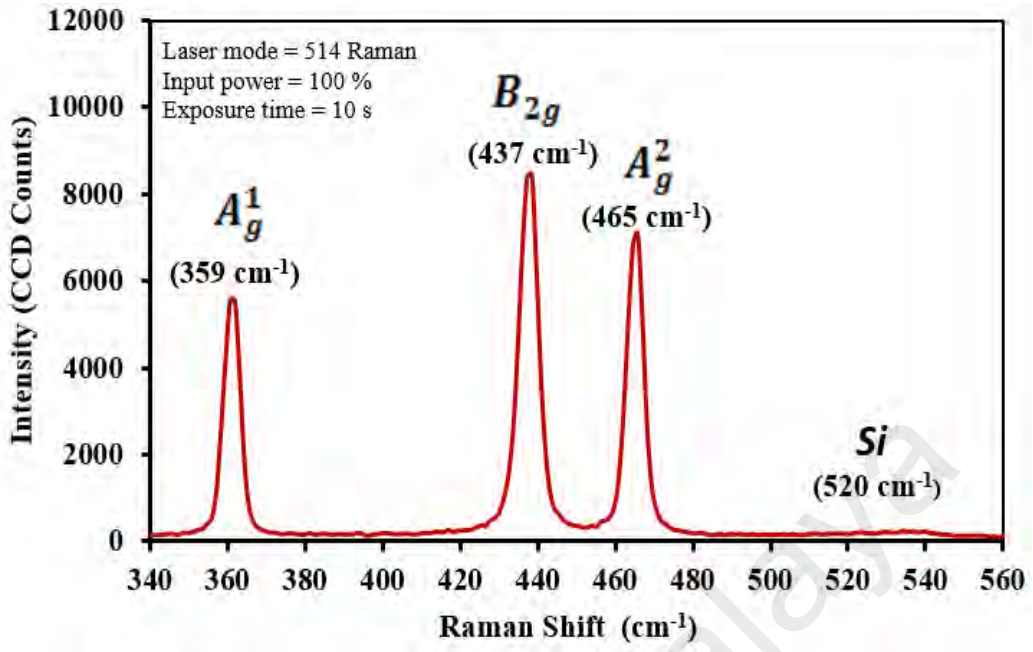

(b)

Figure 5.2, continued

The nonlinear optical response property for the multilayer BP on the scotch tape is then investigated to confirm its saturable absorption with different thicknesses. In the investigation, a self-constructed mode-locked fiber laser operating at 1557 nm wavelength with 1.5 ps pulse width and 17.4 MHz repetition rate, was used as the input pulse source as shown in Figure 5.3 (a). The transmitted power and also a reference power for normalization are recorded as a function of incident intensity on the tape by varying the input laser power. Figures 5.3 (b) and (c) show the nonlinear response for thick and thin samples, respectively. With increasing peak intensity, the material absorption decreases as shown in both figures, confirming the saturable absorption. The experimental data for absorption are fitted according to a simple two-level SA model (Mu et al., 2015);

$$\alpha(I) = \frac{\alpha_s}{1+I/I_{sat}} + \alpha_{ns} \qquad (5.1)$$

where α(I) is the absorption, α_s is the modulation depth, I is the input intensity, I_{sat} is the saturation intensity, and α_{ns} is the non-saturable absorption. The modulation depth and saturation intensity of two BP-SAs are obtained at 6.1 % and 0.30 MW/cm^2 for thick sample as shown in Figure 5.3 (b). On the hand, the thinner sample provides modulation depth and saturation intensity of 7% and 0.25 MW/cm^2 respectively as shown in Figure 5.3 (c). Taking into account its nonlinear optical response leading to absorption saturation at relatively low fluence, the mechanically exfoliated BP meets basic criteria of a passive SA for fibre lasers.

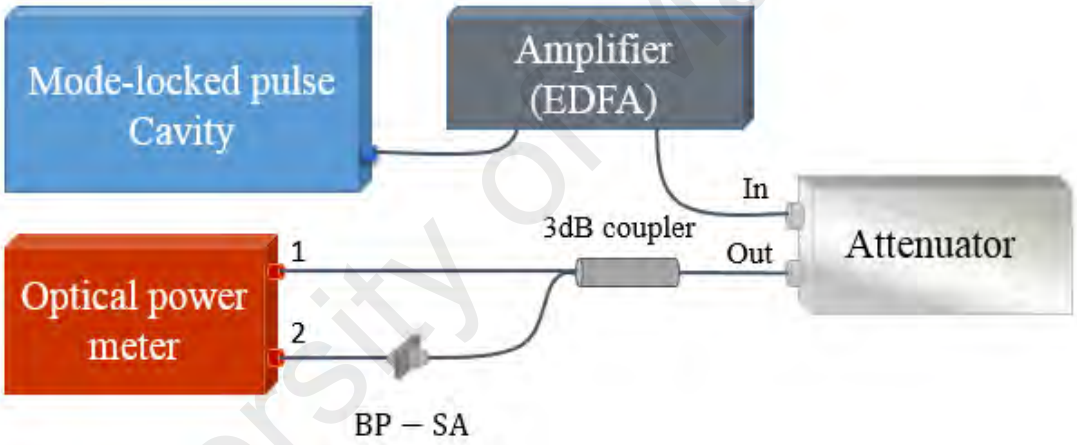

(a)

Figure 5.3: (a) Configuration for measuring the nonlinear absorption, and nonlinear saturable absorption profile showing saturable absorption for (b) thick and (c) thin BP-SAs

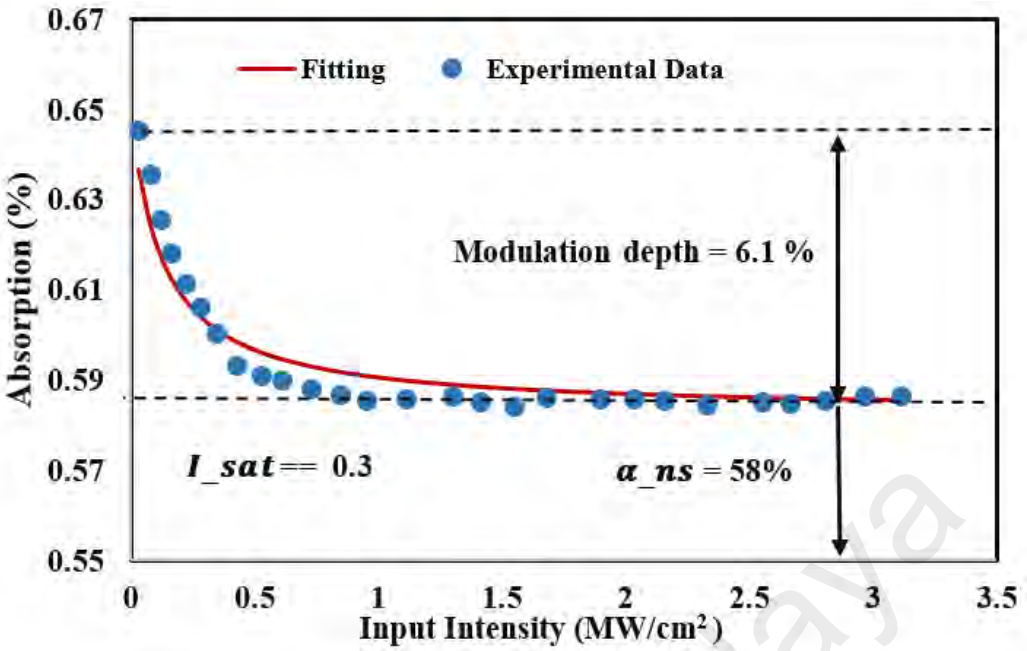

(b)

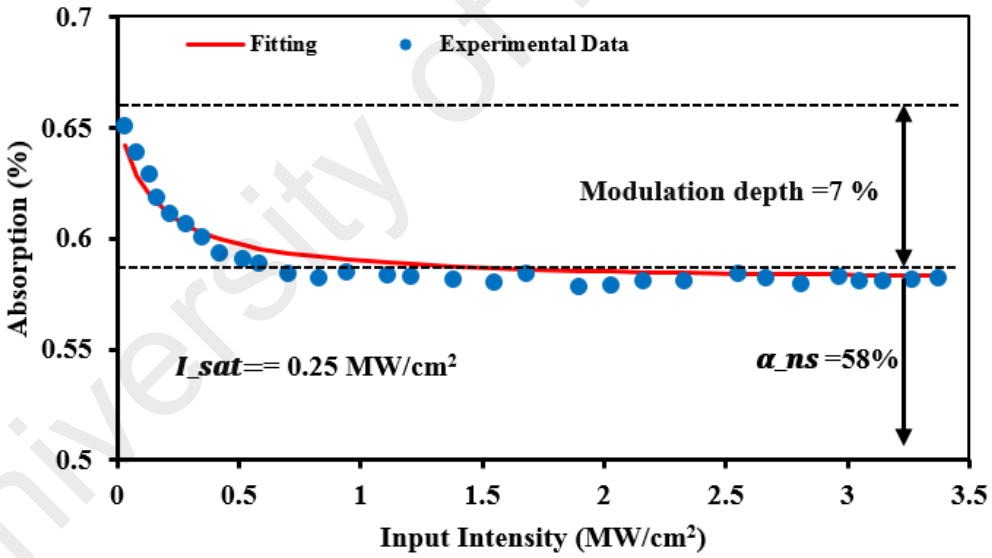

(c)

Figure 5.3, continued

5.3 Q-switched EDFL Using Black phosphorus As Saturable Absorber

To test the passively Q-switching ability of the BP-SAs, the first BP-SA with a modulation depth of 6.1 % and saturation intensity of 0.30 MW/cm^2 was integrated in an erbium doped fiber ring laser with a cavity configuration as shown in Figure 5.4. The ring EDFL employs a 3 m long Erbium-doped fiber (EDF) as the gain medium. The EDF has core and cladding diameters of 4 µm and 125 µm respectively, a numerical aperture (NA) of 0.16 and Erbium ion absorption of 23 dB/m at 980 nm. It is pumped by a 980 nm laser diode (LD) via a 980/1550 nm wavelength division multiplexer (WDM). An isolator is used in the laser setup to avoid the backward reflection and ensure unidirectional propagation of the oscillating laser. All the components are made of single mode fiber (SMF-28) or pigtailed with SMF-28 with a length of 9 m. The total cavity length of the laser is 12 m. The output laser is tapped via a 50/50 coupler which keeps 50% of the light oscillating in the ring cavity. The optical spectrum analyzer (OSA) with a spectral resolution of 0.07 nm was used for the spectral analysis of the wavelength Q-switched laser and an oscilloscope (OSC) was used to analyze the output pulse train of the Q-switching operation via a photo-detector (PD).

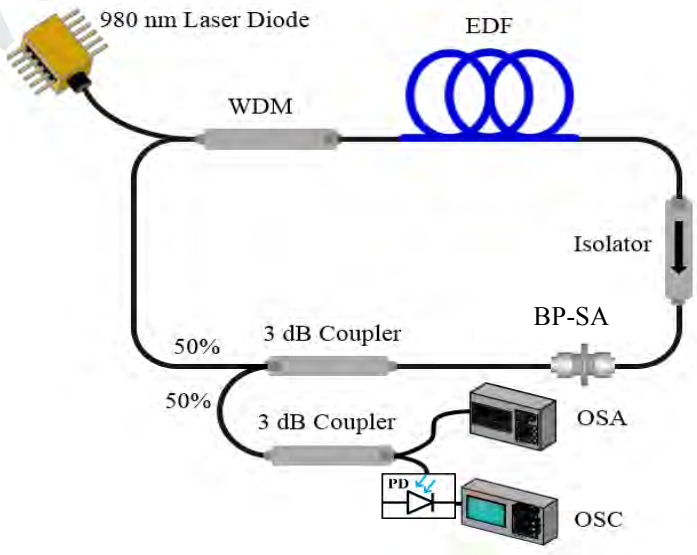

Figure 5.4: Configuration of the Q-switched EDFL using BP based SA

The performance of the EDFL cavity was then investigated by varying the 980 nm pump power. Initially, the EDFL starts to generate continuous wave (CW) laser as the pump power reached 46 mW, but as the pump power is further increased above 50 mW, it transformed into a self-started Q-switched pulse. As the pump power was increased to the available maximum power of 170 mW, the BP SA were maintained stably without thermal damage. Figure 5.5 shows the typical spectrum of Q-switched operation at pump power of 170 mW. The output optical spectrum centered at 1552.9 nm with a 3dB spectral bandwidth 0.05 nm. Figure 5.6 (a) shows the oscilloscope trace of the Q-switched pulse train obtained by BP SA at pump power of 170 mW. The pulse period is measured to be around 22.5 µs. The Q-switching operation is also stable since we didn't observed any distinct amplitude modulation in the entire Q-switched envelop of the spectrum. This indicates that the self-mode locking effect on the Q-switching is weak. Figure 5.6 (b) depicts the enlarged single envelop of the pulse train, which indicated the pulse width of 7.04 µs.

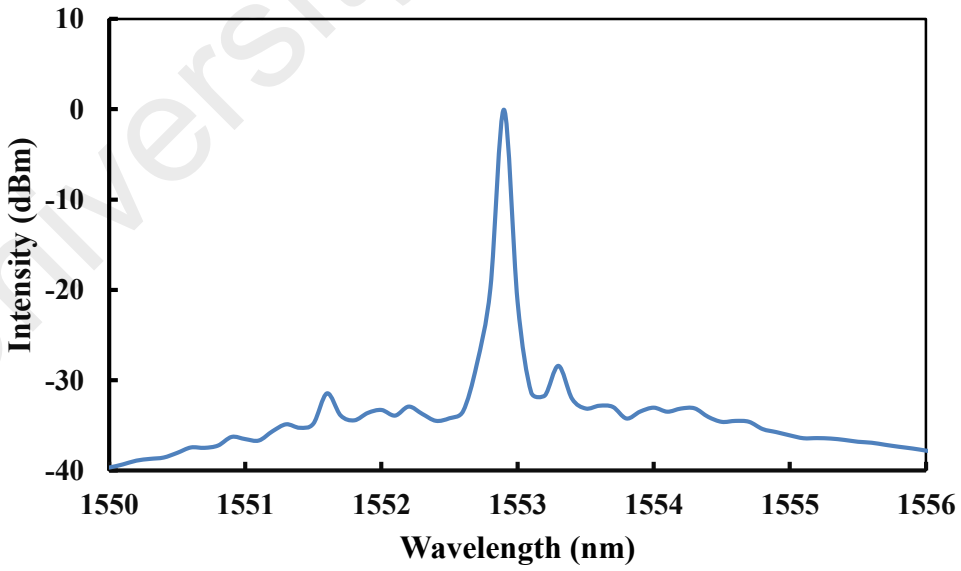

Figure 5.5: Optical spectra of the Q-switched EDFL with BP SAs at pump power of 170 mW

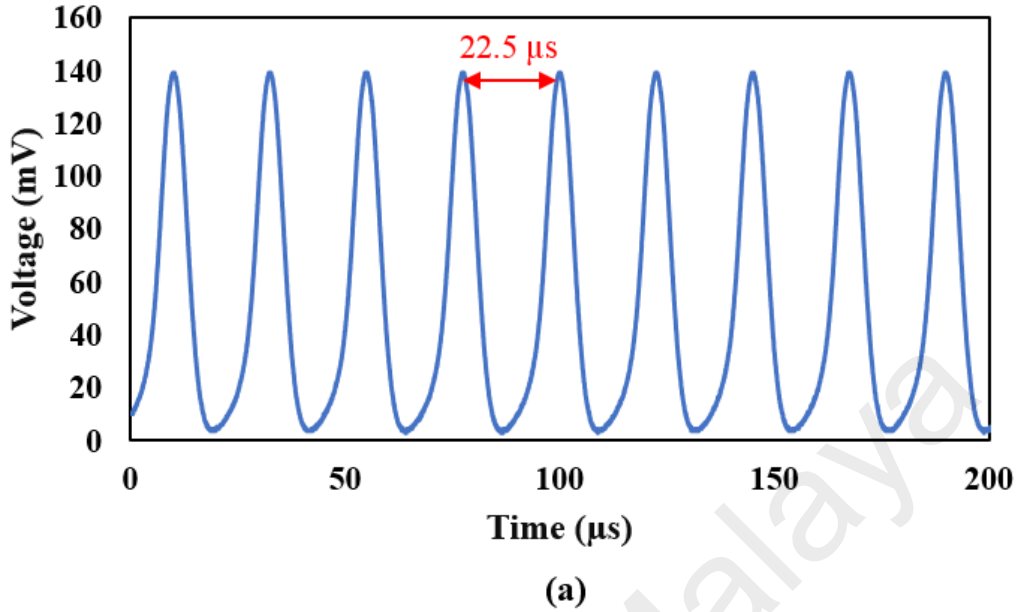

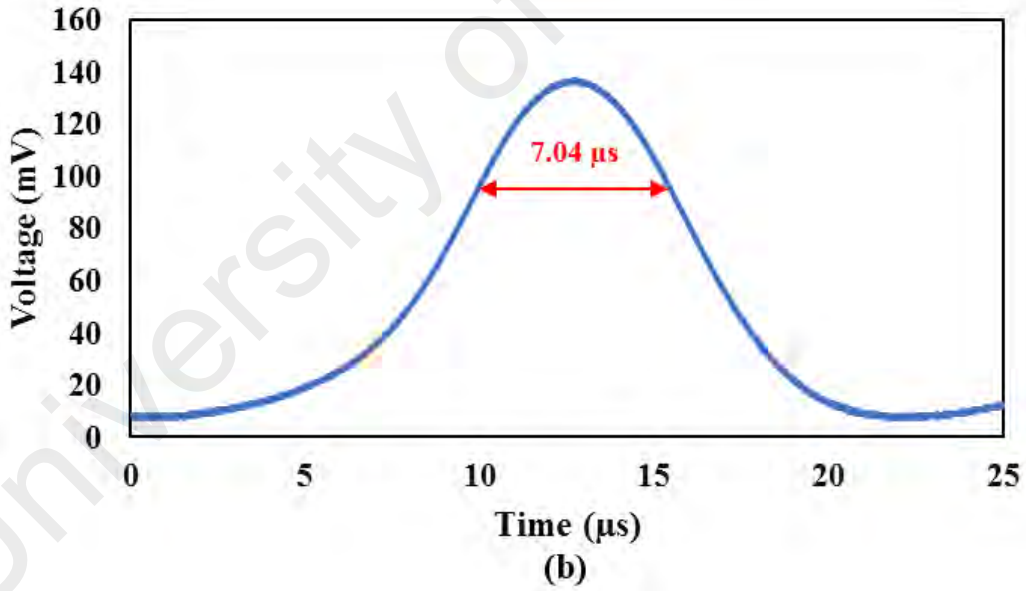

Figure 5.6: Typical Q-switched pulse emitted from the EDFL with BP at pump power of 170 mW. (a) oscilloscope trace of the Q-switched pulse train (b) single-pulse profile

According to the theory of passive Q-switching with SA, the repetition rate as well as the pulse width changes with the changing of incident pump power. Figure 5.7 shows the relationship between the repetition rate and pulse width with the pump power. By varying the 980 nm laser pump from 50 mW to 170 mW, the pulse repetition rate is seen to increase linearly with the pump power, while the pulse width decrease almost linearly. The repetition rate could be widely varied from 9.1 to 44.33 KHz, while its pulse width reduced from 20.75 to 7.04 µs. The pulse width is expected to drop further if the pump power increased more, as long as the damage threshold of the SA is not exceeded.

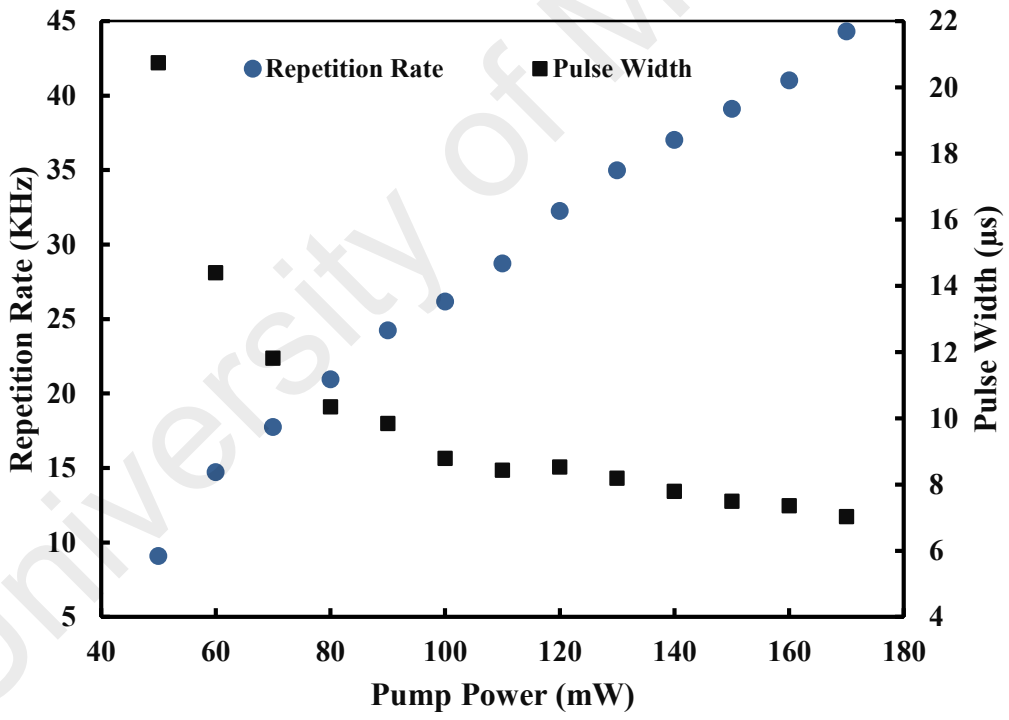

Figure 5.7: Repetition rate and pulse width of the Q-switched EDFL as functions of pump power

The average output power as well as single pulse energy of Q-switched EDFL at different pump power are shown in Figure 5.8. As shown in the figure, the average output power rose almost linearly with the increment of the pump power. The pulse energy was calculated based on the measured average output power and the repetition rate. The maximum output power was 5.94 mW, while the maximum pulse energy was 134 nJ at a pump power of 170 mW. Due to the limited output power of the pump 170 mW, we could not measure the exact damage threshold of the BP SA. Compared to the demonstrated Q-switched fiber lasers our pulse width and pulse energy for BP-SA have been improved, where Chen et al. reported pulse width of 10.32 μs and pulse energy of 94.3 nJ, also Ismail et al. demonstrated pulse width and pulse energy of 5.52 μs and 50 nJ respectively (Y Chen et al., 2015; Ismail et al., 2016). To investigate the laser stability, we characterize the radio frequency (RF) spectra. Figure 5.9 displays the RF spectra of the lasers, which is recorded in a span of 180 KHz and a resolution bandwidth (RBW) of 3 KHz. The fundamental repetition rates is 44.33 kHz. The corresponding signal to noise ratios (SNR) is ~50 dB, which indicating good Q-switching stability.

These results clearly show that BP has a big potential for superior Q-switching and saturable absorption by optimizing the SAs parameters of the layer and the different cavity design. Also the fabrication of the SA is simple and thus the cost of the laser should be low. The simple and low cost laser is suitable for applications in metrology, optical communication, environmental sensing and biomedical diagnostics.

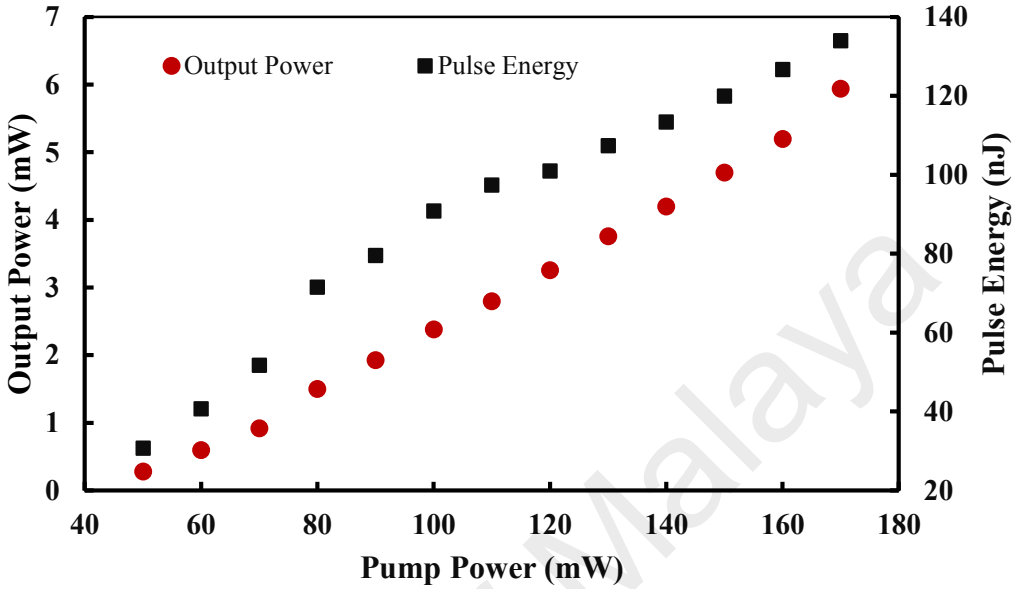

Figure 5.8: Average output power and pulse energy versus incident pump power for Q-switched EDFLs

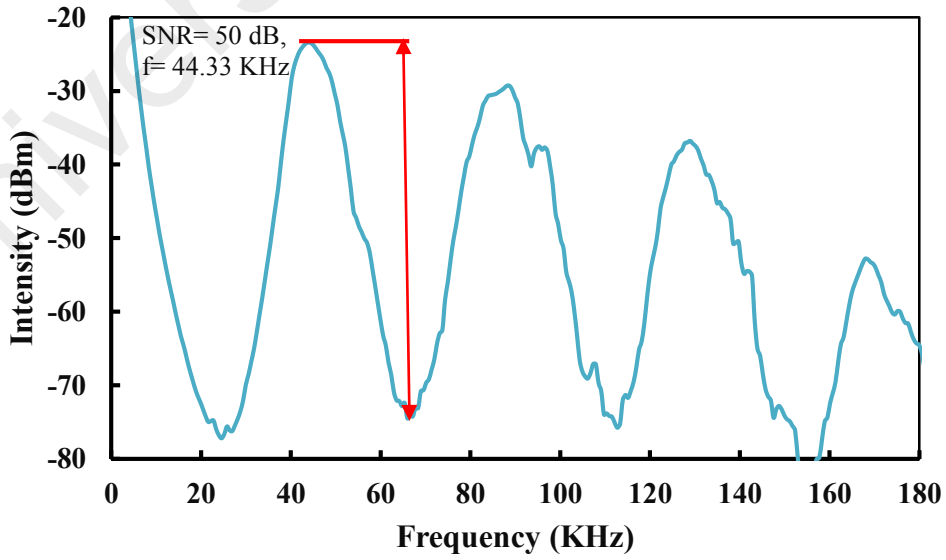

Figure 5.9: RF spectra of the Q-switched EDFLs at pump power of 170 mW

5.4 Ultrafast EDFL Mode Locked With a Black Phosphorus Saturable Absorber

Another passive BP SA that has modulation depth of 7% and saturable intensity of 0.25 MW/cm^2 was then integrated in another cavity to function as a mode-locker. The configuration of the proposed mode locked EDFL is schematically shown in Figure 5.10. The gain medium is a 3 m long EDF with same specifications in the Q-switched configuration and group velocity dispersion (GVD) of 27.6 ps^2/km. The cavity consists of the EDF, a segment of 0.5 m HI 1060 wavelength division multiplexer (WDM) fiber with GVD of - 48.5 ps^2/km, a 20 m long standard single mode fiber (SMF-28) incorporated into the cavity to increase the non-linearity and dispersion and other components such as output coupler, the BP-SA and optical isolator. All the components made of SMF-28 or pigtailed with SMF-28 with long of 5.5 m. The GVD parameter of SMF-28 is - 21.7 ps^2/km. The total cavity length of the mode-locked EDFL is 29 m, which operates in anomalous fiber dispersion of -0.495 ps^2. The active fiber is pumped by a 980 nm laser diode (LD) via a 980/1550 nm WDM. An isolator is incorporated in the ring cavity to prevent backward reflection so that unidirectional propagation of the oscillating laser is ensured. The 80/20 coupler is used to extract the output laser, which keeps the 80% of the light to continue oscillating. The OSA with a spectral resolution of 0.07 nm is used to analyze the spectrum of the mode locked laser, an oscilloscope (OSC) via a fast photo-detector (PD) is used to analyse the output pulse train of the mode locking operation and auto-correlator (AC) for monitoring the pulse duration.

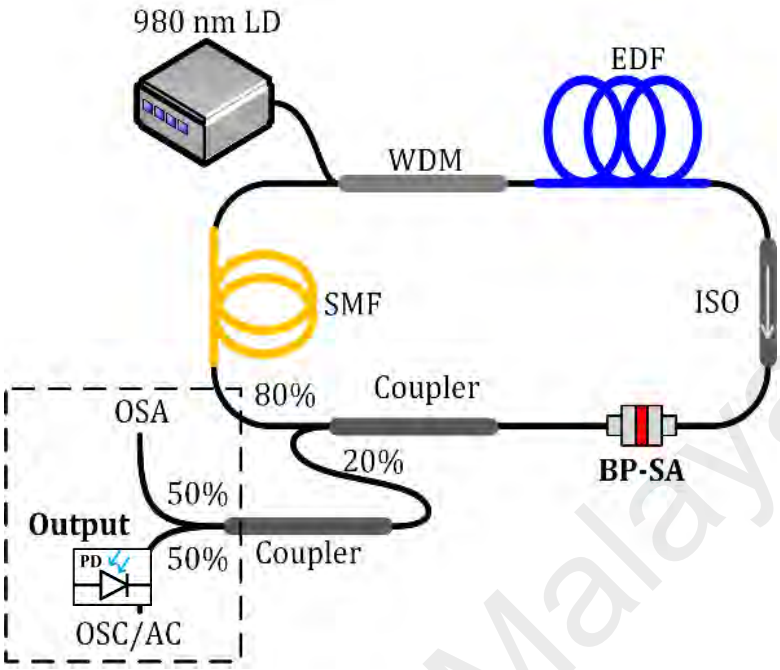

Figure 5.10: Schematic configuration of the proposed mode-locked EDFL

The BP functions as an SA that preferentially passed the light through at higher power to promote the formation of a pulse from noise. By varying the 980 nm pump power the laser started to operate at a low pump power threshold of 20 mW due to the significantly low insertion loss of the thin BP-SA compared to the thick one that used for Q-switched. The EDFL started to operate in the continuous wave (CW) but as the pump power increased above 30 mW, it transformed into the self-started soliton mode locked pulse. As the pump power was increased to the maximum power of 140 mW, the BP-SA was retained stably without thermal damage. Figure 5.11 shows the output spectrum of the soliton mode locked EDFL centered at 1560.7 nm with 3 dB bandwidth of 6.4 nm, which was obtained at pump power of 140 mW. The net cavity GVD in the laser cavity is anomalous, which facilitates soliton pulse shaping via the interplay of GVD and self-phase modulation (SPM) in the cavity. As seen in the figure the appearance of Kelly

sidebands is confirmed the soliton pulse due to resonant coupling interaction between soliton and dispersive wave components emitted after soliton perturbations. The separation of the Kelly sidebands from the center to the left and right of the soliton spectrum are approximately ± 7.7 nm. Based on the sideband separation (Smith et al., 1992), and Eq (3.2) the actual total dispersion is estimated to be -0.276 ps^2, which is contributed by the three types of fiber used (EDF, SMF-28, HI 1060) and SA (BP) dispersions. Based on this total dispersion value, the BP SA dispersion is calculated to be around 0.22 ps^2.

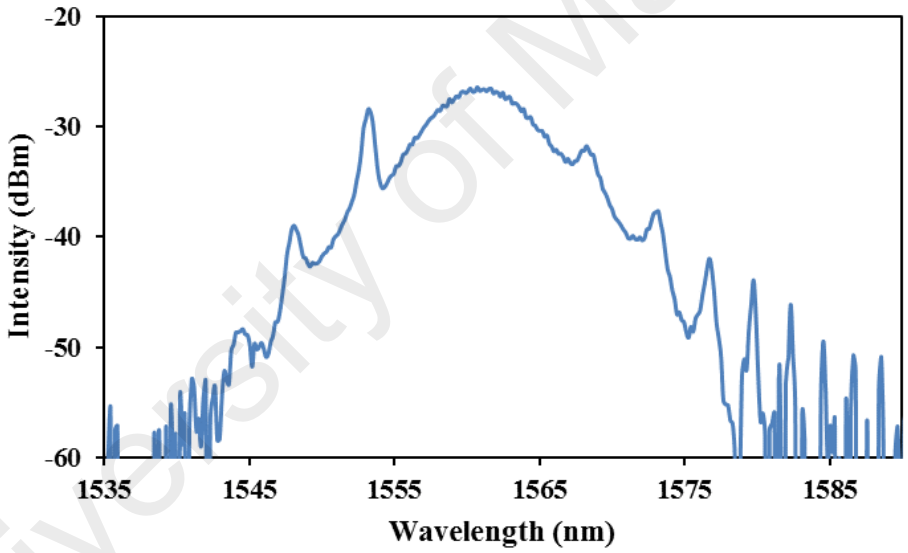

Figure 5.11: Optical spectrum of the mode-locked EDFL at pump power of 140 mW

Figure 5.12 shows the oscilloscope trace of the mode-locked EDFL, which was obtained at the maximum pump power of 140 mW. As seen in the figure, the pulse train is quite uniform with a pulse period of 145 ns. The fundamental repetition rate of the pulses is approximately 6.88 MHz, which is corresponding to the calculated value, taking

into account the length and the refractive indices of the different fibers that make up the laser cavity. Figure 5.13 shows the typical output autocorrelation trace of the mode-locked pulse, which indicates the measured pulse duration is in line with $sech^2$ pulse profile with the full width half maximum (FWHM) of 570 fs. By using this pulse duration value and the above mentioned spectral width, a time-bandwidth product (TBP) of ~0.45 is attained. To investigate the laser stability, we characterize the radio frequency (RF) spectrum. Figure 5.14 shows the RF spectrum for our laser, which is recorded in a span of 100 MHz and a resolution bandwidth (RBW) of 300 kHz. A high signal to background ratio of ~59 dB is observed at the fundamental frequency of 6.88 MHz, which confirms the stability of the pulse. This BP-SA can last more than a day with maximum pump power level launching into the laser cavity. Keeping the BP-SA inside an airtight container would protect it against oxygen and water molecules. The RF spectrum also presents higher cavity harmonics without significant spectral modulation, implying no Q-switching instabilities, showing good mode-locking stability. The average output power and pulse energy of the mode-locked EDFL at various pump power are also investigated and the results are shown in figure 5.15. Both output power and pulse energy are linearly related with the pump power. At the maximum pump power of 140 mW, the average output power is 5.1 mW. Therefore, the pulse energy and peak power are estimated at 0.74 nJ and 1.22 kW respectively. Compare to the demonstrated mode-locked fiber lasers based BP (Y Chen et al., 2015; D Li et al., 2015), our pulse width is shorter with high pulse energy. These results affirm that the BP SA may have a great potential for applications in ultrafast fiber lasers.

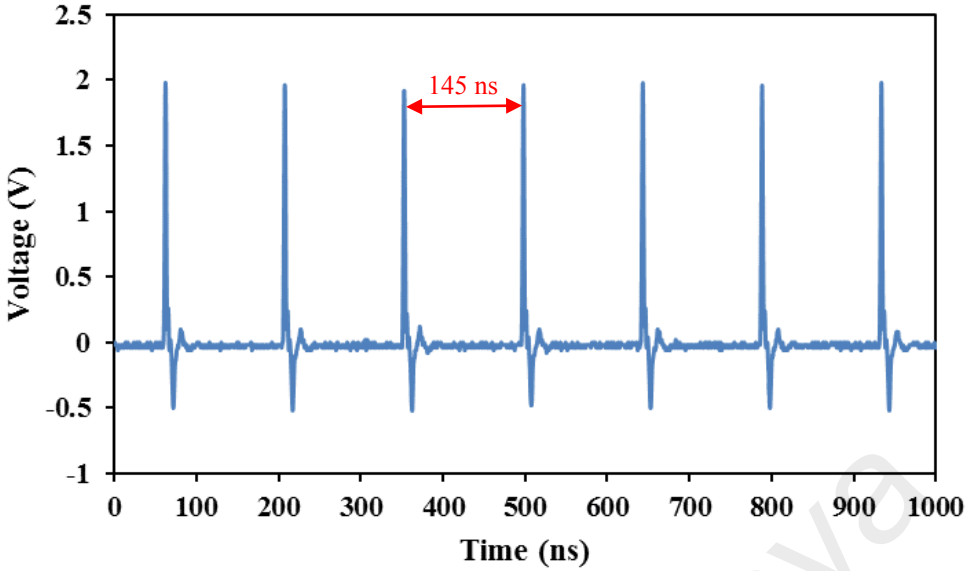

Figure 5.12: Oscilloscope trace of the mode-locked EDFL at pump power of 140 mW

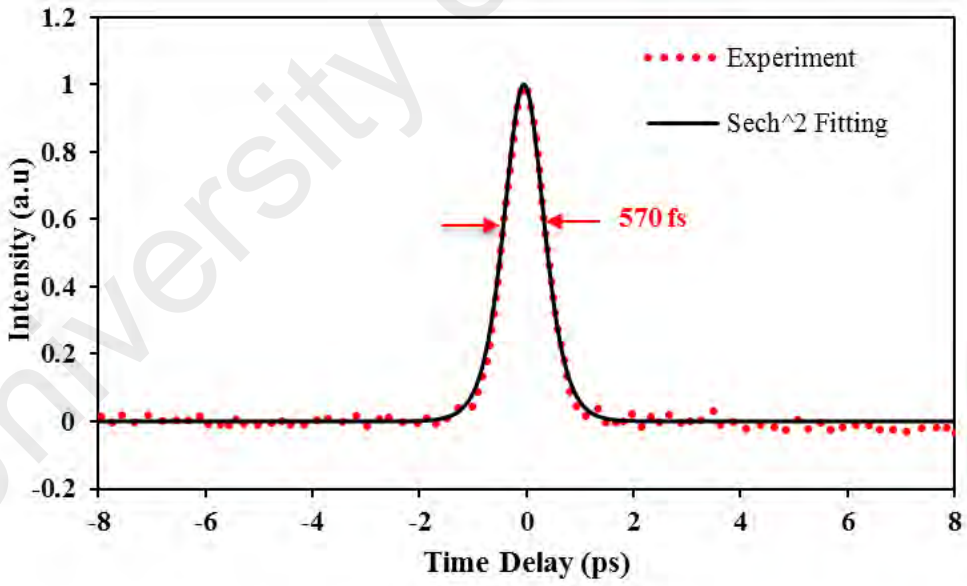

Figure 5.13: Autocorrelation trace of the mode-locked EDFL at pump power of 140 mW

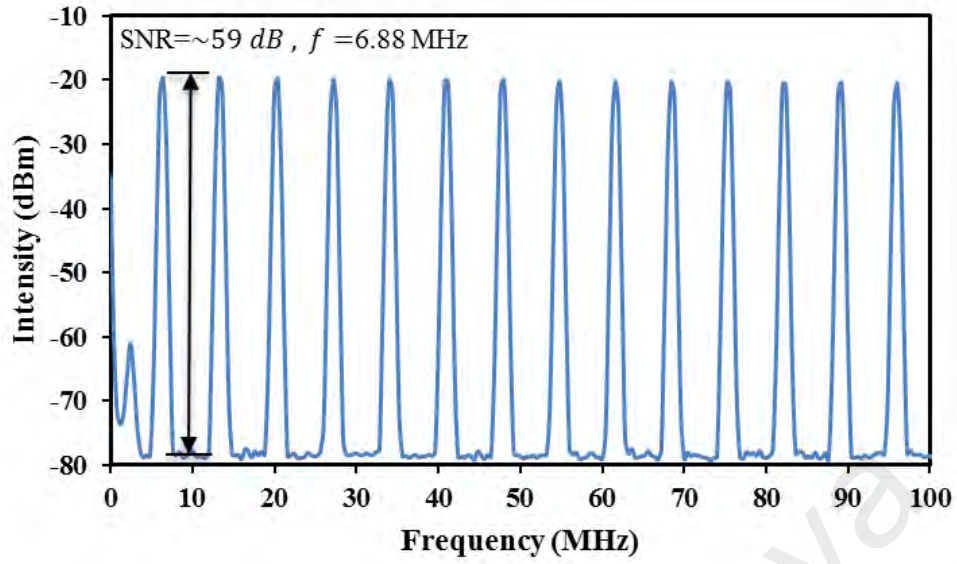

Figure 5.14: RF spectrum of the mode-locked EDFL with a 100 MHz span

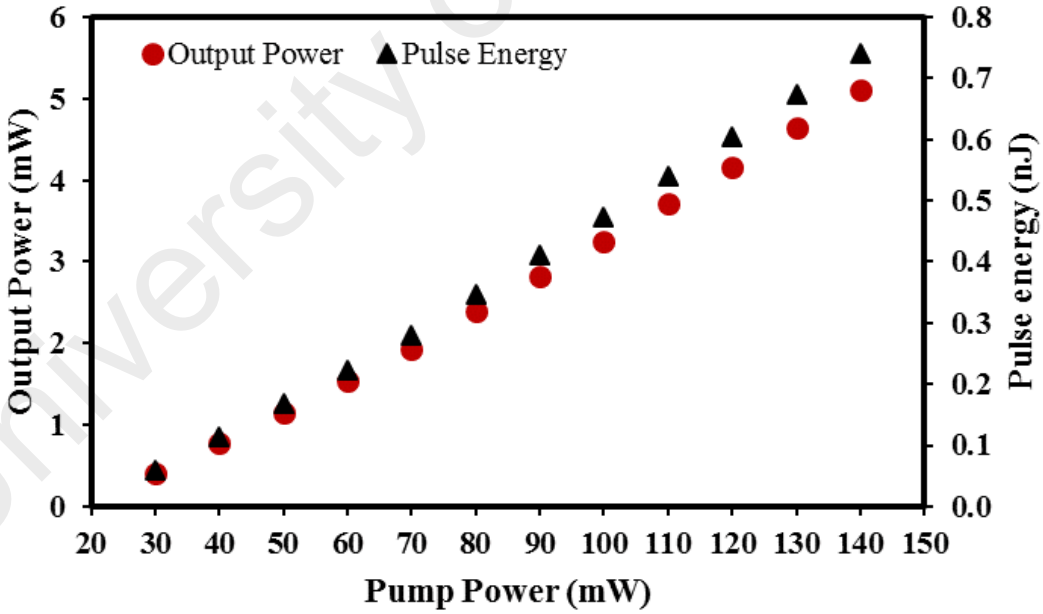

Figure 5.15: Average output power and pulse energy as a function of 980 nm pump power

5.5 Summary

The BP was experimentally demonstrated as an effective SA for both Q-switching and mode-locking applications. The BP was prepared by a simple mechanical exfoliation technique and sandwiched between two fiber ferrules via a fiber adapter to form a fiber-compatible SA. Depending on the thickness of the BP used, the thick BP-based SA with a modulation depth of 6.1% and saturation intensity 0.30 MW/cm^2, Q-switched pulse is achieved with 7.04 μs pulse width and pulse energy of 134 nJ. On the other hand, thin BP-SA with a modulation depth of 7% and saturation intensity of 0.25 MW/cm^2, a mode-locked pulse is obtained with consistent pulse repetition rate of 6.88 MHz and pulse width of 570 fs. The maximum pulse energy is calculated as 0.74 nJ at a pump power of 140 mW, whereas the peak power is estimated at 1.22 kW. BP based-SA is easy to fabricate and cheap, which makes it a suitable component for generating Q-switched and mode-locked fiber lasers in the 1.5 μm wavelength region.

CHAPTER 6: CONCLUSION AND FUTURE OUTLOOK

6.1 Conclusion

This research was started by noticing that fast progress has been accomplished in fiber laser technology since its origins in the mid-twentieth century. Today, optical fibers and short pulse fiber lasers are mature technologies, which have a revolutionary impact on science, industry, and medicine, yielding tangible benefits to society (the Internet is the most obvious example). Despite great progress in the developments of fiber lasers, however, user requirements for fiber laser systems continue to grow as their applications increase, driving further research. This research aimed to construct and demonstrate ultrafast erbium-doped fiber lasers (EDFLs), which are mode-locked pulses by using two-dimensional (2D) nanomaterials for possible applications in high-speed telecommunications, environmental sensing, ultra-sensitive laser spectroscopy, metrology, materials processing and biomedical diagnostics.

This work involved the fabrication and characterization of new passive saturable absorbers (SAs) based on 2D nanomaterials. In Chapter 3, graphite and graphene were demonstrated as SAs for mode-locked EDFL. At first, a nonconductive graphite pencil-core was prepared by mechanical exfoliation and integrated into EDFL ring cavity to realize a self-started mode-locked pulse train at 1562 nm wavelength with a pulse width of 3.05 ps. Next, stretched and soliton femtosecond mode-locked EDFL with graphene SA were generated by manipulating the cavity dispersion. With the dispersion management, the total dispersion can be decreased to -0.028 ps^2, where we obtained stretched pulse with pulse width of 750 fs at a repetition rate of 35.1 MHz and pulse energy of 0.054 nJ at a maximum output power of 1.9 mW. With a variation of the net cavity dispersion, the total dispersion can be -0.3 ps^2, where anomalous dispersion has been achieved by generating soliton mode-locked pulse with pulse width of 820 fs at a repetition rate of 11.5 MHz and pulse energy of 0.42 nJ at an output power of 4.85 mW.

In chapter 4, various types of mode locking operations have been demonstrated based on few-layer MoS_2 SA. First, the MoS_2 SA was prepared by the mechanically exfoliating MoS_2 crystal. The exfoliated acquired MoS_2 flakes were fixed onto the end surface of a standard FC/PC fiber connector and integrated into the EDFL ring cavity. In an anomalous regime with estimated net dispersion of -0.1151 ps^2, the soliton mode-locked EDFL pulse was generated at 1598.94 nm wavelength with a repetition rate of 17.1 MHz and pulse width of 830 fs. Second, a free-standing few-layer MoS_2 polymer composite was fabricated by liquid phase exfoliation of chemically pristine MoS_2 crystals. By using the MoS_2-SA film based EDFL, a stable 630 fs pulse was generated in the anomalous net dispersion of -0.094 ps^2 at 1573.7 nm wavelength with a repetition rate of 27.1 MHz and pulse energy of 0.141 nJ. On the other hand, by inserting a 850 m long dispersion shifted fiber (DSF) in the cavity, a dissipative soliton with square pulse train is obtained in the normal dispersion regime with estimated net dispersion of 4.26 ps^2, where the operating wavelength is centered at 1567.44 nm with a 3dB bandwidth of 19.68 nm, repetition rate of 231.5 KHz and pulse width of 90 ns. These results indicated that the MoS_2-SA could be used as a simple, low cost, low insertion loss, ultrafast saturable absorption device for ultrafast photonic applications.

In chapter 5, Q-switched and mode-locked EDFL are experimentally demonstrated based on multi-layer black phosphorus (BP) SA. The BP was prepared by mechanical exfoliation technique and sandwiched between two fiber ferrules via a fiber adapter to form a fiber-compatible SA. Depending on the thickness of the BP used, the Q-switched pulse is achieved by thick BP-SA with a modulation depth of 6.1%. On the other hand, mode-locked pulse is obtained by thin BP-SA with a modulation depth of 7%. The mode-locked operated from threshold pump power of 30 mW to 140 mW with consistent pulse repetition rate of 6.88 MHz and pulse width of 570 fs, whereas the peak power is estimated at 1.22 kW. These results indicate that a multi-layer BP SA is a promising

material for generating Q-switched and mode-locked fiber lasers in the 1.5 μm wavelength region.

In summary, three new 2D nanomaterials SA (graphene, MoS_2, and BP) were successfully fabricated, characterized and utilized in generating mode-locked EDFLs. The saturable absorption of 2D nanomaterials was characterized and compared in the aspects of modulation depth, saturation intensity and non-saturable absorption (refer to Table 6.1). The MoS_2 exhibits the highest modulation depth compare to graphene and BP. Also, mode locking operations based on these SAs are achieved and compared in the aspects of output power, pulse width, repetition rate, signal to noise ratio (SNR) RF and pulse energy (refer to Table 6.1). Mode-locked EDFL based on MoS_2-PVA is the most stable pulse train with highest SNR in the RF spectrum. Furthermore, mode-locked EDFL using BP has shorter pulse width with highest pulse energy. Tables 6.2 and 6.3 summarize the mode-locked fiber lasers performance of this work using MoS_2 and BP based SAs in comparison with the previously demonstrated works. Compared with the reported mode-locked fiber lasers based on MoS_2 and BP, this work demonstrated shorter pulse width at low pump power.

Table 6.1: Comparison of mode locking EDFL based on 2D nanomaterials saturable absorbers

	Properties	Graphene Film		MoS_2 Scotch Tape	MoS_2 Film		BP Scotch Tape
Materials	**Modulation depth**	5.9 %		11.3%	9.7 %		7 %
	Saturation intensity	21 MW/cm^2		23.5 MW/cm^2	40 MW/cm^2		0.25 MW/cm^2
	Non-saturable absorbance	47%		23%	10.9%		58 %
Mode Locking		**Stretched Pulse**	**Soliton Pulse**	**Soliton Pulse**	**Soliton Pulse**	**Dissipative Pulse**	**Soliton Pulse**
	Wavelength	1575 nm	1557.7 nm	1598.9 nm	1573.7 nm	1567.44nm	1560.7 nm
	Pump range	50 - 170 mW	40 - 130 mW	50 - 110 mW	25-170 mW	50-170 mW	30-140 mW
	Output power	1.9 mW	4.85 mW	1.26 mW	3.82 mW	0.58 mW	5.1 mW
	Pulse width	750 fs	820 fs	830 fs	630 fs	90 ns	570 fs
	Repetition rate	35.1 MHz	11.5 MHz	17.1 MHz	27.1 MHz	231.5 KHz	6.88 MHz
	Signal to noise ratio (SNR)in RF spectrum	55 dB	45 dB	41 dB	61 dB	35 dB	59 dB
	Pulse energy	0.054 nJ	0.42 nJ	0.074 nJ	0.14 nJ	-	0.74 nJ

Table 6.2: Performance Comparison among Various Mode-Locked Pulsed Lasers with Few-Layer MoS_2 SAs

Laser Type	MoS_2 Fabrication Method	Integration Platform	Layers in MoS_2	λ (nm)	Laser Performance			References
					Pulse Width	Repetition Rate	Threshold Pump Power	
Mode-Locked		Fiber facet	1-3	1054.3	800 ps	6.6 MHz	60 mW	(H Zhang et al., 2014)
	SP-I	Microfiber	1-3	1042.6	656 ps	6.7 MHz	120 mW	(Du et al., 2014)
	CVD	Fiber facet	4-5	1568.9	1.28 ps	8.3 MHz	31 mW	(H Xia et al., 2014)
		Side polished fiber	>10	1568	4.98 ps	26 MHz	322 mW	(Khazaeizhad et al., 2014)
		Side polished fiber	>10	1568	637 fs	33.5 MHz	56 mW	(Khazaeizhad et al., 2014)
	SP-I	PVA composite	4-5	1569.5	710 fs	12.1 MHz	22 mW	(Liu et al., 2014)
	LPE	PVA composite	4-5	1535-1565 tunable	~1 ps	13 MHz	-	(Zhang et al., 2015)
	LPE	Coating on mirror	~4	1905	843 ps	9.7 MHz	700 mW	(Tian et al., 2015)
	ME	**Fiber facet**	**~2-5**	**1598.94**	**830 fs**	**17.1 MHz**	**50 mW**	**This Work (2015)**
	LPE	**PVA composite**	**~2-3**	**1573.7**	**630 fs**	**27.1 MHz**	**25 mW**	**This Work (2015)**

Note: (SP-I) solution processed using intercalation; (CVD) chemical vapor deposition; (LPE) liquid phase exfoliation; (ME) mechanical exfoliation.

Table 6.3: Performance Comparison among Various Mode-Locked Pulsed Lasers with Black Phosphorus SAs

Laser Type	BP Fabrication Method	Integration Platform	Layers in BP	Wavelength λ (nm)	Laser Performance			References
					Pulse Width	Repetition Rate	Mode Locking Threshold Pump Power	
Mode-Locked	ME	Fiber facet	~2-5	1571.45	946 fs	5.96 MHz	63.7 mW	(Y Chen et al., 2015)
	-	Film	-	1558.7	786 fs	14.7 MHz	-	(D Li et al., 2015)
	LPE	Microfiber	1-3	1566.5	940 fs	4.96 MHz	70 mW	(Luo et al., 2015)
	ME	Fiber facet	~500	1910	739 fs	36.8 MHz	300 mW	(Sotor, Sobon, Kowalczyk, et al., 2015)
	ME	**Fiber facet**	**~2-50**	**1560.7**	**570 fs**	**6.88 MHz**	**30 mW**	**This Work (2016)**

Note: (ME) mechanical exfoliation; (LPE) liquid phase exfoliation.

6.2 Future Outlook

Up to date, the advances in ultrafast fiber lasers using 2D nanomaterials as saturable absorber have been rapidly adopted in various field and applications and have approved to be promising candidates for many applications in optical communications, biomedical diagnostics, material processing and spectroscopy. Ultrafast fiber lasers exhibit more advantages over solid-state sources, including diffraction limited beam quality, compact size, high efficiency and extremely low noise.

The discovery of remarkable optical properties of graphene has started an extremely quick advance in the study of 2D nanomaterials, which strongly contributed to the improvement of novel ultrafast fiber laser sources. It is clear that the enthusiasm for 2D nanomaterials based photonics will not slow down in the following years.

The progress in the field of ultrafast fiber lasers pulse generation has been rapid and continuous, and has a long lifetime ahead. Throughout the following couple of years, there will be an extension of the utilization of ultrafast fiber laser by replacing conventional solid-state lasers and as ultrafast fiber laser technology continues to develop more applications will be found for it. Furthermore, ultrafast fiber lasers will be continuously pushing for shorter pulse width (<100 fs), higher pulse energy (>μJ) and peak power (>kW). Although, the origin of ultrafast fiber laser generation was not long ago, it is clear that it is shaping up for a long lifetime ahead and beyond our imagination and without boundary.

REFERENCES

Agrawal, G. (2007). *Self-phase modulation in optical fiber communications: good or bad?* Paper presented at the Photonic Applications Systems Technologies Conference.

Agrawal, G. P. (2005). *Lightwave technology: telecommunication systems*: John Wiley & Sons.

Agrawal, G. P. (2007). *Nonlinear fiber optics*: Academic press.

Ahmad, F., Harun, S., Nor, R., Zulkepely, N., Ahmad, H., & Shum, P. (2013). A Passively Mode-Locked Erbium-Doped Fiber Laser Based on a Single-Wall Carbon Nanotube Polymer. *Chinese Physics Letters, 30*(5), 054210.

Ahmad, H., Muhammad, F., Zulkifli, M., & Harun, S. (2013). Graphene-Based Mode-Locked Spectrum-Tunable Fiber Laser Using Mach–Zehnder Filter. *IEEE Photonics Journal, 5*(5), 1501709-1501709.

Ahmed, M., Ali, N., Salleh, Z., Rahman, A., Harun, S., Manaf, M., & Arof, H. (2014). All fiber mode-locked Erbium-doped fiber laser using single-walled carbon nanotubes embedded into polyvinyl alcohol film as saturable absorber. *Optics & Laser Technology, 62*, 40-43.

Balog, R., Jørgensen, B., Nilsson, L., Andersen, M., Rienks, E., Bianchi, M., . . . Lizzit, S. (2010). Bandgap opening in graphene induced by patterned hydrogen adsorption. *Nature materials, 9*(4), 315-319.

Bao, Q., Zhang, H., Wang, Y., Ni, Z., Yan, Y., Shen, Z. X., . . . Tang, D. Y. (2009). Atomic-layer graphene as a saturable absorber for ultrafast pulsed lasers. *Advanced Functional Materials, 19*(19), 3077-3083.

Becker, M., Kuizenga, D., & Siegman, A. (1972). Harmonic mode locking of the Nd: YAG laser. *IEEE Journal of Quantum Electronics, 8*(8), 687-693.

Bertolazzi, S., Brivio, J., & Kis, A. (2011). Stretching and breaking of ultrathin MoS2. *ACS nano, 5*(12), 9703-9709.

Boehm, H., Setton, R., & Stumpp, E. (1986). Nomenclature and terminology of graphite intercalation compounds. *Carbon, 24*(2), 241-245.

Boehm, H. P., Clauss, A., Fischer, G. O., & Hofmann, U. (1962). Das Adsorptionsverhalten sehr dünner Kohlenstoff-Folien. *Zeitschrift für anorganische und allgemeine Chemie, 316*(3-4), 119-127.

Bonaccorso, F., Lombardo, A., Hasan, T., Sun, Z., Colombo, L., & Ferrari, A. C. (2012). Production and processing of graphene and 2d crystals. *Materials Today, 15*(12), 564-589.

Bonaccorso, F., & Sun, Z. (2014). Solution processing of graphene, topological insulators and other 2d crystals for ultrafast photonics. *Optical Materials Express, 4*(1), 63-78.

Bonaccorso, F., Sun, Z., Hasan, T., & Ferrari, A. (2010). Graphene photonics and optoelectronics. *Nature Photonics, 4*(9), 611-622.

Bonaccorso, F., Zerbetto, M., Ferrari, A. C., & Amendola, V. (2013). Sorting nanoparticles by centrifugal fields in clean media. *The Journal of Physical Chemistry C, 117*(25), 13217-13229.

Boyd, R. W. (2008). *Nonlinear Optics, Third Edition*: Academic Press.

Bridgman, P. (1914). TWO NEW MODIFICATIONS OF PHOSPHORUS. *Journal of the American Chemical Society, 36*(7), 1344-1363.

Castellanos-Gomez, A., Vicarelli, L., Prada, E., Island, J. O., Narasimha-Acharya, K., Blanter, S. I., . . . Alvarez, J. (2014). Isolation and characterization of few-layer black phosphorus. *2D Materials, 1*(2), 025001.

Castro Neto, A., & Novoselov, K. (2011). Two-dimensional crystals: beyond graphene. *Materials Express, 1*(1), 10-17.

Castro Neto, A. H. (2007). Graphene: Phonons behaving badly. *Nat Mater, 6*(3), 176-177.

Chang, W., Ankiewicz, A., Soto-Crespo, J., & Akhmediev, N. (2008). Dissipative soliton resonances. *Physical Review A, 78*(2), 023830.

Chang, Y. M., Kim, H., Lee, J. H., & Song, Y.-W. (2010). Multilayered graphene efficiently formed by mechanical exfoliation for nonlinear saturable absorbers in fiber mode-locked lasers. *Applied Physics Letters, 97*(21), 211102.

Chang, Y. M., Lee, J., & Lee, J. H. (2012). Active Mode-Locking of an Erbium-Doped Fiber Laser Using an Ultrafast Silicon-Based Variable Optical Attenuator. *Japanese journal of applied physics, 51*(7R), 072701.

Chen, B., Zhang, X., Wu, K., Wang, H., Wang, J., & Chen, J. (2015). Q-switched fiber laser based on transition metal dichalcogenides MoS2, MoSe2, WS2, and WSe2. *Optics Express, 23*(20), 26723-26737.

Chen, S., Brown, L., Levendorf, M., Cai, W., Ju, S.-Y., Edgeworth, J., . . . Piner, R. D. (2011). Oxidation resistance of graphene-coated Cu and Cu/Ni alloy. *ACS nano, 5*(2), 1321-1327.

Chen, Y., Analytis, J., Chu, J.-H., Liu, Z., Mo, S.-K., Qi, X.-L., . . . Fang, Z. (2009). Experimental realization of a three-dimensional topological insulator, Bi2Te3. *Science, 325*(5937), 178-181.

Chen, Y., Jiang, G., Chen, S., Guo, Z., Yu, X., Zhao, C., . . . Tang, D. (2015). Mechanically exfoliated black phosphorus as a new saturable absorber for both Q-switching and Mode-locking laser operation. *Optics Express, 23*(10), 12823-12833.

Chen, Y., Zhao, C., Huang, H., Chen, S., Tang, P., Wang, Z., . . . Tang, D. (2013). Self-Assembled Topological Insulator: Bi Se Membrane as a Passive Q-Switcher in an Erbium-Doped Fiber Laser. *Journal of lightwave technology, 31*(17), 2857-2863.

Chong, C. Y. (2008). *Femtosecond fiber lasers and amplifiers based on the pulse propagation at normal dispersion.* Cornell University.

Churchill, H. O., & Jarillo-Herrero, P. (2014). Two-dimensional crystals: Phosphorus joins the family.

Churchill, H. O., & Jarillo-Herrero, P. (2014). Two-dimensional crystals: Phosphorus joins the family. *Nature nanotechnology, 9*(5), 330-331.

Coleman, J. N., Lotya, M., O'Neill, A., Bergin, S. D., King, P. J., Khan, U., . . . Smith, R. J. (2011). Two-dimensional nanosheets produced by liquid exfoliation of layered materials. *Science, 331*(6017), 568-571.

Collings, B. C., Mitchell, M. L., Boivin, L., & Knox, W. H. (2000). A 1021 channel WDM system. *Optics and Photonics News, 11*(3), 31-35.

Cui, Y., & Liu, X. (2013). Graphene and nanotube mode-locked fiber laser emitting dissipative and conventional solitons. *Optics Express, 21*(16), 18969-18974.

Cunningham, G., Lotya, M., Cucinotta, C. S., Sanvito, S., Bergin, S. D., Menzel, R., . . . Coleman, J. N. (2012). Solvent exfoliation of transition metal dichalcogenides: dispersibility of exfoliated nanosheets varies only weakly between compounds. *ACS nano, 6*(4), 3468-3480.

De Silvestri, S., Laporta, P., & Svelto, O. (1984). The role of cavity dispersion in cw mode-locked dye lasers. *IEEE Journal of Quantum Electronics, 20*(5), 533-539.

DeMaria, A., Stetser, D., & Heynau, H. (1966). Self mode-locking of lasers with saturable absorbers. *Applied Physics Letters, 8*(7), 174-176.

Dennis, M. L., & Duling, I. N. (1994). Experimental study of sideband generation in femtosecond fiber lasers. *IEEE Journal of Quantum Electronics, 30*(6), 1469-1477.

Desurvire, E., Simpson, J. R., & Becker, P. (1987). High-gain erbium-doped traveling-wave fiber amplifier. *Optics letters, 12*(11), 888-890.

Diament, P. (1990). *Wave Transmission and Fiber Optics*: Macmillan.

DiDomenico Jr, M. (1964). Small-signal analysis of internal (coupling-type) modulation of lasers. *Journal of Applied Physics, 35*(10), 2870-2876.

Digonnet, M. J. (2001). *Rare-earth-doped fiber lasers and amplifiers, revised and expanded*: CRC press.

Dong, L., & Samson, B. (2016). *Fiber Lasers: Basics, Technology, and Applications*: CRC Press.

Doran, N., & Wood, D. (1988). Nonlinear-optical loop mirror. *Optics letters, 13*(1), 56-58.

Druffel, E. R. M. (1997). Geochemistry of corals: Proxies of past ocean chemistry, ocean circulation, and climate. *Proceedings of the National Academy of Sciences, 94*(16), 8354-8361.

Du, J., Wang, Q., Jiang, G., Xu, C., Zhao, C., Xiang, Y., . . . Zhang, H. (2014). Ytterbium-doped fiber laser passively mode locked by few-layer Molybdenum Disulfide (MoS2) saturable absorber functioned with evanescent field interaction. *Scientific Reports, 4*, 6346.

El-Sherif, A. F., & King, T. A. (2003). High-energy, high-brightness Q-switched Tm3+-doped fiber laser using an electro-optic modulator. *Optics communications, 218*(4–6), 337-344.

Fermann, M. E., Galvanauskas, A., & Sucha, G. (2002). *Ultrafast lasers: Technology and applications* (Vol. 80): CRC Press.

Fermann, M. E., & Hartl, I. (2013). Ultrafast fibre lasers. *Nat Photon, 7*(11), 868-874.

Ferrari, A. C. (2007). Raman spectroscopy of graphene and graphite: disorder, electron–phonon coupling, doping and nonadiabatic effects. *Solid state communications, 143*(1), 47-57.

Ferrari, A. C., Meyer, J., Scardaci, V., Casiraghi, C., Lazzeri, M., Mauri, F., . . . Roth, S. (2006). Raman spectrum of graphene and graphene layers. *Physical review letters, 97*(18), 187401.

Fork, R., Greene, B., & Shank, C. V. (1981). Generation of optical pulses shorter than 0.1 psec by colliding pulse mode locking. *Applied Physics Letters, 38*(9), 671-672.

Freudiger, C. W., Yang, W., Holtom, G. R., Peyghambarian, N., Xie, X. S., & Kieu, K. Q. (2014). Stimulated Raman scattering microscopy with a robust fibre laser source. *Nature Photonics, 8*(2), 153-159.

Frindt, R. (1965). Optical Absorption of a Few Unit-Cell Layers of Mo S 2. *Physical Review, 140*(2A), A536.

Frindt, R., & Yoffe, A. (1963). *Physical properties of layer structures: optical properties and photoconductivity of thin crystals of molybdenum disulphide.* Paper presented at the Proceedings of the Royal Society of London A: Mathematical, Physical and Engineering Sciences.

Fu, B., Hua, Y., Xiao, X., Zhu, H., Sun, Z., & Yang, C. (2014). Broadband graphene saturable absorber for pulsed fiber lasers at 1, 1.5, and 2 μm. *IEEE Journal of selected topics in QUANTUM ELECTRONICS, 20*(5), 411-415.

Ganatra, R., & Zhang, Q. (2014). Few-layer MoS2: a promising layered semiconductor. *ACS nano, 8*(5), 4074-4099.

Garmire, E. (2000). Resonant optical nonlinearities in semiconductors. *IEEE Journal of selected topics in QUANTUM ELECTRONICS, 6*(6), 1094-1110.

Gattass, R. R., & Mazur, E. (2008). Femtosecond laser micromachining in transparent materials. *Nature Photonics, 2*(4), 219-225.

Geim, A., Novoselov, K., Yazyev, O. V., Louie, S. G., Ghosh, S., Bao, W., . . . Lau, C. N. (2007). Nobel Prize for graphene. *Nature materials, 6*, 183-192.

Geim, A. K., & Novoselov, K. S. (2007). The rise of graphene. *Nature materials, 6*(3), 183-191.

Gomez, L. A. (2004). Picosecond Sesam-Baed Ytterbium Mode-Locked Fiber Laser. *IEEE Journal of selected topic in Quantum electronics, 10*(1), 129.136.

Govind, P. (2013). Nonlinear fiber optics: Elsevier/Academic Press.

Graf, D., Molitor, F., Ensslin, K., Stampfer, C., Jungen, A., Hierold, C., & Wirtz, L. (2007). Spatially Resolved Raman Spectroscopy of Single- and Few-Layer Graphene. *Nano letters, 7*(2), 238-242.

Grelu, P., & Akhmediev, N. (2012). Dissipative solitons for mode-locked lasers. *Nat Photon, 6*(2), 84-92.

Grelu, P., & Akhmediev, N. (2012). Dissipative solitons for mode-locked lasers. *Nature Photonics, 6*(2), 84-92.

Guo, Z., Zhang, H., Lu, S., Wang, Z., Tang, S., Shao, J., . . . Yu, X. F. (2015). From black phosphorus to phosphorene: basic solvent exfoliation, evolution of Raman scattering, and applications to ultrafast photonics. *Advanced Functional Materials, 25*(45), 6996-7002.

Gupta, A., Sakthivel, T., & Seal, S. (2015). Recent development in 2D materials beyond graphene. *Progress in Materials Science, 73*, 44-126.

Hanna, D., Kazer, A., Phillips, M., Shepherd, D., & Suni, P. (1989). Active mode-locking of an Yb: Er fibre laser. *Electronics Letters, 2*(25), 95-96.

Hargrove, L., Fork, R. L., & Pollack, M. (1964). Locking of He–Ne laser modes induced by synchronous intracavity modulation. *Applied Physics Letters, 5*(1), 4-5.

Hargrove, L. E., Fork, R. L., & Pollack, M. A. (1964). LOCKING OF He–Ne LASER MODES INDUCED BY SYNCHRONOUS INTRACAVITY MODULATION. *Applied Physics Letters, 5*(1), 4-5.

Hasan, T., Sun, Z., Wang, F., Bonaccorso, F., Tan, P. H., Rozhin, A. G., & Ferrari, A. C. (2009). Nanotube–polymer composites for ultrafast photonics. *Advanced Materials, 21*(38-39), 3874-3899.

Hasan, T., Torrisi, F., Sun, Z., Popa, D., Nicolosi, V., Privitera, G., . . . Ferrari, A. (2010). Solution-phase exfoliation of graphite for ultrafast photonics. *physica status solidi (b), 247*(11-12), 2953-2957.

Hasegawa, A. (1984). Generation of a train of soliton pulses by induced modulational instability in optical fibers. *Optics letters, 9*(7), 288-290.

Haus, H., Tamura, K., Nelson, L., & Ippen, E. (1995). Stretched-pulse additive pulse mode-locking in fiber ring lasers: theory and experiment. *IEEE Journal of Quantum Electronics, 31*(3), 591-598.

Haus, H. A. (1975). Theory of mode locking with a fast saturable absorber. *Journal of Applied Physics, 46*(7), 3049-3058.

Haus, H. A. (2000). Mode-locking of lasers. *IEEE Journal of selected topics in QUANTUM ELECTRONICS, 6*(6), 1173-1185.

Haus, H. A., Fujimoto, J. G., & Ippen, E. P. (1992). Analytic theory of additive pulse and Kerr lens mode locking. *IEEE Journal of Quantum Electronics, 28*(10), 2086-2096.

Huang, Y., Luo, Z., Li, Y., Zhong, M., Xu, B., Che, K., . . . Weng, J. (2014). Widely-tunable, passively Q-switched erbium-doped fiber laser with few-layer MoS 2 saturable absorber. *Optics Express, 22*(21), 25258-25266.

Ikezawa, M., Kondo, Y., & Shirotani, I. (1983). Infrared optical absorption due to one and two phonon processes in black phosphorus. *Journal of the Physical Society of Japan, 52*(5), 1518-1520.

Ippen, E. P. (1994). Principles of passive mode locking. *Applied Physics B: Lasers and Optics, 58*(3), 159-170.

Islam, M. N., Simpson, J., Shang, H., Mollenauer, L., & Stolen, R. (1987). Cross-phase modulation in optical fibers. *Optics letters, 12*(8), 625-627.

Ismail, E., Kadir, N., Latiff, A., Ahmad, H., & Harun, S. (2016). Black phosphorus crystal as a saturable absorber for both a Q-switched and mode-locked erbium-doped fiber laser. *RSC Advances, 6*(76), 72692-72697.

Jamieson, J. C. (1963). Crystal structures adopted by black phosphorus at high pressures. *Science, 139*(3561), 1291-1292.

Joensen, P., Frindt, R., & Morrison, S. R. (1986). Single-layer MoS 2. *Materials research bulletin, 21*(4), 457-461.

Kasap, S., & Capper, P. (2006). *Springer handbook of electronic and photonic materials*: Springer Science & Business Media.

Kataura, H., Kumazawa, Y., Maniwa, Y., Umezu, I., Suzuki, S., Ohtsuka, Y., & Achiba, Y. (1999). Optical properties of single-wall carbon nanotubes. *Synthetic metals, 103*(1), 2555-2558.

Kelleher, E., Travers, J., Sun, Z., Ferrari, A., Golant, K., Popov, S., & Taylor, J. (2010). Bismuth fiber integrated laser mode-locked by carbon nanotubes. *Laser Physics Letters, 7*(11), 790.

Keller, U. (2003). Recent developments in compact ultrafast lasers. *Nature, 424*(6950), 831-838.

Keller, U., Miller, D., Boyd, G., Chiu, T., Ferguson, J., & Asom, M. (1992). Solid-state low-loss intracavity saturable absorber for Nd: YLF lasers: an antiresonant semiconductor Fabry–Perot saturable absorber. *Optics letters, 17*(7), 505-507.

Keller, U., Miller, D. A. B., Boyd, G. D., Chiu, T. H., Ferguson, J. F., & Asom, M. T. (1992). Solid-state low-loss intracavity saturable absorber for Nd:YLF lasers: an antiresonant semiconductor Fabry–Perot saturable absorber. *Optics letters, 17*(7), 505-507.

Keller, U., Weingarten, K. J., Kartner, F. X., Kopf, D., Braun, B., Jung, I. D., . . . Der Au, J. A. (1996). Semiconductor saturable absorber mirrors (SESAM's) for femtosecond to nanosecond pulse generation in solid-state lasers. *IEEE Journal of selected topics in QUANTUM ELECTRONICS, 2*(3), 435-453.

Khazaeizhad, R., Kassani, S. H., Jeong, H., Yeom, D.-I., & Oh, K. (2014). Mode-locking of Er-doped fiber laser using a multilayer MoS 2 thin film as a saturable absorber in both anomalous and normal dispersion regimes. *Optics Express, 22*(19), 23732-23742.

Kim, K. S., Zhao, Y., Jang, H., Lee, S. Y., Kim, J. M., Kim, K. S., . . . Hong, B. H. (2009). Large-scale pattern growth of graphene films for stretchable transparent electrodes. *Nature, 457*(7230), 706-710.

Kuizenga, D., & Siegman, A. (1970). FM and AM mode locking of the homogeneous laser-Part I: Theory. *IEEE Journal of Quantum Electronics, 6*(11), 694-708.

Lamb Jr, W. E. (1964). Theory of an optical maser. *Physical Review, 134*(6A), A1429.

Latiff, A., Shamsudin, H., Ahmad, H., & Harun, S. (2016). Q-switched thulium-doped fiber laser operating at 1940 nm region using a pencil-core as saturable absorber. *Journal of Modern Optics, 63*(8), 783-787.

Lee, C., Yan, H., Brus, L. E., Heinz, T. F., Hone, J., & Ryu, S. (2010). Anomalous lattice vibrations of single-and few-layer MoS2. *ACS nano, 4*(5), 2695-2700.

Lee, J., Lee, J., Koo, J., & Lee, J. H. (2016). Graphite saturable absorber based on the pencil-sketching method for Q-switching of an erbium fiber laser. *Applied optics, 55*(2), 303-309.

Li, D., Jussila, H., Karvonen, L., Ye, G., Lipsanen, H., Chen, X., & Sun, Z. (2015). Polarization and thickness dependent absorption properties of black phosphorus: new saturable absorber for ultrafast pulse generation. *Scientific Reports, 5*, 15899.

Li, H., Xia, H., Lan, C., Li, C., Zhang, X., Li, J., & Liu, Y. (2015). Passively-Switched Erbium-Doped Fiber Laser Based on Few-Layer MoS 2 Saturable Absorber. *IEEE photonics technology letters, 27*(1), 69-72.

Li, H., Zhang, Q., Yap, C. C. R., Tay, B. K., Edwin, T. H. T., Olivier, A., & Baillargeat, D. (2012). From bulk to monolayer MoS2: evolution of Raman scattering. *Advanced Functional Materials, 22*(7), 1385-1390.

Lin, G., & Lin, Y. (2011). Directly exfoliated and imprinted graphite nano-particle saturable absorber for passive mode-locking erbium-doped fiber laser. *Laser Physics Letters, 8*(12), 880.

Lin, Y.-H., & Lin, G.-R. (2013). Kelly sideband variation and self four-wave-mixing in femtosecond fiber soliton laser mode-locked by multiple exfoliated graphite nano-particles. *Laser Physics Letters, 10*(4), 045109.

Lin, Y.-H., Yang, C.-Y., Lin, S.-F., & Lin, G.-R. (2015). Triturating versatile carbon materials as saturable absorptive nano powders for ultrafast pulsating of erbium-doped fiber lasers. *Optical Materials Express, 5*(2), 236-253.

Lin, Y., & Lin, G. (2012). Free-standing nano-scale graphite saturable absorber for passively mode-locked erbium doped fiber ring laser. *Laser Physics Letters, 9*(5), 398.

Linde, D. (1986). Characterization of the noise in continuously operating mode-locked lasers. *Applied Physics B: Lasers and Optics, 39*(4), 201-217.

Ling, X., Wang, H., Huang, S., Xia, F., & Dresselhaus, M. S. (2015). The renaissance of black phosphorus. *Proceedings of the National Academy of Sciences, 112*(15), 4523-4530.

Liu, H., Luo, A.-P., Wang, F.-Z., Tang, R., Liu, M., Luo, Z.-C., . . . Zhang, H. (2014). Femtosecond pulse erbium-doped fiber laser by a few-layer MoS 2 saturable absorber. *Optics letters, 39*(15), 4591-4594.

Liu, X. (2011). Soliton formation and evolution in passively-mode-locked lasers with ultralong anomalous-dispersion fibers. *Physical Review A, 84*(2), 023835.

Liu, X., Cui, Y., Han, D., Yao, X., & Sun, Z. (2015). Distributed ultrafast fibre laser. *Scientific Reports, 5*.

Liu, X. M., Yang, H. R., Cui, Y. D., Chen, G. W., Yang, Y., Wu, X. Q., . . . Tong, L. M. (2016). Graphene-clad microfibre saturable absorber for ultrafast fibre lasers. *Scientific Reports, 6*, 26024.

Low, T., Rodin, A., Carvalho, A., Jiang, Y., Wang, H., Xia, F., & Neto, A. C. (2014). Tunable optical properties of multilayer black phosphorus thin films. *Physical Review B, 90*(7), 075434.

Lu, S., Miao, L., Guo, Z., Qi, X., Zhao, C., Zhang, H., . . . Fan, D. (2015). Broadband nonlinear optical response in multi-layer black phosphorus: an emerging infrared and mid-infrared optical material. *Optics Express, 23*(9), 11183-11194.

Luo, A., Luo, Z., Xu, W., Dvoyrin, V., Mashinsky, V., & Dianov, E. (2011). Tunable and switchable dual-wavelength passively mode-locked Bi-doped all-fiber ring laser based on nonlinear polarization rotation. *Laser Physics Letters, 8*(8), 601.

Luo, A. P., Luo, Z. C., Xu, W. C., Dvoyrin, V., Mashinsky, V., & Dianov, E. (2011). Tunable and switchable dual-wavelength passively mode-locked Bi-doped all-fiber ring laser based on nonlinear polarization rotation. *Laser Physics Letters, 8*(8), 601-605.

Luo, Z.-C., Liu, M., Guo, Z.-N., Jiang, X.-F., Luo, A.-P., Zhao, C.-J., . . . Zhang, H. (2015). Microfiber-based few-layer black phosphorus saturable absorber for ultra-fast fiber laser. *Optics Express, 23*(15), 20030-20039.

Luo, Z.-C., Luo, A.-P., & Xu, W.-C. (2011). Tunable and switchable multiwavelength passively mode-locked fiber laser based on SESAM and inline birefringence comb filter. *Photonics Journal, IEEE, 3*(1), 64-70.

Luo, Z., Huang, Y., Weng, J., Cheng, H., Lin, Z., Xu, B., . . . Xu, H. (2013). 1.06 μm Q-switched ytterbium-doped fiber laser using few-layer topological insulator Bi 2 Se 3 as a saturable absorber. *Optics Express, 21*(24), 29516-29522.

Luo, Z., Zhou, M., Weng, J., Huang, G., Xu, H., Ye, C., & Cai, Z. (2010). Graphene-based passively Q-switched dual-wavelength erbium-doped fiber laser. *Optics letters, 35*(21), 3709-3711.

Mak, K. F., He, K., Shan, J., & Heinz, T. F. (2012). Control of valley polarization in monolayer MoS2 by optical helicity. *Nat Nano, 7*(8), 494-498.

Mak, K. F., Lee, C., Hone, J., Shan, J., & Heinz, T. F. (2010). Atomically thin MoS 2: a new direct-gap semiconductor. *Physical review letters, 105*(13), 136805.

Mao, D., She, X., Du, B., Yang, D., Zhang, W., Song, K., . . . Zhao, J. (2016). Erbium-doped fiber laser passively mode locked with few-layer WSe2/MoSe2 nanosheets. *Scientific Reports, 6*, 23583.

Mao, N., Tang, J., Xie, L., Wu, J., Han, B., Lin, J., . . . Liu, K. (2016). Optical anisotropy of black phosphorus in the visible regime. *J. Am. Chem. Soc, 138*(1), 300-305.

Margulis, V. A., & Sizikova, T. (1998). Theoretical study of third-order nonlinear optical response of semiconductor carbon nanotubes. *Physica B: Condensed Matter, 245*(2), 173-189.

Martinez, A., Fuse, K., & Yamashita, S. (2011). Mechanical exfoliation of graphene for the passive mode-locking of fiber lasers. *Applied Physics Letters, 99*(12), 121107.

Martinez, A., & Sun, Z. (2013). Nanotube and graphene saturable absorbers for fibre lasers. *Nature Photonics, 7*(11), 842-845.

Martinez, A., & Yamashita, S. (2013). 5 - Carbon nanotube and graphene-based fiber lasers *Carbon Nanotubes and Graphene for Photonic Applications* (pp. 121-147e): Woodhead Publishing.

Mas-Balleste, R., Gomez-Navarro, C., Gomez-Herrero, J., & Zamora, F. (2011). 2D materials: to graphene and beyond. *Nanoscale, 3*(1), 20-30.

Maxwell, J. C. (1865). A dynamical theory of the electromagnetic field. *Philosophical transactions of the Royal Society of London, 155*, 459-512.

Mears, R., Reekie, L., Jauncey, I., & Payne, D. (1987). Low-noise erbium-doped fibre amplifier operating at 1.54μm. *Electronics Letters, 19*(23), 1026-1028.

Milam, D. (1998). Review and assessment of measured values of the nonlinear refractive-index coefficient of fused silica. *Applied optics, 37*(3), 546-550.

Milonni, P. W., & Eberly, Joseph H. (2010). *Laser Physics*. USA: Wiley.

Mocker, H. W., & Collins, R. (1965). Mode competition and self-locking effects in aq-switched ruby laser. *Applied Physics Letters, 7*(10), 270-273.

Mocker, H. W., & Collins, R. J. (1965). MODE COMPETITION AND SELF-LOCKING EFFECTS IN A Q-SWITCHED RUBY LASER. *Applied Physics Letters, 7*(10), 270-273.

Morita, A. (1986). Semiconducting black phosphorus. *Applied Physics A: Materials Science & Processing, 39*(4), 227-242.

Mu, H., Lin, S., Wang, Z., Xiao, S., Li, P., Chen, Y., . . . Pan, C. (2015). Black Phosphorus–Polymer Composites for Pulsed Lasers. *Advanced Optical Materials, 3*(10), 1447-1453.

Mulvad, H. C. H., Galili, M., Oxenløwe, L. K., Hu, H., Clausen, A. T., Jensen, J. B., . . . Jeppesen, P. (2010). Demonstration of 5.1 Tbit/s data capacity on a single-wavelength channel. *Optics Express, 18*(2), 1438-1443.

Nagy, Z., Takacs, A., Filkorn, T., & Sarayba, M. (2009). Initial clinical evaluation of an intraocular femtosecond laser in cataract surgery. *Journal of refractive surgery, 25*(12).

Nair, R. R., Blake, P., Grigorenko, A. N., Novoselov, K. S., Booth, T. J., Stauber, T., . . . Geim, A. K. (2008). Fine structure constant defines visual transparency of graphene. *Science, 320*(5881), 1308-1308.

Nakazawa, M. (2000). Solitons for breaking barriers to terabit/second WDM and OTDM transmission in the next millennium. *Selected Topics in Quantum Electronics, IEEE Journal of, 6*(6), 1332-1343.

Nakazawa, M., Yoshida, E., & Kimura, Y. (1991). Low threshold, 290 fs erbium-doped fiber laser with a nonlinear amplifying loop mirror pumped by InGaAsP laser diodes. *Applied Physics Letters, 59*(17), 2073-2075.

Nelson, L. E., Jones, D. J., Tamura, K., Haus, H. A., & Ippen, E. P. (1997). Ultrashort-pulse fiber ring lasers. *Applied Physics B, 65*(2), 277-294.

Ngo, N. Q. (2010). *Ultra-fast fiber lasers: principles and applications with MATLAB® models*: CRC Press.

Nishii, T., Maruyama, Y., Inabe, T., & Shirotani, I. (1987). Synthesis and characterization of black phosphorus intercalation compounds. *Synthetic Metals, 18*(1), 559-564.

Novoselov, K. (2011). Nobel lecture: graphene: materials in the flatland. *Reviews of Modern Physics, 83*(3), 837.

Novoselov, K. S., Geim, A. K., Morozov, S. V., Jiang, D., Zhang, Y., Dubonos, S. V., . . . Firsov, A. A. (2004). Electric field effect in atomically thin carbon films. *Science, 306*(5696), 666-669.

Okhotnikov, O., Grudinin, A., & Pessa, M. (2004). Ultra-fast fibre laser systems based on SESAM technology: new horizons and applications. *New journal of physics, 6*(1), 177.

Paschotta, R. (2008). *Field guide to laser pulse generation* (Vol. 14): SPIE Press Bellingham.

Peccianti, M., Pasquazi, A., Park, Y., Little, B., Chu, S. T., Moss, D., & Morandotti, R. (2012). Demonstration of a stable ultrafast laser based on a nonlinear microcavity. *Nature communications, 3*, 765.

Plamann, K., Aptel, F., Arnold, C., Courjaud, A., Crotti, C., Deloison, F., . . . Legeais, J.-M. (2010). Ultrashort pulse laser surgery of the cornea and the sclera. *Journal of Optics, 12*(8), 084002.

Popa, D., Sun, Z., Hasan, T., Torrisi, F., Wang, F., & Ferrari, A. (2010). Graphene Q-switched, tunable fiber laser. *arXiv preprint arXiv:1011.0115*.

Proctor, B., Westwig, E., & Wise, F. (1993). Characterization of a Kerr-lens mode-locked Ti: sapphire laser with positive group-velocity dispersion. *Optics letters, 18*(19), 1654-1656.

Quimby, R. S. (2006). *Photonics and lasers: an introduction*: John Wiley & Sons.

Reich, S., & Thomsen, C. (2004). Raman spectroscopy of graphite. *Philosophical Transactions of the Royal Society of London A: Mathematical, Physical and Engineering Sciences, 362*(1824), 2271-2288.

Ren, J., Wang, S., Cheng, Z., Yu, H., Zhang, H., Chen, Y., . . . Wang, P. (2015). Passively Q-switched nanosecond erbium-doped fiber laser with MoS 2 saturable absorber. *Optics Express, 23*(5), 5607-5613.

Rudenko, A. N., & Katsnelson, M. I. (2014). Quasiparticle band structure and tight-binding model for single-and bilayer black phosphorus. *Physical Review B, 89*(20), 201408.

Salehi, J. A., Weiner, A. M., & Heritage, J. P. (1990). Coherent ultrashort light pulse code-division multiple access communication systems. *Lightwave Technology, Journal of, 8*(3), 478-491.

Schawlow, A. L., & Townes, C. H. (1958). Infrared and optical masers. *Physical Review, 112*(6), 1940.

Schmidt, W., & Schäfer, F. (1968). Self-mode-locking of dye-lasers with saturated absorbers. *Physics Letters A, 26*(11), 558-559.

Schweizer, M. (2002). Pen or pencil: Google Patents.

Set, S. Y., Yaguchi, H., Tanaka, Y., & Jablonski, M. (2004). Laser mode locking using a saturable absorber incorporating carbon nanotubes. *Lightwave Technology, Journal of, 22*(1), 51-56.

Shank, C., & Ippen, E. (1974). Subpicosecond kilowatt pulses from a mode-locked cw dye laser. *Applied Physics Letters, 24*(8), 373-375.

Smith, N. J., Blow, K., & Andonovic, I. (1992). Sideband generation through perturbations to the average soliton model. *Journal of lightwave technology, 10*(10), 1329-1333.

Smith, N. J., Blow, K., & Andonovic, I. (1992). Sideband generation through perturbations to the average soliton model. *Lightwave Technology, Journal of, 10*(10), 1329-1333.

Sobon, G. (2016). Application of 2D Materials to Ultrashort Laser Pulse Generation *Two-dimensional Materials-Synthesis, Characterization and Potential Applications*: InTech.

Sobon, G. (2016). *Application of 2D Materials to Ultrashort Laser Pulse Generation*.

Sobon, G., Sotor, J., & Abramski, K. (2012). All-polarization maintaining femtosecond Er-doped fiber laser mode-locked by graphene saturable absorber. *Laser Physics Letters, 9*(8), 581.

Sotor, J., Pasternak, I., Krajewska, A., Strupinski, W., & Sobon, G. (2015). Sub-90 fs a stretched-pulse mode-locked fiber laser based on a graphene saturable absorber. *Optics Express, 23*(21), 27503-27508.

Sotor, J., Sobon, G., Kowalczyk, M., Macherzynski, W., Paletko, P., & Abramski, K. M. (2015). Ultrafast thulium-doped fiber laser mode locked with black phosphorus. *Optics letters, 40*(16), 3885-3888.

Sotor, J., Sobon, G., Macherzynski, W., Paletko, P., & Abramski, K. M. (2015). Black phosphorus a new saturable absorber material for ultrashort pulse generation. *arXiv preprint arXiv:1504.04731*.

Sotor, J., Sobon, G., Macherzynski, W., Paletko, P., & Abramski, K. M. (2015). Black phosphorus saturable absorber for ultrashort pulse generation. *Applied Physics Letters, 107*(5), 051108.

Sotor, J., Sobon, G., Macherzynski, W., Paletko, P., Grodecki, K., & Abramski, K. M. (2014). Mode-locking in Er-doped fiber laser based on mechanically exfoliated Sb 2 Te 3 saturable absorber. *Optical Materials Express, 4*(1), 1-6.

Spence, D. E., Kean, P. N., & Sibbett, W. (1991). 60-fsec pulse generation from a self-mode-locked Ti: sapphire laser. *Optics letters, 16*(1), 42-44.

Splendiani, A., Sun, L., Zhang, Y., Li, T., Kim, J., Chim, C.-Y., . . . Wang, F. (2010). Emerging photoluminescence in monolayer MoS2. *Nano letters, 10*(4), 1271-1275.

Sugai, S., & Shirotani, I. (1985). Raman and infrared reflection spectroscopy in black phosphorus. *Solid State Communications, 53*(9), 753-755.

Sun, Z., Hasan, T., Torrisi, F., Popa, D., Privitera, G., Wang, F., . . . Ferrari, A. C. (2010). Graphene mode-locked ultrafast laser. *ACS nano, 4*(2), 803-810.

Sun, Z., Hasan, T., Wang, F., Rozhin, A. G., White, I. H., & Ferrari, A. C. (2010). Ultrafast stretched-pulse fiber laser mode-locked by carbon nanotubes. *Nano Research, 3*(6), 404-411.

Sutter, D. H., Steinmeyer, G., Gallmann, L., Matuschek, N., Morier-Genoud, F., Keller, U., . . . Tschudi, T. (1999). Semiconductor saturable-absorber mirror–assisted Kerr-lens mode-locked Ti: sapphire laser producing pulses in the two-cycle regime. *Optics letters, 24*(9), 631-633.

Tamura, K., Ippen, E. P., Haus, H. A., & Nelson, L. E. (1993). 77-fs pulse generation from a stretched-pulse mode-locked all-fiberring laser. *Optics letters, 18*(13), 1080-1082.

Tamura, K., Nelson, L., Haus, H., & Ippen, E. (1994). Soliton versus nonsoliton operation of fiber ring lasers. *Applied Physics Letters, 64*(2), 149-151.

Tausenev, A., Obraztsova, E., Lobach, A., Chernov, A., Konov, V., Kryukov, P., . . . Dianov, E. (2008). 177fs erbium-doped fiber laser mode locked with a cellulose polymer film containing single-wall carbon nanotubes. *Applied Physics Letters, 92*(17), 171113.

Tian, Z., Wu, K., Kong, L., Yang, N., Wang, Y., Chen, R., . . . Tang, Y. (2015). Mode-locked thulium fiber laser with MoS2. *Laser Physics Letters, 12*(6), 065104.

Tran, V., Soklaski, R., Liang, Y., & Yang, L. (2014). Layer-controlled band gap and anisotropic excitons in few-layer black phosphorus. *Physical Review B, 89*(23), 235319.

Wallace, P. R. (1947). The band theory of graphite. *Physical Review, 71*(9), 622.

Wang, J., Liang, X., Hu, G., Zheng, Z., Lin, S., Ouyang, D., . . . Sun, Z. (2016). 152 fs nanotube-mode-locked thulium-doped all-fiber laser. *Scientific Reports, 6*.

Wang, K., Wang, J., Fan, J., Lotya, M., O'Neill, A., Fox, D., . . . Zhao, Q. (2013). Ultrafast saturable absorption of two-dimensional MoS2 nanosheets. *ACS nano, 7*(10), 9260-9267.

Wang, Q. H., Kalantar-Zadeh, K., Kis, A., Coleman, J. N., & Strano, M. S. (2012). Electronics and optoelectronics of two-dimensional transition metal dichalcogenides. *Nature nanotechnology, 7*(11), 699-712.

Wang, S., Yu, H., Zhang, H., Wang, A., Zhao, M., Chen, Y., . . . Wang, J. (2014). Broadband Few-Layer MoS2 Saturable Absorbers. *Advanced Materials, 26*(21), 3538-3544.

Warschauer, D. (1963). Electrical and optical properties of crystalline black phosphorus. *Journal of Applied Physics, 34*(7), 1853-1860.

Weill, R., Bekker, A., Smulakovsky, V., Fischer, B., & Gat, O. (2011). Spectral sidebands and multipulse formation in passively mode-locked lasers. *Physical Review A, 83*(4), 043831.

Wienke, A., Haxsen, F., Wandt, D., Morgner, U., Neumann, J., & Kracht, D. (2012). Ultrafast, stretched-pulse thulium-doped fiber laser with a fiber-based dispersion management. *Optics letters, 37*(13), 2466-2468.

Wilson, J., & Yoffe, A. (1969). The transition metal dichalcogenides discussion and interpretation of the observed optical, electrical and structural properties. *Advances in Physics, 18*(73), 193-335.

Wittig, J., & Matthias, B. (1968). Superconducting phosphorus. *Science, 160*(3831), 994-995.

Woodward, R. (2015). *Exploiting nonlinearity in optical fibres and nanomaterials for short-pulse laser technology.* (PhD), Imperial College London.

Woodward, R., Howe, R., Hu, G., Torrisi, F., Zhang, M., Hasan, T., & Kelleher, E. (2015). Few-layer MoS 2 saturable absorbers for short-pulse laser technology: current status and future perspectives [Invited]. *Photonics Research, 3*(2), A30-A42.

Woodward, R., Kelleher, E., Howe, R., Hu, G., Torrisi, F., Hasan, T., . . . Taylor, J. (2014). Tunable Q-switched fiber laser based on saturable edge-state absorption in few-layer molybdenum disulfide (MoS 2). *Optics Express, 22*(25), 31113-31122.

Woodward, R. I., & Kelleher, E. J. (2015). 2D Saturable Absorbers for Fibre Lasers. *Applied Sciences, 5*(4), 1440-1456.

Woodward, R. I., Kelleher, E. J., Runcorn, T. H., Popov, S. V., Torrisi, F., Howe, R. T., & Hasan, T. (2014, 2014/06/08). *Q-switched Fiber Laser with MoS2 Saturable Absorber.* Paper presented at the CLEO: 2014, San Jose, California.

Woodward, R. I., Kelleher, E. J. R., Howe, R. C. T., Hu, G., Torrisi, F., Hasan, T., . . . Taylor, J. R. (2014). Tunable Q-switched fiber laser based on saturable edge-state absorption in few-layer molybdenum disulfide (MoS2). *Optics Express, 22*(25), 31113-31122.

Wu, K., Chen, B., Zhang, X., Zhang, S., Guo, C., Li, C., . . . Zou, W. (2017). High-performance mode-locked and Q-switched fiber lasers based on novel 2D materials of topological insulators, transition metal dichalcogenides and black phosphorus: review and perspective. *Optics Communications*.

Wu, K., Zhang, X., Wang, J., & Chen, J. (2015). 463-MHz fundamental mode-locked fiber laser based on few-layer MoS 2 saturable absorber. *Optics letters, 40*(7), 1374-1377.

Xia, F., Wang, H., & Jia, Y. (2014). Rediscovering black phosphorus as an anisotropic layered material for optoelectronics and electronics. *Nature communications, 5*.

Xia, H., Li, H., Lan, C., Li, C., Zhang, X., Zhang, S., & Liu, Y. (2014). Ultrafast erbium-doped fiber laser mode-locked by a CVD-grown molybdenum disulfide (MoS2) saturable absorber. *Optics Express, 22*(14), 17341-17348.

Xia, H., Li, H., Lan, C., Li, C., Zhang, X., Zhang, S., & Liu, Y. (2014). Ultrafast erbium-doped fiber laser mode-locked by a CVD-grown molybdenum disulfide (MoS 2) saturable absorber. *Optics Express, 22*(14), 17341-17348.

Xu, C., & Wise, F. (2013). Recent advances in fibre lasers for nonlinear microscopy. *Nature Photonics, 7*(11), 875-882.

Xu, J., Liu, J., Wu, S., Yang, Q.-H., & Wang, P. (2012). Graphene oxide mode-locked femtosecond erbium-doped fiber lasers. *Optics Express, 20*(14), 15474-15480.

Xu, M., Liang, T., Shi, M., & Chen, H. (2013). Graphene-like two-dimensional materials. *Chemical reviews, 113*(5), 3766-3798.

Yamashita, S. (2012). A tutorial on nonlinear photonic applications of carbon nanotube and graphene. *Journal of lightwave technology, 30*(4), 427-447.

Yang, C.-Y., Wu, C.-L., Lin, Y.-H., Tsai, L.-H., Chi, Y.-C., Chang, J.-H., . . . Lin, G.-R. (2013). Fabricating graphite nano-sheet powder by slow electrochemical exfoliation of large-scale graphite foil as a mode-locker for fiber lasers. *Optical Materials Express, 3*(11), 1893-1905.

Zabusky, N. J., & Kruskal, M. D. (1965). Interaction of" solitons" in a collisionless plasma and the recurrence of initial states. *Physical review letters, 15*(6), 240.

Zhan, Y., Liu, Z., Najmaei, S., Ajayan, P. M., & Lou, J. (2012). Large-area vapor-phase growth and characterization of MoS2 atomic layers on a SiO2 substrate. *Small, 8*(7), 966-971.

Zhang, H., Liu, C.-X., Qi, X.-L., Dai, X., Fang, Z., & Zhang, S.-C. (2009). Topological insulators in Bi2Se3, Bi2Te3 and Sb2Te3 with a single Dirac cone on the surface. *Nature physics, 5*(6), 438-442.

Zhang, H., Lu, S., Zheng, J., Du, J., Wen, S., Tang, D., & Loh, K. (2014). Molybdenum disulfide (MoS 2) as a broadband saturable absorber for ultra-fast photonics. *Optics Express, 22*(6), 7249-7260.

Zhang, H., Lu, S. B., Zheng, J., Du, J., Wen, S. C., Tang, D. Y., & Loh, K. P. (2014). Molybdenum disulfide (MoS2) as a broadband saturable absorber for ultra-fast photonics. *Optics Express, 22*(6), 7249-7260.

Zhang, H., Tang, D., Zhao, L., Bao, Q., & Loh, K. (2009). Large energy mode locking of an erbium-doped fiber laser with atomic layer graphene. *Optics Express, 17*(20), 17630-17635.

Zhang, M., Howe, R. C., Woodward, R. I., Kelleher, E. J., Torrisi, F., Hu, G., . . . Hasan, T. (2015). Solution processed MoS2-PVA composite for sub-bandgap mode-locking of a wideband tunable ultrafast Er: fiber laser. *Nano Research, 8*(5), 1522-1534.

Zhang, M., Kelleher, E., Popov, S., & Taylor, J. (2014). Ultrafast fibre laser sources: Examples of recent developments. *Optical Fiber Technology, 20*(6), 666-677.

Zhang, M., Kelleher, E., Torrisi, F., Sun, Z., Hasan, T., Popa, D., . . . Taylor, J. (2012). Tm-doped fiber laser mode-locked by graphene-polymer composite. *Optics Express, 20*(22), 25077-25084.

Zhang, Y., Tang, T.-T., Girit, C., Hao, Z., Martin, M. C., Zettl, A., . . . Wang, F. (2009). Direct observation of a widely tunable bandgap in bilayer graphene. *Nature, 459*(7248), 820-823.

Zhao, C., Zhang, H., Qi, X., Chen, Y., Wang, Z., Wen, S., & Tang, D. (2012). Ultra-short pulse generation by a topological insulator based saturable absorber. *Applied Physics Letters, 101*(21), 211106.

Zhao, L., Tang, D., & Wu, J. (2006). Gain-guided soliton in a positive group-dispersion fiber laser. *Optics letters, 31*(12), 1788-1790.

Zhong, Y., Zhang, Z., & Tao, X. (2010). Passively mode-locked fiber laser based on nonlinear optical loop mirror with semiconductor optical amplifier. *Laser physics, 20*(8), 1756-1759.

Zhou, D.-P., Wei, L., Dong, B., & Liu, W.-K. (2010). Tunable passively-switched erbium-doped fiber laser with carbon nanotubes as a saturable absorber. *IEEE photonics technology letters, 22*(1), 9-11.

Zhou, X., Yoshitomi, D., Kobayashi, Y., & Torizuka, K. (2008). Generation of 28-fs pulses from a mode-locked ytterbium fiber oscillator. *Optics Express, 16*(10), 7055-7059.

LIST OF PUBLICATIONS AND PAPERS PRESENTED

The following publications form the basis of the thesis:

ISI Journal Papers

1. **M.H.M. Ahmed**, A.A. Latiff, H. Arof, H. Ahmad, S.W. Harun, *Soliton mode-locked erbium-doped fibre laser with mechanically exfoliated molybdenum disulfide saturable absorber,* IET Optoelectronics 10(2016) 169-173. *(ISI-Indexed)*

2. **M.H.M. Ahmed,** A.A. Latiff, H. Arof, H. Ahmad, S.W. Harun, *Femtosecond mode-locked erbium-doped fiber laser based on MoS2–PVA saturable absorber,* Optics & Laser Technology 82 (2016) 145-149. *(ISI-Indexed)*

3. **M.H.M. Ahmed,** A.A. Latiff, H. Arof, S.W. Harun, *Mode-locking pulse generation with MoS 2–PVA saturable absorber in both anomalous and ultra-long normal dispersion regimes*, Applied Optics 55(2016) 4247-4252. *(ISI-Indexed)*

4. **M.H.M. Ahmed**, A.A. Latiff, H. Arof, S.W. Harun, *Ultrafast erbium-doped fiber laser mode-locked with a black phosphorus saturable absorber,* Laser Physics Letters 13(2016) 095104. *(ISI-Indexed)*

5. **M. H. M. Ahmed**, A. H. H. Al-Masoodi, M. Yasin, H. Arof, S. W. Harun, *Stretched and soliton femtosecond pulse generation with graphene saturable absorber by manipulating cavity dispersion*, Optik-International Journal for Light and Electron Optics 138(2017) 250-255. *(ISI-Indexed)*

6. **M. H. M Ahmed**, A. H. H. Al-Masoodi, A. A. Latiff, H. Arof, S. W. Harun, *Mechanically exfoliated 2D nanomaterials as saturable absorber for Q-switched erbium-doped fiber laser,* Indian Journal of Physics (2017)1-6. *(ISI-Indexed)*

Conference Papers

1. **M. H. M. Ahmed,** A. H. H. Al-Masoodi and S. W. Harun, *Passively Q-switched Erbium-Doped Fiber Laser Based on Mechanically Exfoliated Black Phosphorus Saturable Absorber,* 1st International Research Conference on Engineering, Science & Humanities November 09th – 10th, 2016 | UKM Malaysia.

Additional ISI Publications

In addition, the following papers were published during the period of PhD, but is beyond the scope of this thesis:

1. **M. H. M. Ahmed**, Banabila, A. M., Latiff, A. A., Irawati, N., Ali, N. M., Harun, S. W., & Arof, H. (2016). *Tunable Q-switched erbium doped fiber laser with graphene oxide paper based saturable absorber*. Optoelectronics And Advanced Materials-Rapid Communications, 10(11-12), 791-796. *(ISI-Indexed)*

2. A. H. H Al-Masoodi, **M. H. M. Ahmed**, A. A. Latiff, H Arof, S. W. Harun, *Q-Switched Ytterbium-Doped Fiber Laser Using Black Phosphorus as Saturable Absorber,* Chinese Physics Letters 33(2016) 054206. *(ISI-Indexed)*

3. A. H. H. Al-Masoodi, F. Ahmad, **M. H. M Ahmed**, H. Arof, S. W. Harun, *Q-switched ytterbium-doped fiber laser with topological insulator-based saturable absorber,* Optical Engineering 56(2017) 056103-056103. *(ISI-Indexed)*

4. A. Nady, **M. H. M. Ahmed**, A. Numan, S. Ramesh, A. A. Latiff, CHR Ooi, H. Arof, S. W. Harun, *Passively Q-switched erbium-doped fibre laser using cobalt oxide nanocubes as a saturable absorber,* Journal of Modern Optics (2017) 1-6. *(ISI-Indexed)*

5. A. Nady, **M. H. M. Ahmed**, A. A. Latiff, A. Numan, C. H. Raymond Ooi, S. W. Harun, *Nickel oxide nanoparticles as a saturable absorber for an all-fiber passively Q-switched erbium-doped fiber laser,* Laser Physics 27(2017) 065105. *(ISI-Indexed)*

6. A. H. H. Al-Masoodi, **M. H. M Ahmed**, A. A. Latiff, H. Arof, S. W. Harun, (2017) *Passively Q-switched Ytterbium doped fiber laser with mechanically exfoliated MoS2 saturable absorber,* Indian Journal of Physics 91(5), 575-580. *(ISI-Indexed)*

7. A. Nady, **M. H. M. Ahmed**, A. A. Latiff, Ooi, C. R., & S. W. Harun, (2017). *Femtoseconds soliton mode-locked erbium-doped fiber laser based on nickel oxide nanoparticle saturable absorber*. Chinese Optics Letters, 15(10), 100602. *(ISI-Indexed)*

8. Al-Masoodi, A. H. H., **Ahmed, M. H. M.**, Latiff, A. A., Azzuhri, S. R., Arof, H., & Harun, S. W. (2017). Passively Mode-locked Ytterbium-doped Fiber Laser Operation with few layer MoS 2 PVA Saturable Absorber. *Optik-International Journal for Light and Electron Optics*. *(ISI-Indexed)*

9. Al-Masoodi, A. H. H., Yasin, M., **Ahmed, M. H. M.**, Latiff, A. A., Arof, H., & Harun, S. W. (2017). Mode-locked ytterbium-doped fiber laser using mechanically exfoliated black phosphorus as saturable absorber. *Optik-International Journal for Light and Electron Optics. (ISI-Indexed)*